Inaugural dissertation

for

obtaining the doctoral degree

of the

Combined Faculty of Mathematics, Engineering and Natural Sciences

of the

Ruprecht - Karls - University

Heidelberg

Presented by

Jana Christin Askani, Master of Science (M.Sc.)

born in: Speyer, Germany

Oral examination: 29th March 2022

# The role of membrane tethering complexes in vacuolar trafficking and vacuole biogenesis

Referees: Prof. Dr. Karin Schumacher

Prof. Dr. Alexis Maizel

# Table of contents

# Zusammenfassung (Deutsch)

Die lytische Vakuole ist für die Pflanzenzelle lebenswichtig, da die Vakuole wesentliche Funktionen wie Abbau, Entgiftung, Speicherung und Erzeugung des Turgordrucks erfüllt. Sekundäre aktive Transport- und Abbauprozesse benötigen die Energie, die von den am Tonoplasten lokalisierten V-ATPase und V-PPase bereitgestellt wird. Durch die Untersuchung des vakuolären Transports der V-ATPase und der V-PPase wurde ein vom Golgi unabhängiger und durch Provakuolen vermittelter Transportweg entdeckt. Zur weiteren Untersuchung des Golgi-unabhängigen Transports und seiner Rolle in der Biogenese von Vakuolen wurde die konditionelle Expression von Sar1b-GTP zur Unterbrechung des COPII-vermittelten Transports analysiert. Die am Tonoplasten lokalisierte V-ATPase kann unabhängig vom COPII-Weg zur Vakuole transportiert werden. Mit einem genetischen Huckepack-System und der konditionellen Expression von VHA-a3 wurden punkt- und schlauchförmige Strukturen, bei denen es sich wahrscheinlich um Provakuolen handelt, in vivo untersucht. Die Fusionsstellen zwischen Provakuolen und der Vakuole befinden sich wahrscheinlich in der Nähe der Kernhülle.

Die Rolle der konservierten Membranbindungskomplexe HOPS und CORVET im vakuolären Transport wurde untersucht. In Arabidopsis vermittelt der HOPS-Komplex den vakuolären Transport vom Golgi über AP-3-Vesikel und vom TGN/EE über MVBs, ähnlich seiner Funktion in Hefe- und Säugetierzellen. CORVET hat eine neue Rolle entwickelt und vermittelt einen pflanzenspezifischen Transportweg vom TGN/EE zur Vakuole. Eine Population der am Tonoplasten lokalisierten V-ATPase und V-PPase tritt in einen Golgi-abhängigen Weg ein, der über das TGN/EE und RAB5-positive LEs verläuft, die den CORVET-Membranbindungskomplex für die Fusion mit der Vakuole benötigen. Allerdings scheinen weder der HOPS- noch der CORVET-Komplex eine Rolle bei der Membranfusion zwischen Provakuolen und der Vakuole zu spielen. Tonoplasten-lokalisierte Protonenpumpen können sowohl in Provakuolen als auch in COPII-Vesikel sortiert werden. Dadurch können Protonenpumpen, die am Tonoplasten lokalisiert sind, das ER über zwei verschiedene Wege verlassen, und die

Verteilung zwischen den beiden Transportwegen könnte an Umwelt- oder Entwicklungsfaktoren angepasst werden.

In meristematischen Wurzelzellen besteht die Vakuole aus einem einzigen, schlauchförmigen Netzwerk, dessen Integrität durch den HOPS-Komplex aufrechterhalten wird. Die homotypische Vakuolenfusion erfolgt durch die Bildung von Vertexringen. Anders als in Hefezellen ist die V-ATPase für die homotypische Vakuolenfusion nicht erforderlich. Das Gleichgewicht des signalgebenden Lipids PI3P an der Vakuolenmembran ist jedoch entscheidend für die ordnungsgemäße Fusion an der Vakuole.

# Summary (English)

The lytic vacuole is vital for the plant cell, as the vacuole fulfills essential functions, such as degradation, detoxification, storage and generation of the turgor pressure. Secondary active transport and degradation processes require the energy provided by the tonoplast-localized V-ATPase and V-PPase. By studying the vacuolar trafficking of the V-ATPase and the V-PPase a trafficking route independent of the Golgi and mediated by provacuoles was discovered. To further investigate the Golgi-independent trafficking and its role in vacuole biogenesis, conditional expression of Sar1b-GTP to disrupt COPII-mediated trafficking was studied. The tonoplast-localized V-ATPase can be transported independent of the COPII route to the vacuole. With a genetic piggyback system and conditional expression of VHA-a3 punctate and tubular structures likely being provacuoles were examined in vivo.

The role of the conserved membrane tethering complexes HOPS and CORVET in vacuolar trafficking was investigated. In Arabidopsis, the HOPS complex mediates vacuolar trafficking from the Golgi via AP-3 vesicles and from the TGN/EE via MVBs, similar to its function in yeast and mammalian cells. CORVET evolved a new role and operates a plant-specific transport route from the TGN/EE to the vacuole. A population of the tonoplast-localized V-ATPase and V-PPase enters a Golgi-dependent pathway, which passes through the TGN/EE and RAB5-positive LEs, which require the CORVET membrane tethering complex for fusion with the vacuole. However, neither the HOPS nor the CORVET complex seems to play a role in membrane fusion between provacuoles and the vacuole. Tonoplast-localized proton pumps can be sorted into provacuoles as well as into COPII vesicles. Thereby, tonoplast-localized proton pumps can exit the ER via two distinct routes and the distribution between the two trafficking routes might be adaptable to environmental or developmental cues.

In meristematic root cells, the vacuole is composed of a single, tubular network, whose integrity is maintained by the HOPS complex. Homotypic vacuole fusion occurs via the formation of vertex rings. Unlike in yeast cells, the V-ATPase is not required for homotypic vacuole fusion. However, the balance of the signaling lipid PI3P at the vacuolar membrane is crucial for proper fusion events at the vacuole.

## Contributions to this work

The author declares that this work was written independently using only the sources indicated and not by services of a third party. Where the work of others was quoted or reproduced, the source is always given. Apart from the author and the supervisor the following persons contributed to the work presented in this thesis as indicated.

The cloning, transformation and selection of the Dex-inducible knockdown against *VPS16* (amiR-*vps16*) was performed by Falco Krüger with Taslima Nahar. The cloning of GFP-VPS16 and the transformation and selection in Arabidopsis thaliana was done by Falco Krüger. The cloning and transformation of the Dex-inducible knockdowns against subunits of the HOPS and CORVET complex was performed during my Master Thesis (Askani, 2015).

Philipp Bellon cloned the Dex-inducible VHA-a3-mCherry and the establishment of the genetic piggyback system was done together with me and Falco Krüger.

Philipp Bellon and Upendo Lupanga planned and executed the cloning of the Dex inducible dominant-negative Sar1b-GTP. The transformations of the cloned constructs into Arabidopsis thaliana plants and selections of Arabidopsis lines were performed by me, Zaida Andrés and Upendo Lupanga.

Together with Florian Hinterberger the cloning of the estradiol-inducible VHA-a3-LinkerGFP was performed.

Marlene Handl performed the selection of the estradiol-inducible VHA-a3-LinkerGFP. She also cloned, transformed and selected UBQ10:INT1-mTurquoise.

Jointly with Sina Pfleger the cloning of the estradiol-inducible ARA7-GDP was performed.

Görkem Patir Nebioglou planned and executed the cloning of pUBQ10:AHA10-mVenus.

Lotte Bald and Stefan Scholl planned and executed the cloning of VHA-a3-mCherry-eGFP, which was selected by Simon Delang. Lotte Bald also cloned the VHP1-mCherry, which was selected by me and Falco Krüger.

Beate Schöfer contributed by taking care of Arabidopsis plants in the growth cambers. In addition, Beate Schöfer crossed Arabidopsis plants expressing DEX:Sar1b-GTP-CFP in 35S:SUC4-GFP with the *pat2-2* mutant.

Sample preparation, processing and imaging of EM samples was performed by me, Upendo Lupanga, Stephanie Gold and Stefan Hillmer.

Parts of this work have been published in:

**Brillada, C., Zheng, J., Krüger, F., Rovira-Diaz, E., Askani, J.C., Schumacher, K., and Rojas-Pierce, M.** (2018). Phosphoinositides control the localization of HOPS subunit VPS41, which together with VPS33 mediates vacuole fusion in plants. Proc. Natl. Acad. Sci. **115**: 201807763.

**Lupanga, U., Röhrich, R., Askani, J., Hilmer, S., Kiefer, C., Krebs, M., Kanazawa, T., Ueda, T., and Schumacher, K.** (2020). The Arabidopsis V-ATPase is localized to the TGN/EE via a seed plant specific motif. Elife **9**.

**Takemoto, K., Ebine, K., Askani, J.C., Krüger, F., Gonzalez, Z.A., Ito, E., Goh, T., Schumacher, K., Nakano, A., and Ueda, T.** (2018). Distinct sets of tethering complexes, SNARE complexes, and Rab GTPases mediate membrane fusion at the vacuole in Arabidopsis. Proc. Natl. Acad. Sci.: 201717839.

# 1 Introduction

## 1.1 Vacuoles and lysosomes – similarities and differences

The main characteristic of eukaryotic cells is the compartmentalization of different reaction spaces within a cell. To degrade and recycle biomolecules, an acidic compartment with low pH and hydrolases is required in all eukaryotic cells. In different kingdoms of life, this lytic compartment has different characteristics and names. In yeast and plant cells, the degradative reaction space is called a vacuole. In metazoan cells, however, the lytic compartment is called lysosome.

**Table 1: Overview of the specific characteristics of the yeast vacuole, the mammalian lysosome and the plant vacuole.** The information given in the table was reviewed in Armstrong, 2010; Epp et al., 2011; Li and Kane, 2009; de Marcos Lousa and Denecke, 2016.

| | Yeast vacuole | Mammalian lysosome | Plant vacuole |
|---|---|---|---|
| **pH** | 5 - 6.5 | 4.5 - 5.5 | 5.5 - 6.2 |
| **Degradative function** | Yes | Yes | Yes |
| **Storage and detoxification** | Yes | No active sequestration of amino acids, metal ions or metabolic byproducts | Yes |
| **Morphology** | One to three round vacuoles | Numerous round lysosomes; about 500 nm in diameter | Filling up to 90 % of cell volume |
| **Hydroskeleton** | No | No | Yes |

The lytic vacuole in Arabidopsis fulfills degradative functions, just like vacuoles in yeast and lysosomes in animal cells. In addition, the plant vacuole serves as storage for nutrients and metabolites. And by actively accumulating harmful molecules, the cytosol can be detoxified to ensure proper reaction processes. The active sequestration of amino acids, metal ions, and metabolic byproducts is a

shared feature of yeast vacuoles and the vacuoles of plants. Lysosomes do not exhibit this function and have been described to exclusively have degradative properties (Table 1; Marty, 1999; de Marcos Lousa and Denecke, 2016).

Plants have two distinct types of degradative compartments: the lytic vacuole (LV), also called the central or vegetative vacuole, and the protein storage vacuole (PSV). The lytic vacuole of higher plants fills almost 90 % of the cell volume in differentiated plant cells and exhibits a brick-like structure in differentiated root cells. This fact led to the alternative naming of the lytic vacuole as the central vacuole. Besides the plant cell wall, the lytic vacuole is the characteristic feature of plant cells compared to organisms from other kingdoms of life.

The latter type of vacuoles, the PSV, forms temporarily during embryogenesis and mainly stores proteins and fats. Degradation processes of proteins and lipids help to supply the plant embryo with the necessary energy during seed germination until the first photosynthetic tissues are formed to ensure autotrophic energy supply (Zheng and Staehelin, 2011).

In the primary root tip of the model plant *Arabidopsis thaliana* (*A. thaliana*; hereafter referred to as Arabidopsis for short), PSVs are present until 4 days after germination (DAG; Zheng and Staehelin, 2011). Therefore, lytic vacuoles in Arabidopsis are usually studied in meristematic root cells of 5 to 8-day-old seedlings (Zouhar and Rojo, 2009). As the following research study focuses exclusively on vacuolar trafficking and biogenesis of the lytic vacuole in Arabidopsis, the lytic vacuole is referred to as vacuole hereafter for simplicity.

In contrast to the large volume of plant vacuoles, the mammalian cell has numerous round lysosomes (50 to 1,000 per cell) ranging in size from 0.1 to 1 $\mu$m (de Marcos Lousa and Denecke, 2016). This size difference leads to the interesting question of why the morphology of a plant vacuole is so different from the lysosomal structure of mammalian cells.

Plants are sessile organisms and the best way to exploit the immediate surrounding is in developing large surfaces like seen in complex root systems in the soil and in elongated flattened structures like plant leaves to collect sunlight

and carbon dioxide. In the scenario of building elongated structures with a high surface-to-volume ratio, two considerations must be considered.

If the subcellular compartments are to be kept stable in their size, the proportion of cytosol, the liquid phase inside the cell surrounding the subcellular organelles, must be increased. However, ion homeostasis in the cytosol is critical with numerous proteins and buffering systems and, therefore, the cytosol is energy intense to produce and maintain. But if the proportion of the costly cytosol remains the same throughout cell development, the size of at least one subcellular compartment must be increased during cell growth – the mainly water filled vacuole (Krüger and Schumacher, 2017; Maugarny-Calès and Laufs, 2018).

A recent study showed that the cytosolic fraction remains stable from meristematic root cells, which are small, to cells of the late elongation zone of the primary root. Moreover, the increase in vacuole volume correlates with the overall increase in cell volume in the meristematic and elongations zone of the root (Dünser et al., 2019). Thereby, vacuolar expansion allows cell growth with a comparatively good energy efficiency and low cost of nutrients and metabolites.

As water is stored to fill the plant vacuole, the vacuole also acts as the water reservoir of the cell. The water also plays an important role in supporting the plant structure. Multicellular plants do not possess an endo – or exoskeleton to support their structure, but by taking up water a so-called hydrostatic skeleton can be formed. Water is stored in the plant vacuole, which acts as the water reservoir of the cell, and together with the cytosol the pressurized cell is enclosed by the cell wall. Plant growth therefore relies on the delicate balance between turgor pressure and the yielding of the cell wall to this pressure (Höfte, 2015).

For acidic hydrolases to function inside the vacuole or lysosome and to generate the necessary membrane potential for secondary active transport, protons ($H^+$) must be accumulated within the vacuole or lysosome. Accumulation against the $H^+$ gradient is facilitated by the vacuolar-type $H^+$-ATPase (V-ATPase or VHA-a). As transport of $H^+$ against the concentration gradient requires energy, cytosolic adenosine triphosphate (ATP) is hydrolyzed by the peripheral $V_1$ subcomplex of

the V-ATPase facing the cytosol. Thus, the V-ATPase is an ATP-dependent proton pump.

The $V_1$ subcomplex consists of eight subunits: VHA-A, VHA-B, VHA-C, VHA-D, VHA-E, VHA-F, VHA-G and VHA-H. Hydrolysis of ATP results in rotation of the subcomplex, and the rotational energy is thereby transferred to the membrane integral $V_0$ sub-complex, which consists of the six subunits VHA-a, VHA-c, VHA-c´; VHA-c´´, VHA-d and VHA-e. The rotational energy of the $V_0$ complex then transports $H^+$ protons across the membrane into the lumen (Beyenbach and Wieczorek, 2006; Nakanishi-Matsui et al., 2010; Schumacher and Krebs, 2010; Sze et al., 2002).

The different isoforms of the VHA-a subunit determine the subcellular localization of the V-ATPase. In yeast cells, there are two isoforms of the VHA-a subunit: Vhp1p (Vacuolar pH 1) and Stv1p (Similar To VPH1). Vph1p is located at the vacuolar membrane and Stv1p localizes to the Golgi (Kawasaki-Nishi et al., 2001; Manolson et al., 1994).

Mammalian cells possess four isoforms of the VHA-a subunit (a1, a2, a3, and a4) that direct the V-ATPase to endosomes or the plasma membrane of specific cell types. The subunit a1 localizes to synaptic vesicles and the presynaptic plasma membrane of neural cells (Morel et al., 2003). a2 directs the V-ATPase to endosomes in epithelial cells (Hurtado-Lorenzo et al., 2006). And the isoforms a3 and a4 are required for localization of the V-ATPase to the plasma membrane of osteoclasts and renal cells, respectively (Toyomura et al., 2003; Wagner et al., 2004; reviewed in Forgac, 2007).

In Arabidopsis, there are three isoforms of VHA-a: VHA-a1, VHA-a2 and VHA-a3. Localization studies found that VHA-a1 localizes to the *trans*-Golgi network (TGN)/early endosome (EE) (TGN/EE) in Arabidopsis (Dettmer et al., 2006; Viotti et al., 2010). The isoforms VHA-a2 and VHA-a3 localize to the tonoplast (Dettmer et al., 2006). By creating chimeric proteins of VHA-a1 and VHA-a3 the targeting signal was located between L132 and E179 in the N-terminus of VHA-a1. The targeting signal consists of an acidic cluster, which exists only in seed plants, and was named VHA-a1-targeting domain (VHA-a1-TD). The identified N-terminal

targeting domain of VHA-a1 is required for ER export and retention at the TGN/EE (Lupanga et al., 2020).

With the exception of VHA-a and VHA-c, all other V-ATPase subunits in Arabidopsis are encoded by a single gene (Sze et al., 2002). The T-DNA mutant lacking VHA-A is male gametophyte lethal, suggesting that the V-ATPase is essential in Arabidopsis (Dettmer et al., 2005). The *vha-a2 vha-a3* double mutant, which lacks V-ATPase complexes at the tonoplast, is viable, but shows severe defects in accumulating nitrate and zinc in the vacuolar lumen (Krebs et al., 2010). Further studies showed that the V-ATPase in the TGN/EE is essential for endocytic and secretory trafficking (Luo et al., 2015). Knock-down of VHA-a1 by RNAi or amiRNA leads to a reduction in cell expansion (Brüx et al., 2008). The CRISPR null mutant *vha-a1* is male gametophyte lethal indicating that VHA-a2 and VHA-a3 containing V-ATPase complexes take over the function of VHA-a1 during vegetative growth (Lupanga et al., 2020).

In plants, there is a second proton pump at the vacuole - the vacuolar $H^+$-pyrophosphatase ($H^+$-PPase, V-PPase or VHP1). The V-PPase is composed of a single polypeptide chain containing 17 predicted transmembrane domains (Segami et al., 2014). Inorganic pyrophosphate (PPi) is hydrolyzed to drive H+ translocation. The combined action of both proton pumps, the V-ATPase and the V-PPase, provides the necessary proton gradient and membrane potential for the proper functionality of the vacuole in Arabidopsis (Gaxiola et al., 2007; Kriegel et al., 2015).

## 1.2 Distinct cellular trafficking pathways operate towards the vacuole

Compartmentalization of eukaryotic cells allows different biochemical processes to occur simultaneously in different reaction spaces. However, this requires the exchange of substances via membrane transport or vesicle trafficking. Various transport pathways traverse the eukaryotic cell like subway lines. Lipids, transmembrane and luminal proteins are synthesized at the ER and transported to their destination. This is called anterograde (lat. ad anteriora; forward directed) transport. The secretory pathway transports transmembrane proteins from the ER to the plasma membrane or the vacuole. Retrograde transport processes, on the other hand, transport proteins back, usually to prevent mislocalization.

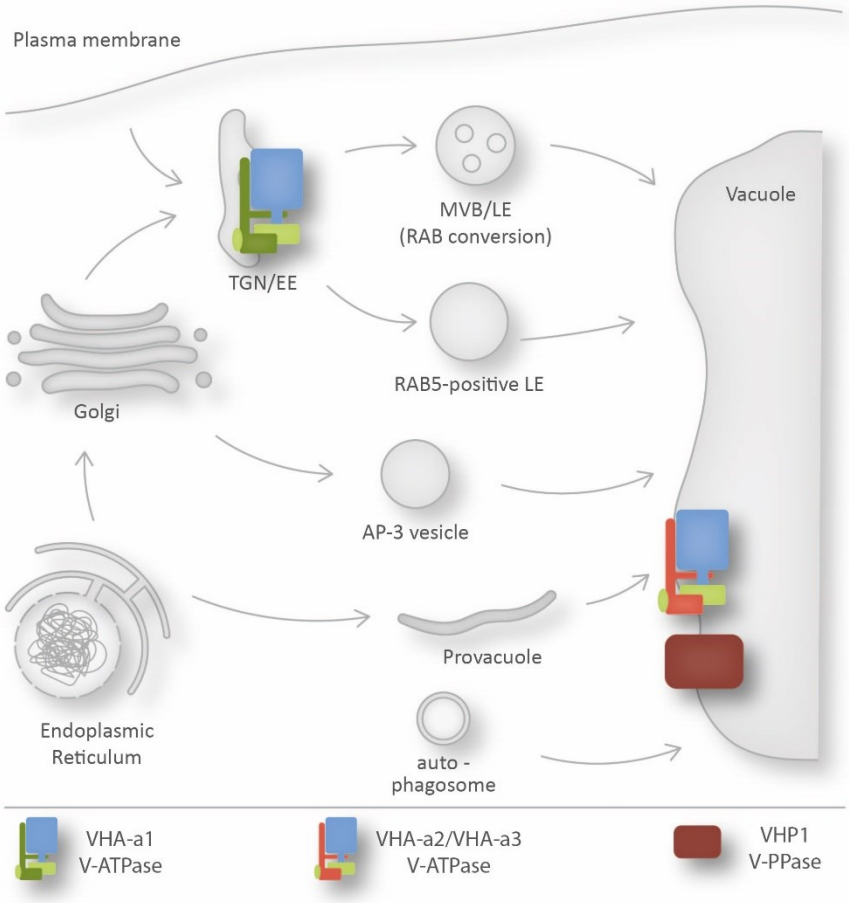


**Figure 1: Schematic representation of trafficking pathways towards the vacuole in Arabidopsis.** Several trafficking pathways lead from the Endoplasmic Reticulum (ER) to the vacuole. The VHA-a1 containing V-ATPase localizes to the trans-Golgi network/early endosome (TGN/EE), whereas the isoforms VHA-a2 and VHA-a4 are located at the tonoplast in Arabidopsis. Modified after Schumacher and Krebs, 2010.

### 1.2.1 ER export to the Golgi is mediated by COPII vesicles

The first step of the secretory pathway is protein export from the ER to the Golgi via coated vesicles. The vesicles are called coat protein complex II or abbreviated COPII and consist of five cytosolic components in yeast: Sar1p, Sec23p, Sec 24p, Sec13p and Sec 31p. Twenty-one paralogs of COPII subunits have been identified in Arabidopsis, making it the organism with the largest number of isoforms (Marti et al., 2010).

COPII vesicle formation is best studied in yeast but appears to be highly conserved throughout all eukaryotic cells. The GTPase Sar1p is activated by its GEF (guanine nucleotide exchange factor) Sec12p, which is a membrane-bound protein at the ER. Sar1p-GTP initiates the formation of the COPII coat by recruiting Sec23p and Sec24p. The complex of Sar1p and the heterodimer Sec23-24p recruits cargo to the forming COPII vesicle and discriminates between cargo and ER-resident proteins, acting like a cargo receptor. The COPII coat is completed by Sec13-31p heterodimers (Miller et al., 2003).

ER-to-Golgi transport can be blocked in eukaryotic cells by introducing Sar1 in its GTP-locked form. A point mutation of a specific histidine in the GTP catalyzing domain of Sar1 renders the GTPase inoperative and GTP cannot be hydrolyzed (Shima et al., 1998). The GTP locked Sar1 (Sar1-GTP) cannot be inactivated by its GAP (GTPase-activating protein). Thus, the COPII coat cannot disassemble, and the vesicle membrane is not exposed and can therefore not fuse with the Golgi membrane. This eventually leads to an accumulation of coated COPII vesicles at the interface of the Golgi and causes a breakdown of protein export from the ER to the Golgi. The retrograde transport form Golgi back to the ER continues and as no new material from COPII vesicles can be integrated into the Golgi, Golgi morphology and function become severely impaired (Shima et al., 1998). In Arabidopsis, five paralogs of Sar1p were identified: Sar1a to Sar1e (Chung et al., 2016).

Previously, inducible gene expression of the tobacco GTP locked Sar1 (Sar1-GTP) was used in *Nicotiana tabacum* and Arabidopsis to investigate the inhibition of ER-

to-Golgi transport. After 24 h of induction, complete Golgi disassembly and redistribution of Golgi markers into the ER was observed (Osterrieder et al., 2010).

The GTP-locked mutant form of Sar1b is achieved by mutating the histidine at position 74 to leucine (H74L). After Dex-induced expression of Sar1b-GTP the exit from the ER is blocked for proteins entering the secretory pathway (Takeuchi et al., 2000).

The Golgi consists of several cisternae, in which the proteins are transported from the cis to the trans side of the Golgi. If the ER is like a biosynthetic factory producing lipids and proteins, the Golgi can be seen as the post office. In the different Golgi cisternae, different enzymes are located to post-translationally modify the proteins. Thereby, the proteins get their travel tickets for their correct locations.

### 1.2.2 The TGN/EE is the sorting hub inside the plant cell

The next location in the classical secretory pathway of a plant cell is the TGN/EE (*trans*-Golgi network / early endosome). The TGN/EE forms from the trans-Golgi stack through cisternal maturation and appears a cluster of tubules and vesicles (Kang et al., 2011). Even though the TGN/EE is transiently associated with the Golgi, the TGN/EE represents an independent compartment. During endocytosis, plasma membrane proteins are internalized via clathrin-coated vesicles and reach the TGN/EE as the first intercellular compartment (Dettmer et al., 2006; Geldner et al., 2007). The TGN/EE is the main sorting station for secretory and endocytic trafficking (Reyes et al., 2011; Viotti et al., 2010). By using super-resolution microscopy, the highly mobile and dynamic features of the plant TGN/EE were described, which underlies constant fission and fusion processes (Uemura et al., 2014, 2019; Viotti et al., 2010).

Protein trafficking at the TGN/EE can be blocked with chemical inhibitors. The V-ATPase inhibitor Concanamycin A (ConcA) leads to the formation of Golgi-TGN/EE hybrids and an inhibition of protein trafficking at the TGN/EE (Scheuring et al., 2011; Viotti et al., 2010) pH homeostasis at the TGN/EE is a crucial determinant for trafficking (Luo et al., 2015).

In yeast and animal cells, Brefeldin A (BFA) inhibits ER-to-Golgi transport (Kreis et al., 1995). In Arabidopsis, Brefeldin A (BFA) does not lead to the redistribution of Golgi proteins to the ER, therefore BFA does not block ER-to-Golgi transport unlike in animal cells (Richter et al., 2007). The application of BFA causes the aggregation of TGN/EEs, also called BFA bodies, and the clustering of Golgi stacks in the periphery of the formed BFA bodies in Col-0 (Richter et al., 2007). The difference in the mode of action arises from the Golgi-localized BFA-insensitive guanine-nucleotide exchange factor (GEF) of the ADP-ribosylation factor (ARF) family (ARF-GEF) GNOM-LIKE1 (GNL1) in Arabidopsis. A mutation in GNL1 renders it BFA-sensitive (GNL1-BFA$^S$) leading to the accumulation of Golgi proteins in the ER and the inhibition of ER-to-Golgi transport after BFA application. This experimental set-up to block COPII-mediated ER-to-Golgi transport requires the operation in the *gnl1* mutant (*gnl1*;GNL1-BFA$^S$).

The RAS superfamily of regulatory GTPases (RAB GTPases) and soluble N-ethylmaleimidine sensitive factor attachment receptor (SNARE) proteins act as determinants for transport specificity at the TGN/EE (Uemura and Ueda, 2014). With the help of GTPase mutants impaired in the binding to guanosine triphosphate (GTP) or guanosine diphosphate (GDP) it is possible to differentiate between distinct trafficking pathway from the TGN/EE to the vacuole (Ebine et al., 2011, 2014; Ito et al., 2018; Uemura and Ueda, 2014).

### 1.2.3 MVBs form ILVs to transport proteins for degradation to the vacuole

ARA7-positive subdomains fission from the TGN/EE and mature over time to multivesicular bodies (MVB) or also called late endosomes (LE). This process requires the exchange of the RAB5 GTPase ARA7 by the RAB7 GTPase RABG3f on the membrane surface of MVBs by the MON1-CCZ1 (MONENSIN SENSITIVITY1/CALCIUM CAFFEINE ZINC SENSITIVITY1) complex. MON1 is also called SAND1. This step is required prior to MVB-to-vacuole fusion (Cui et al., 2014, 2016; Singh et al., 2014).

At the same time plasma membrane receptors are sorted into intraluminal vesicles (ILVs) inside the MVB. As the limiting membrane of an MVB fuses with the tonoplast, the ILVs are released into the vacuolar lumen, in which acidic hydrolases

degrade the ILVs and their content. Receptors at the plasma membrane cannot be degraded in the vacuolar lumen, if the RAB GTPase exchange, also called RAB conversion, is non-functional. Not only plasma membrane proteins but also vacuolar membrane proteins can be transported from the ER, the place of their protein synthesis and membrane insertion, to the tonoplast via MVBs, such as INOSITOL TRANSPORTER 1 (INT1) (Wolfenstetter et al., 2012). The difference is that vacuolar membrane proteins are not sorted into ILVs but stay at the limiting membrane of the MVB to end up in the vacuolar membrane after MVB -to- vacuole fusion.

### 1.2.4 RAB conversion independent pathways to the vacuole

The RAB conversion dependent pathway is not the only transport pathway, which transports vacuolar membrane proteins to their destination. There are also RAB7-independent trafficking pathways to the vacuole (Ebine et al., 2014).

The vacuolar Q-SNARE SYNTAXIN OF PLANTS 22 (SYP22) relies on the action of ARA7, a RAB5 GTPase, but does not require RABG3f, a RAB7 GTPase, for proper trafficking to the vacuole (Ebine et al., 2014). This trafficking pathway from the TGN to the vacuole, in which RAB GTPase exchange by CCZ1/Mon1 or SAND1 is not required, was therefore termed RAB conversion independent (Ebine et al., 2014). The transport vesicles mediating this transport route directly from the TGN/EE to the vacuole were referred to as MVEs (multivesicular endosomes) or RAB5-positive LEs. However, it remains unknown, whether RAB5-positive LEs have the same structure and morphology as the well-studied MVBs (Ebine et al., 2014).

The adaptor protein complex 3 (AP-3) is involved in the sorting of VACUOLAR SUCROSE TRANSPORTER 4 (SUC4) and vacuolar R-SNAREs, such as Vesicle ASSOCIATED MEMBRANE PROTEIN 711 and 713 (VAMP711, VAMP713), from the Golgi to the vacuole (Ebine et al., 2014; Feng et al., 2017a; Wolfenstetter et al., 2012).

Autophagosomes deliver cytoplasmic proteins and organelles for degradation to the vacuole and consist of a double membrane. The outer membrane of autophagosomes fuses with the vacuolar membrane to release the content of

autophagosomes into the vacuolar lumen for subsequent degradation. It appears that autophagosomes do not transport newly synthesized proteins to the vacuole (Michaeli et al., 2016).

## 1.3 HOPS and CORVET - gatekeepers in membrane fusion

### 1.3.1 HOPS and CORVET mediate endo-lysosomal membrane fusion events in yeast and metazoans

Yeast mutants defective in protein sorting to the vacuole and vacuole biogenesis, also called *vacuolar protein sorting* (*vps*) mutants, were investigated with light and electron microscopy and subsequently grouped in distinct classes. Class A *vps* mutants contain one to three large vacuoles and are therefore morphologically not distinguishable from wild-type yeast cells. Mutants grouped in class B show multiple (20 – 40) fragmented vacuoles. Class C mutants exhibit the most severe phenotypes, as cells lack vacuoles and instead accumulate vesicles and multi-membranous structures. However, heterozygous zygotes can form proper vacuoles, indicating that the accumulated structures are intermediate components for the formation of vacuoles. The class C proteins include the four core proteins forming the Homotypic Protein Sorting (HOPS) and Class C Core Vacuole/Endosome Tethering (CORVET) membrane tethering complexes: Vps11p, Vps16p, Vps18p, and Vps33p (Banta et al., 1988).

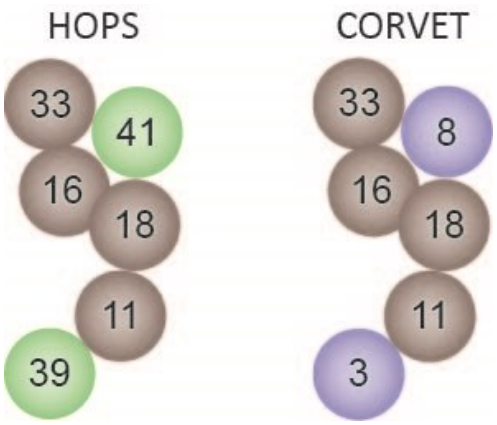


**Figure 2: Schematic representation of the HOPS and CORVET membrane tethering complexes.** The class C core proteins Vps11p, Vps16p, Vps18, and Vps33 are depicted in brown. The two accessory subunits of the HOPS complex Vps41p and Vps39p are shown in green. The CORVET-specific subunits Vps8p and Vps3p are shown in purple. Changed after (Balderhaar and Ungermann, 2013) and modified after Krüger, 2017.

In yeast, the HOPS complex functions in the fusion of MVBs/LEs and AP-3 vesicles with the vacuole and in vacuole-to-vacuole fusions, also called homotypic vacuole fusions. The CORVET complex mediates fusion events between EEs and LEs and

therefore acts upstream of HOPS in the MVB/LE-mediated trafficking pathway (Balderhaar and Ungermann, 2013). The specificity of the two complexes is derived from two specific subunits binding Rab GTPases. The two subunits Vps39p and Vps41p are specific for HOPS, bind to Rab7 and were described to belong to the Class B *vps* mutants with multiple fragmented vacuoles (Balderhaar and Ungermann, 2013; Raymond et al., 1992). The CORVET complex additionally consists of Vps8p and Vps3p, which bind to Rab5 (Figure 2). Vps8p belongs to the class A Vps proteins as the mutant has an unaltered vacuole morphology, whereas the lack of Vps3p causes a single, enlarged vacuole (Balderhaar and Ungermann, 2013; Raymond et al., 1992).

The homotypic fusion between vacuoles is a well-studied process. In yeast, the signaling lipid phosphatidylinositol 3-phosphate (PI3P) is enriched at fusion sites between vacuoles. The Rab7 GTPase is recruited to the vacuolar membrane by PI3P. The HOPS-specific subunits Vps39p and Vps41p bind to Rab7 and Rab7 as an effector for the HOPS complex. During membrane fusion, HOPS proofreads the correct assembly of the SNARE proteins (one R-SNARE and three Q-SNAREs) and thereby orchestrates homotypic vacuole fusion (Balderhaar and Ungermann, 2013; Wickner, 2010).

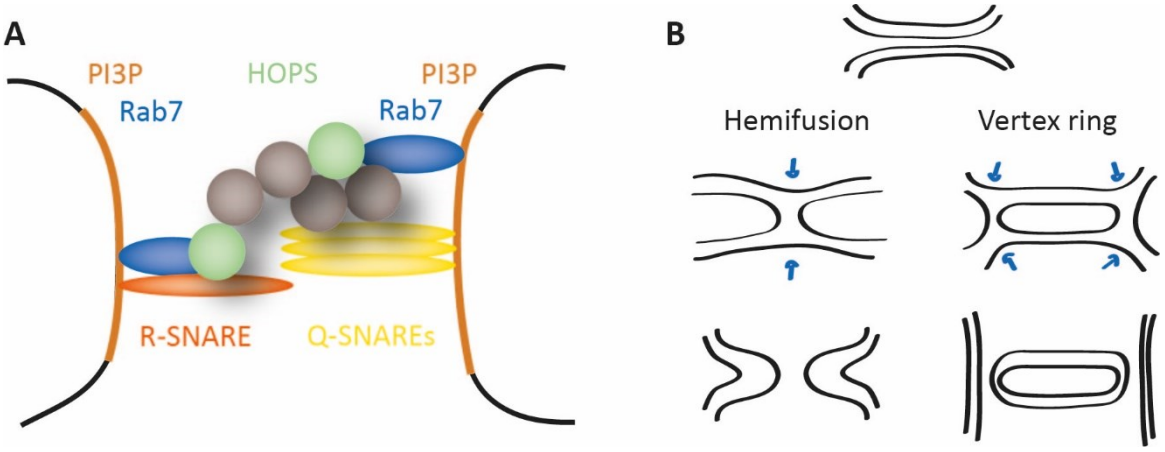


**Figure 3: Schematic representation of homotypic vacuole fusion in yeast.** (A) Molecular players at fusion sites between vacuoles. (B) Models of homotypic vacuole fusion in yeast. (A) and (B) changed after (Balderhaar and Ungermann, 2013) and (A) modified after Krüger, 2017.

To achieve membrane mixing during homotypic vacuole fusion different models were proposed. In recent years, evidence points to the formation of vertex rings as the mode for membrane fusion between vacuoles. Around the contact site of two

vacuolar membranes a vertex ring forms, at which the HOPS complex and SNARE proteins accumulate and mediate membrane fusion. The completion of membrane fusion at the vertex rings leads to the formation of luminal vesicles (Wickner, 2010).

Subunits of the HOPS complex interact with microtubules and actin filaments in mammalian cells indicating that the activity of the HOPS complex might be coordinated with cytoskeletal functions in animal cells (van der Beek et al., 2019; Kim et al., 2004; Richardson et al., 2004).

### 1.3.2 HOPS/CORVET knockout mutants are embryo lethal in Arabidopsis

Subunits of the HOPS and CORVET complex are evolutionary well conserved and also in Arabidopsis homologous genes were identified (Vukašinović and Žárský, 2016) (Table 2).

**Table 2: Summary of homologous subunits of the HOPS and CORVET membrane tethering complexes *in Arabidopsis thaliana*.** The table gives information about the gene name in *S. cerevisiae* and *A. thaliana* and the gene locus in *A. thaliana*. A similar table was previously presented in Askani, 2015.

| Standard name *Saccharomyces cerevisiae* | Trivial name *Arabidopsis thaliana* | Gene locus *Arabidopsis thaliana* |
|---|---|---|
| VPS16 | VPS16<br>VCL1 | At2g38020 |
| VPS11 | VPS11 | At2g05170 |
| VPS18 | VPS18 | At1g12470 |
| VPS33 | VPS33 | At3g54860 |
| VPS39 | VPS39<br>EMB2754 | At4g36630 |
| VPS41 | VPS41<br>VAM2 | At1g08190 |
| VPS3 | VPS3 | At1g22860 |
| VPS8 | VPS8<br>SETH5 | At4g00800 |

The knockout mutant of the Arabidopsis orthologue of yeast Vps16p, a shared subunit between HOPS and CORVET, is embryo lethal in the late torpedo stage and the embryo was described to lack discernable vacuoles. Therefore, the mutant was termed *vacuoleless1* (*vcl1*). Instead of vacuoles, the *vcl1/vps16* mutant embryo accumulates vesicles and autophagosomes. It was suggested that the lack of vacuoles leads to aberrant cell divisions and cell elongation in the embryo and

therefore ultimately, to incorrect morphogenesis of the embryo and embryo lethality (Rojo et al., 2001).

VPS16 forms a membrane associated complex with VPS11 and VPS33 (orthologues to yeast Vps11p and Vps33p) at the tonoplast in Arabidopsis, suggesting a similar role in vacuolar membrane fusion in Arabidopsis as in yeast. In addition, the vacuolar Q-SNARE SYP22 was found to co-immunoprecipitate with VPS16 (Rojo et al., 2003).

In an ethylmethane sulfonate (EMS) screen for mutants, which suppress the zigzag growth of *zigzag1* (*zig-1*), which is defective in the Qb-SNARE VTI11, a missense mutation in *VPS41* was found and termed *zig suppressor 2* (*zip2*). The *zip2* mutant has no apparent phenotype, but the T-DNA mutant of *VPS41* is lethal (Hao et al., 2016; Niihama et al., 2009). And also the T-DNA mutants of *VPS18*, *VPS3* and *VPS39* are embryo lethal (Takemoto et al., 2018).

The T-DNA knockout mutant *vps3-2* is embryo lethal and arrests in the late torpedo stage. Embryonic cells of *vps3-2* cells have abnormal vacuoles filled with electron-dense material, vesicles and organelles. The undigested content within the unusual vacuoles of the *vps3-2* embryo could result from a mistargeting of hydrolases, whose vacuolar trafficking may be disrupted (Delgadillo et al., 2020).

As knockout mutants of the HOPS and CORVET membrane tethering complexes are embryo lethal (Delgadillo et al., 2020; Rojo et al., 2001), it is difficult to study their function in Arabidopsis.

To affect both membrane tethering complexes, a dexamethasone (Dex) inducible knockdown against *VPS16*, a shared subunit between HOPS and CORVET, was created. In meristematic root cells, vacuoles of the induced knockdown against *VP16* are spherical and fragmented (Askani, 2015; Krüger, 2017). To be able to assign specific functions to each complex, knockdowns against VPS39 and VSP41, subunits specific for the HOPS complex, and against the CORVET-specific subunits VPS3 and VPS8, were introduced (Master Thesis Jana Christin Askani, 2015).

The knock downs were created as dexamethasone (Dex) inducible artificial microRNAs (amiRNAs). For this approach the WMD3 micro RNA design tool

(Schwab et al., 2006) was used to obtain adequate amiRNA sequences, which were derived from the endogenous miR319a precursor sequence (Master Thesis Jana Christin Askani, 2015). The chimeric LhG4-GR transcription factor is a fusion between a mutant lac repressor, a GAL4 transcription-activation-domain-II and a ligand-binding domain of the glucocorticoid receptor. Upon binding of Dex to the ligand-binding domain of the glucocorticoid receptor, the LhG4-GR transcription factor is released from the interaction with the HSP90 complex, translocates into the cell nucleus and activates the p6xOP promoter to express the introduced amiRNA (Craft et al., 2005).

## 1.4 How do vacuoles form and develop in Arabidopsis?

Antonie van Leeuwenhoek discovered plant vacuoles in 1676. As vacuoles appear as empty spaces filling the cell in light microscopy, van Leeuwenhoek named vacuoles after the Latin word for empty “vacuus” (Hoole and Leeuwenhoek, 1800).

In the 20th century, two opposing hypotheses on the origin of the vacuoles were published. The first hypothesis was based on EM images showing ER stretches to be connected with the vacuole. These ER stretches were termed provacuoles. In addition, vacuole development was described to take place through homotypic vacuole fusion to push the cytosol to the cell wall instead of enclosing the cytosol to digest it (Matile & Moor, 1968; Mesquita, 1969). The second hypothesis described the TGN to be the main membrane source for vacuole biogenesis (Marty, 1978, 1999).

With advanced methods in Molecular and Cellular Biology in the last decade, new insights into the formation and development of the vacuole were obtained. Lately, two conflicting models of vacuole biogenesis were published. The two models differ in the source compartment, from which the vacuole mainly develops, and in the vacuole morphology in meristematic root cells. On the one hand, MVBs form small vacuoles (SVs), which form larger vacuoles by homotypic fusion. Thus, vacuoles in meristematic root cells consist of separated compartments (Cui et al., 2018). On the other hand, the vacuole was found to originate from the ER and Golgi-independent trafficking via provacuoles. Here, vacuoles in meristematic root cells consist of constricted, yet connected tubules (Viotti et al., 2013).

### 1.4.1 Vacuole morphology in meristematic root cells

An EM-based whole cell tomography study found that most vacuoles in the root meristem are separated (Cui et al., 2018). By examining vacuoles of the *free1* mutant (also called *fyve1-1* mutant, see Kolb et al., 2015) with the EM-based tomography method, vacuoles were described to be smaller, but still separated (Cui et al., 2018). This finding is in contradiction to the results of 3D reconstructions with BCECF. Even though the *fyve1-1* vacuole stained with BCECF shows multiple small subvolumes, the subvolumes are connected and form a complex structure (Kolb et al., 2015). Other studies using 3 D reconstruction with BCECF staining

found that the vacuole remains an interconnected compartment, when auxin (Scheuring et al., 2016) or a genetic mutation (*alix* mutant see Kalinowska et al., 2015) causes severe changes in overall vacuole morphology.

Serial block-face SEM (scanning electron microscopy) was used to generate 3D models in nanometer resolution of the vacuoles in meristematic root cells to compare the morphology of Col-0 vacuoles and auxin-treated vacuoles. The vacuole in a meristematic root cell displayed a single connected compartment, even though the auxin-induced vacuolar constrictions severely altered vacuole morphology (Scheuring et al., 2016).

An argument raised by Cui et al., 2018 was that the fluorescent dye BCECF used to stain the vacuolar lumen could alter vacuole morphology. By comparing 3D reconstructions of vacuoles from roots expressing the vacuole marker spRFP-AFVY (Hunter et al., 2007) stained with and without BCECF, it could be shown that BCECF does not affect vacuole morphology and that vacuoles close to the QC consist of tubules (Minina et al., 2021).

Cui et al., 2018 performed photoconversion on the luminal vacuolar marker aleurain (Aleu) attached to the fluorophore Kaede (green-to-red photoconvertible fluorescent protein; Ando et al., 2002) to track the diffusion of the photoconverted red fluorescence inside the vacuoles. In vacuoles of the elongation zone the red fluorescence from photoconverted Kaede took up 60 sec to spread across all vacuolar subvolumes. And in 80 % of the vacuoles in the meristematic zone the red fluorescence was restricted to the subvolume, which was photoconverted, indicating that 80 % of the vacuoles are separated (Cui et al., 2018).

Whereas fluorescence recovery after photobleaching (FRAP) on BCECF stained vacuoles was used to quantify the vacuolar connectivity in Scheuring et al., 2016. The fluorescence of BCECF recovered rapidly in Col-0 vacuoles with an average of around 1 sec, whereas the auxin treatment led to a slower recovery of the fluorescence. This suggests that vacuolar subvolumes are connected and that auxin treatment increases the constrictions of the connected tubular network (Scheuring et al., 2016).

This result is corroborated by FRAP measurements with spRFP-AVFY showing that the connectivity of the vacuole is similar in all stages of root development. This underscores that vacuole morphology is connected throughout the root (Minina et al., 2021).

Several publications come independently to the conclusion of a tubular, but connected vacuole by using 3 D reconstruction of vacuoles stained with BCECF or FRAP methods: Kalinowska et al., 2015; Kolb et al., 2015; Löfke et al., 2015; Scheuring et al., 2015. 3 D Renderings of Col-0 vacuoles derived from confocal techniques are supported by SBF-SEM, in which vacuolar structures are connected. And FRAP assay with spL-RFP and BCECF showed that vacuoles in the root meristem are interconnected. Therefore, the vacuole is a single compartment with a network-like structure and a highly dynamic morphology (Viotti et al., 2013). Moreover, techniques based on CLSM methods are sufficient to examine vacuole morphology in vivo.

### 1.4.2 Source for vacuole biogenesis

The EM-based whole cell tomography was performed in meristematic cells of the root cortex (Cui et al., 2018), which is remarkable as other research groups performed their investigations about vacuolar trafficking and vacuole biogenesis in epidermal cells (Kalinowska et al., 2015; Kolb et al., 2015; Scheuring et al., 2016; Viotti et al., 2013; Zheng et al., 2014a). The analysis showed that small vacuoles (SVs) constitute the majority of vacuoles in meristematic cells. As early stages of SVs contain ILVs, it was concluded that MVBs are the source for the formation of SVs. To form large vacuoles, the homotypic fusion between matured SVs was proposed. This assumption was supported by the finding that the number of SVs was increased in the vacuolar Qb-SNARE mutant *vesicle transport v-SNARE 11* (*vti11*) mutant suggesting that the fusion of SVs was inhibited.

The two tonoplast-localized proton pumps, the V-ATPase and the V-PPase, are the most abundant proteins at the tonoplast (Carter et al., 2004). Therefore, their intracellular trafficking was investigated (Viotti et al., 2013). Several approaches showed that the trafficking of VHA-a3, the tonoplast-localized VHA-a isoform, and VHP1 is independent of the Golgi. The inhibitor ConcA did not lead to an accumulation of VHA-a3 in TGN/EE aggregates. In the *pat2-1* mutant impaired in the formation of AP-3 coated transport vesicles VHA-a3 was detected exclusively at the tonoplast. This indicates that the trafficking of VHA-a3 does not require the TGN/EE or the AP-3 pathway (Viotti et al., 2013).

By using the BFA-sensitive mutant of GNL1 (*gnl1*;GNL1-BFA$^{S}$) to block ER-to-Golgi transport, VHA-a1 was retained in the ER, but the vacuolar trafficking of VHA-a3 was not affected. In addition, the trafficking of sterol-enriched membranes to the tonoplast was not affected when ER-to-Golgi transport was blocked. Thus, an alternative trafficking route from the ER to the vacuole, which is independent of COPII vesicles, the Golgi and post-Golgi trafficking, was proposed (Viotti et al., 2013).

Both tonoplast-localized proton pumps were found in circular double-membrane structures enclosing cytosol in immunogold-labeled EM (electron microscopy) images. These structures were called provacuoles and their formation does not

require the function of the Golgi or post-Golgi trafficking. Also, rare cases were observed, in which provacuoles were connected with ER. In EM images provacuoles show a similar structure to autophagosomes, but provacuole formation and vacuole morphology was not affected in autophagy mutants. Taken together, vacuole biogenesis and trafficking of tonoplast proteins and lipids is facilitated directly from the ER independent of the Golgi and post-Golgi trafficking. Based on 2D EM images, a model was proposed on how provacuoles develop from double-membrane sheets via cup-shaped structures to spherical or tubular structures (Viotti et al., 2013).

In contrast, the EM-based whole cell tomography identified tubular vacuoles labeled with VHP1 and structurally reminiscent of provacuoles. As only ca. 4 % of vacuolar structures were provacuoles, the contribution of provacuoles to vacuole biogenesis was qualified as minor. The formation and morphology of tubular vacuoles or provacuoles was not affected in the *free1, mon1* and *vti11* mutants confirming that the formation is independent of post-Golgi trafficking (Cui et al., 2018).

In vivo imaging of provacuoles would allow for 3D reconstructions determining the morphology and structure of provacuoles in detail. By determining the surface and volume of provacuoles, calculations could be made to determine how much vacuolar membrane is contributed to the increasing vacuolar surface during cell expansion by provacuoles. Several approaches to detect provacuoles *in vivo* with CLSM have been undertaken.

The assembly factor AtVMA12 biochemically interacts with the V-ATPase at the ER to ensure proper assembly of the holo-complex (Neubert et al., 2008). However, AtVMA12-RFP and VHA-a3-GFP display completely separate fluorescent signals and do not colocalize (Viotti et al., 2013). As the fluorescence of VHA-a3-GFP / VHA-a3-RFP can only be detected at the end point of its trafficking - the tonoplast, the intracellular trafficking of VHA-a3-GFP/RFP seems to be faster than the folding of the attached fluorophore (Viotti et al., 2013).

*VHA-AP2* (*V-ATPase Associated Protein 2*) is a homologue of the mammalian (Pro)renin receptor ATP6AP2 (or PRR), which was recently shown to be a V-

ATPase subunit in bovine brain cells (Wang et al., 2020). In Col-0, VHA-AP2-GFP localizes to the TGN/EE and the tonoplast. In the *vha-a2 vha-a3* double mutant lacking V-ATPase complexes at the tonoplast, VHA-AP2-GFP cannot be detected at the tonoplast, but at the TGN/EE and in the ER. This means that the subcellular localization of VHA-AP2-GFP depends on the presence of the V-ATPase.

This feature of VHA-AP2 was used to create a conditional system, in which VHA-a3-mCherry is expressed under the control of the Dex-inducible promotor in the *vha-a2 vha-a3* double mutant. The created genetic background was termed piggyback or PRV-tool01. By expressing VHA-a3-mCherry new V-ATPase complexes destined for the tonoplast are synthesized at the ER. In these newly synthesized VHA-a3-mCherry containing V-ATPase complexes already fluorescent VHA-AP2-GFP is integrated and transported to the vacuole. By following the fluorescent signal of VHA-AP2-GFP from the ER to the vacuole, intermediate structures likely resembling provacuoles were identified. Super-resolution microscopy was applied to obtain 3D images for the computation of surface and volume renderings. Taking the overall vacuolar volume of an elongating root cell into account, the independent provacuolar structures provide up to 60 % of the vacuolar membrane (Dissertation Falco Krüger, 2017).

First evidence that the vacuolar trafficking of VHA-a3 is not entirely facilitated in a Golgi and post-Golgi independent manner was raised by a publication showing that the trafficking of VHA-a3 relies on the action of RAB5-GTPase ARA7 at the TGN/EE (Feng et al., 2017b).

The generation of a CRISPR/Cas9 null mutant of *VHA-a1* exhibited that VHA-a1 is required during the development of the male gametophyte, but vegetative growth is not affected by the loss of *VHA-a1*. As the action of the V-ATPase at the TGN/EE is crucial and the knockdown of *VHA-a1* causes defects in cell expansion (Brüx et al., 2008; Luo et al., 2015), the VHA-a2 and VHA-a3 isoforms might compensate for VHA-a1. This assumption was proven by the reduction of *VHA-a2* and *VHA-a3* alleles in the *vha-a1* knockout mutant, which lead to a dwarf phenotype in heterozygous plants. Plants containing no *VHA-a2* and *VHA-a3* allele in the *vha-a1* mutant cannot be generated, suggesting that VHA-a2 and VHA-a3 substitute

VHA-a1 and that a mutant without VHA-a isoforms is not viable (Lupanga et al., 2020).

Notably, the genome of the liverwort *Marchantia polymorpha* encodes for only one VHA-a subunit (MpVHA-a), which localizes to the TGN/EE and the tonoplast in Arabidopsis. MpVHA-a cannot replace the function of VHA-a1 in the CRISPR *vha-a1* mutant but compensates for the loss of VHA-a2 and VHA-a3 at the tonoplast in the *vha-a2 vha-a3* double mutant. This finding supports the model of an ancestral state, in which the V-ATPase localizes to the tonoplast and acidifies the TGN/EE on the transit to the vacuole (Lupanga et al., 2020).

Thus, the hypothesis was proposed that VHA-a isoforms compete for the entry into COPII-vesicles in Arabidopsis root cells. VHA-a1 is assumed to have a higher preference for the recognition by the COPII receptor due to the targeting domain (VHA-a1-TD).

The point mutation R729N in VHA-a3 is predicted to render the V-ATPase non-functional in pumping protons across the vacuolar membrane (Dissertation Christoph Neubert 2012). VHA-a3-R729N-GFP localizes to the ER in Col-0 and the tonoplast in the *vha-a2 vha-a3* double mutant indicating that non-functional V-ATPase complexes do not leave the ER due to an unknown ER-based quality control, when enough functional V-ATPase complexes are present (Dissertation Christoph Neubert 2012).

# 2 Aims and objectives of this study

This study aimed to investigate the vacuolar trafficking of the tonoplast-localized V-ATPase and V-PPase. To manipulate COPII-mediated ER export, the effect of the dominant-negative Sar1b (Sar1b-GTP) was examined. To learn more about the structure and morphology of provacuoles, which mediate the Golgi-independent trafficking of proton pumps to the vacuole, it was necessary to extend the in vivo imaging of provacuoles. For this purpose, a genetic piggyback system (Krüger, 2017) and the conditional expression of VHA-a3 was used.

Knockout mutants of subunits of the HOPS and CORVET membrane tethering complex (*vcl1*/*vps16*, *vps41* and *vps3*) are not viable in Arabidopsis (Delgadillo et al., 2020; Hao et al., 2016; Rojo et al., 2001). Inducible knockdowns against subunits of the HOPS and CORVET complex were used to examine the role of HOPS and CORVET in vacuolar trafficking and mediating transport pathways to the vacuole. Of special interest was the question whether the HOPS or CORVET complex plays a role in vacuolar trafficking of the tonoplast-localized V-ATPase and V-PPase.

To examine the function of the HOPS and CORVET complex in vacuole development, the vacuolar morphology in the induced knockdowns against subunits of the HOPS and CORVET complex was studied.

# 3 Results

## 3.1 Investigating the ER exit of tonoplast proteins by blocking COPII-mediated ER export in a conditional manner

### 3.1.1 Dominant-negative Sar1b disrupts COPII-mediated ER export in root cells of Arabidopsis

The BFA-sensitive form of GNL1 (GNL1-BFA$^S$) in the *gnl1* mutant leads to the block of COPII-mediated ER export to the Golgi after BFA application and was used to show that VHA-a3 is transported to the vacuole in a COPII-independent manner (Viotti et al., 2013). To disrupt COPII-mediated ER export in a conditional approach in Col-0 for further studies on the Golgi-independent trafficking of the tonoplast-localized proton pumps, the dominant-negative form of Sar1b (GTP-locked Sar1b or Sar1b-GTP) was introduced. Sar1b-GTP blocks the COPII-mediated ER export in yeast, mammalian organisms, tobacco and Arabidopsis suspension cells (daSilva, 2004; Osterrieder et al., 2010; Takeuchi et al., 2000).

Blocking ER export to the Golgi in a long-term manner leads to various secondary effects and is harmful for the cells (Osterrieder et al., 2010). By using an inducible expression system, secondary effects may be avoided and immediate effects on cellular trafficking should be observable. Therefore, Sar1b-GTP was cloned with an attached CFP (cyan fluorescent protein) or mVenus (monomeric yellow fluorescent protein) under the control of the dexamethasone (Dex) inducible expression system (DEX:Sar1b-GTP-CFP or DEX:Sar1b-GTP-mVenus) (Craft et al., 2005).

To confirm the disruption of ER-to-Golgi transport in Arabidopsis root cells, the Dex-inducible Sar1b-GTP-CFP was observed with the ER-resident V-ATPase assembly factor VMA21-GFP (Vacuolar Membrane ATPase 21; Neubert et al., 2008), the Golgi marker ST-GFP (last 58 aa of the rat sialyl transferase; Boevink et al., 1998) or the plasma membrane localized brassinosteroid receptor BRI1-GFP (Brassinosteroid Insensitive 1; Geldner et al., 2007).

After Dex treatment, Sar1b-GTP-CFP colocalized with VMA21-GFP at the ER and was additionally found in punctate structures independent of the ER-localized

VMA21-GFP (Supplementary Figure 1). This observation showed that Sar1b-GTP partially localizes to the ER in Arabidopsis root cells.

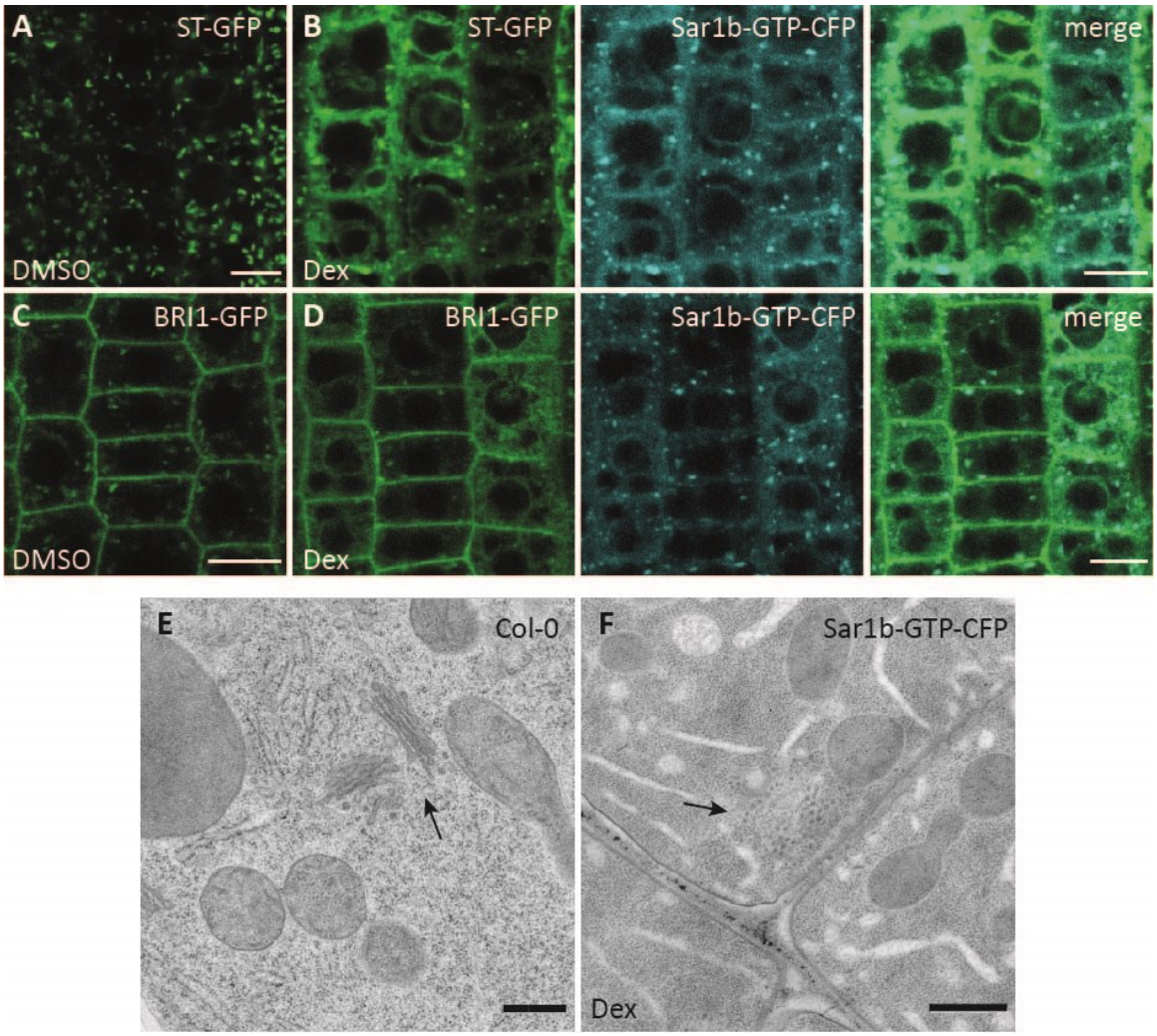


**Figure 4: Dexamethasone (Dex) induced expression of dominant-negative Sar1b (Sar1b-GTP) blocks COPII-mediated ER export in root cells of Arabidopsis**. (A) to (D) 6-days-old Arabidopsis seedlings were treated with DMSO or 60 µM Dex for 6 hr. Scale bars are equal to 10 µm. (A) ST-GFP localized to the Golgi in DMSO treated roots. (B) After Dex treatment, ST-GFP accumulated in the ER and colocalized with Sar1b-GTP-CFP at the ER and in punctae. (C) BRI1-GFP localized to the plasma membrane and endosomes in the DMSO control. (D) BRI1-GFP was retained in the ER and colocalized with Sar1b-GTP-CFP after Dex application. (E) and (F) EM images of high-pressure frozen and freeze-substituted Arabidopsis root tips of Col-0 and Dex-induced Sar1b-GTP-CFP. Scale bars are equal to 500 nm. EM images were obtained by Upendo Lupanga and Stefan Hillmer.

ST-GFP labeled the Golgi in the DMSO control (Figure 4 A), but colocalized with Sar1b-GTP-CFP at the ER and in punctate structures after Dex treatment (Figure 4 B). As expected, BRI1-GFP localized to the plasma membrane and endosomes in the DMSO control (Figure 4 C). After applying Dex, BRI1-GFP colocalized with

Sar1b-GTP-CFP at the ER and in punctae. Residual signal of BRI1-GFP at the plasma membrane remained after 6 hr of Dex induction (Figure 4 D).

The accumulation of ST-GFP and BRI1-GFP in the ER after Dex treatment indicates that both proteins are retained in the ER when COPII-mediated ER export is disrupted by the induced expression of Sar1b-GTP. The punctae labeled with Sar1b-GTP-CFP and ST-GFP or BRI1-GFP may be ER-independent, COPII vesicle remnants.

Next, electron microscopy (EM) was used to investigate the disruption of COPII-mediated ER export in meristematic root cells. After Dex treatment, Golgi stacks were disorganized and lacked the typical cisternae as seen in the Col-0 control (black arrows in Figure 4 E and F). Vesicles accumulated at Golgi remnants and ER tubules were swollen after the expression of Sar1b-GTP-CFP (Figure 4 F) indicating an accumulation of proteins in the ER and the collapse of the Golgi as COPII-mediated ER export is disrupted.

The ER-independent punctate structures of Sar1b-GTP-CFP observed in vivo (Supplementary Figure 1 B) could resemble the abnormal vesicular Golgi remnants in the EM images (Figure 4 F). Taken together, expressing the GTP-locked form of Sar1b blocks COPII-mediated ER export to the Golgi and leads to the retention of secretory cargo in the ER. This shows that Sar1b-GTP is a useful tool in epidermal root cells of Arabidopsis to disrupt COPII-mediated ER export similar to experimental setups in yeast, mammalian cells and tobacco (daSilva, 2004; Osterrieder et al., 2010; Takeuchi et al., 2000).

In Arabidopsis, the different Sar1 isoforms showed different affinities for different cargo meaning that COPII vesicles might have different cargo compositions (Chung et al., 2016). These differences in cargo specificity might lead to a selective retention of cargo in the ER by expressing only one GTP-locked Sar1 isoform. However, the Golgi morphology and the COPII-mediated ER export were corrupted by using the GTP-locked form of Sar1b. As a consequence, the cargo specificity of the Sar1b isoform for different COPII cargos is neglectable for the inhibition of the COPII trafficking pathway. Thus, inducible Sar1b-GTP was used to block COPII-mediated ER export in further experiments.

### 3.1.2 Disrupted COPII-mediated ER exit does not affect the ER exit of VHA-a3

Next, the effects of Sar1-GTP on the trafficking of the TGN/EE-localized V-ATPase containing VHA-a1 and of the tonoplast-localized V-ATPase containing VHA-a3 were tested. VHA-a1-GFP localized to the TGN/EE in the DMSO control (Figure 5 A) and accumulated in the ER after Dex-induced expression of Sar1b-GTP-CFP (Figure 5 B). In addition, the punctate structures of VHA-a1-GFP and Sar1b-GTP-CFP colocalized after Dex treatment (Figure 5 B) indicating that the trafficking of VHA-a1 is dependent on COPII vesicles.

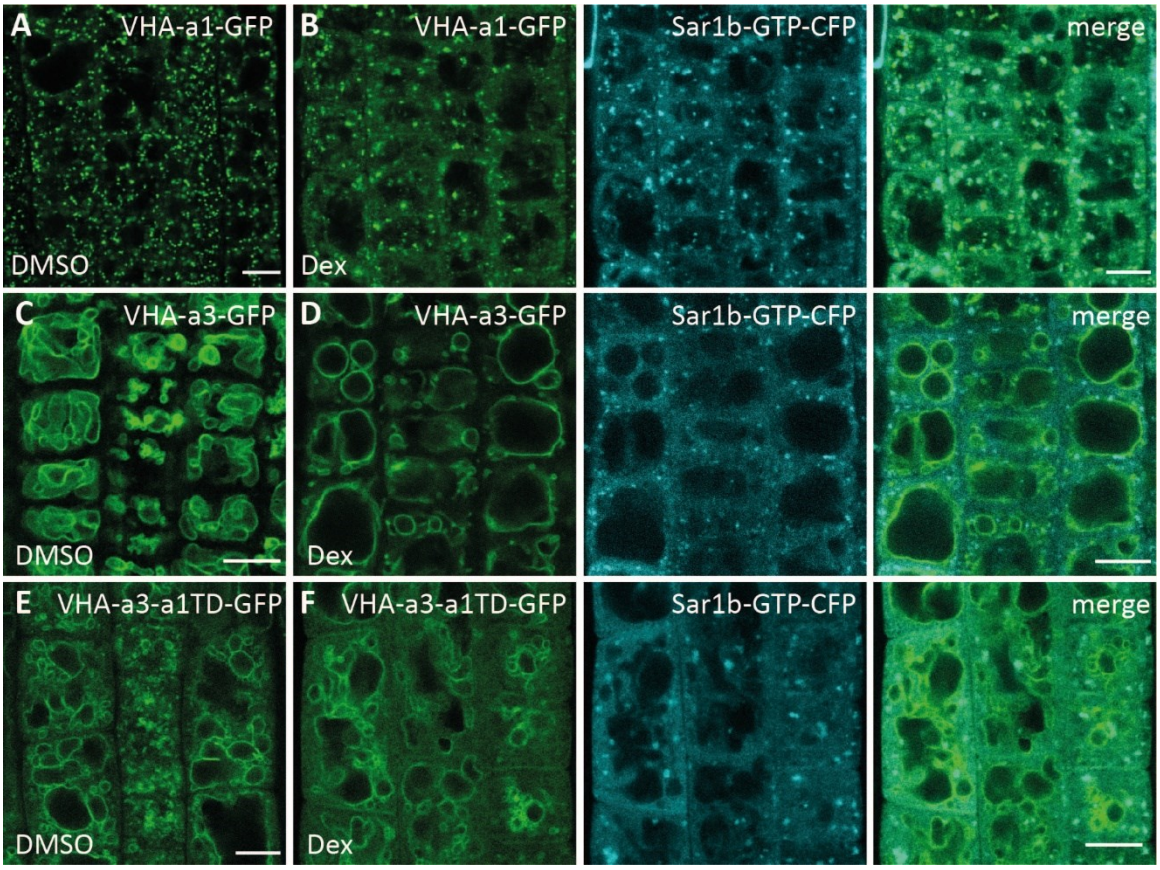


**Figure 5: After blocking COPII-mediated ER export, VHA-a1-GFP accumulates in the ER, whereas VHA-a3-GFP is not retained in the ER.** 6-days-old Arabidopsis seedlings were treated with DMSO or 60 µM Dex for 6hr. (A) VHA-a1-GFP localized to the TGN/EE after DMSO treatment. (B) Upon Dex induction, VHA-a1-GFP accumulated in the ER and colocalized with Sar1b-GTP-CFP at the ER and in punctae. (C) VHA-a3-GFP was located at the tonoplast in the DMSO control. (D) After Dex treatment, the tonoplast localization remained unaltered. (E) The chimeric protein of VHA-a3 with the VHA-a1 targeting domain (VHA-a3-a1-TD-GFP) localized to the TGN/EE and the tonoplast after DMSO application. (F) Upon Dex induction, VHA-a3-a1-TD-GFP accumulated in the ER. Scale bars are equal to 10 µm.

The tonoplast localization of VHA-a3-GFP did not change after Dex induction in comparison to the DMSO control (Figure 5 C and D) confirming that VHA-a3 is not retained in the ER after blocking COPII-mediated ER export. This holds further evidence that VHA-a3 is transported to the vacuole in a COPII- and Golgi-independent manner. However, the fact that VHA-a3-GFP does not remain in the ER could also be caused by a degradation process in the ER, an insufficient amount of newly synthesized protein, a relatively high turnover rate or a different timing of Dex induction in different Arabidopsis lines.

To exclude that VHA-a3-GFP is degraded in the ER after expressing Sar1b-GTP-CFP, the VHA-a1 targeting domain inserted into VHA-a3 (VHA-a3-a1-TD) (Lupanga et al., 2020) was used. VHA-a3-a1-TD-GFP localized to the TGN/EE and the tonoplast in the DMSO control showing a dual subcellular localization (Figure 5 E). After Dex treatment, VHA-a3-a1-TD-GFP accumulated in the ER and localized to the tonoplast. Punctae of VHA-a3-a1-TD-GFP, which colocalized with Sar1b-GTP-CFP, were not observed (Figure 5 F). The ER retention of the chimeric protein contradicts the suggestions that degradation or low protein biosynthesis cause the missing ER accumulation of VHA-a3-GFP, when COPII-mediated ER export is blocked. In addition, the missing colocalization of VHA-a3-a1-TD-GFP and Sar1b-GTP-CFP indicates that the information for the Sar1 isoform specificity is included somewhere else in VHA-a1. This further strengthens the assumption that the GTP-locked form of Sar1b leads to a general collapse of COPII-mediated ER export even though each Sar1 isoform recognizes specific cargo.

The non-pumping mutant form of VHA-a3 (VHA-a3R729N) localizes to the ER in Col-0 and is stabilized by inhibiting the proteasomal degradation with MG132 (Dissertation Christoph Neubert 2012). Therefore, it was tested if VHA-a3-GFP accumulates in the ER after Dex-induction of Sar1b-GTP, when proteasomal degradation is inhibited. Therefore, VHA-a3-GFP seedlings were treated with Dex to induce the expression of Sar1b-GTP-CFP and with MG132 to block proteasomal degradation. After Dex and MG132 treatment, VHA-a3-GFP did not accumulate in the ER (Supplementary Figure 2) indicating that VHA-a3-GFP is not degraded through the proteasome after blocking COPII-mediated ER export.

To exclude variations in Dex-induced expression of Sar1b-GTP-CFP, VHA-a3-RFP and Dex-inducible Sar1b-GTP-CFP was observed with either VHA-a1-GFP, ST-GFP or BRI1-GFP. This three-color imaging approach allowed us to simultaneously observe the effects of disrupted COPII-mediated ER export on VHA-a3-RFP and a reference protein, which depends on the COPII trafficking pathway.

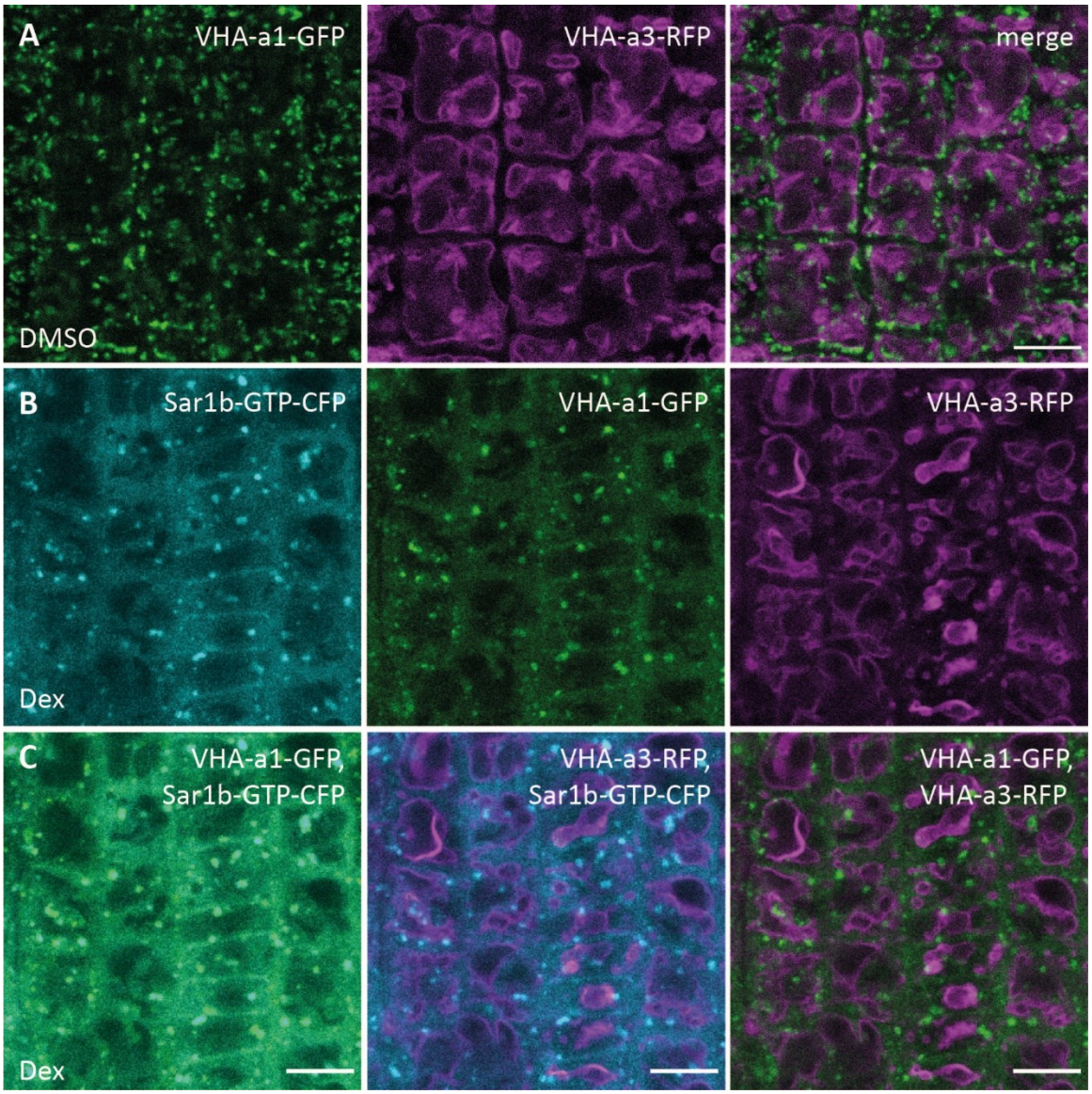


**Figure 6: Three-color imaging excludes temporal differences in Dex-induced expression of Sar1b-GTP regarding the localization of VHA-a3.** 6-days-old Arabidopsis seedlings were treated with DMSO or 60 µM Dex for 6 h. (A) In the DMSO control, VHA-a1-GFP localized to the TGN/EE and VHA-a3-RFP to the tonoplast. (B) After Dex treatment, VHA-a1-GFP was found in the ER and punctae, whereas VHA-a3-RFP was located at the tonoplast. (C) Different dual overlays of color channels depicted in (B) showed that blocking COPII-mediated ER export led to ER retention of VHA-a1-GFP, but not of VHA-a3-RFP. Scale bars are equal to 10 µm.

In the DMSO control, VHA-a1-GFP localized to the TGN/EE and VHA-a3-RFP to the tonoplast (Figure 6 A). After Dex treatment, VHA-a1-GFP accumulated in the ER and punctae, which colocalized with Sar1b-GTP-CFP (Figure 6 B and C). VHA-a3-RFP localized to the tonoplast, but neither accumulated in the ER nor colocalized with Sar1b-GTP-CFP or VHA-a1-GFP (Figure 6 B and C).

ST-GFP as well as BRI1-GFP accumulated in the ER after the induced expression of Sar1b-GTP-CFP, whereas VHA-a3-RFP was solely detected at the tonoplast in three-colour imaging (Supplementary Figure 3). Thus, simultaneous observation of VHA-a3-RFP with proteins depending on COPII-mediated trafficking ensured the disruption of the COPII trafficking and supported the finding of a COPII-independent ER export of VHA-a3. Taken together, blocking COPII-mediated ER export to the Golgi does not affect the ER exit of VHA-a3.

### 3.1.3 Investigating the trafficking of tonoplast-localized proteins with Sar1b-GTP

The vacuolar pyrophosphatase VHP1 is also transported to the vacuole in a Golgi-independent manner; so both tonoplast-localized proton pumps are transported via a Golgi-independent pathway (Viotti et al., 2013). Therefore, the effect of Dex-inducible Sar1b-GTP on VHP1-GFP was examined.

VHP1-GFP localized to the tonoplast in the DMSO control (Figure 7 A). After Dex induced expression of Sar1b-GTP-CFP, VHP1-GFP labeled the tonoplast, but could not be observed in the ER or in punctae (Figure 7 B) indicating that blocked ER-to-Golgi transport does not influence the localization of VHP1. This provides further evidence that VHA-a3 and VHP1 are transported to the vacuole independent of the Golgi.

Moreover, Dex-inducible Sar1b-GTP was used to investigate the effects of blocked COPII-mediated ER export on the localization of additional tonoplast proteins. It was attempted to determine proteins, other than the two proton pumps, that are localized at the tonoplast and whose localization is not altered when ER export to the Golgi is blocked.

The vacuolar glucose exporter named ERDL6 (Early Response to Dehydration-Like 6; Poschet et al., 2011) localized to the tonoplast in control conditions (Figure

7 C) and did not accumulate in the ER after Dex-induced expression of Sar1b-GTP-CFP (Figure 7 D). The lack of ER retention, when ER-to-Golgi transport is disrupted, marks ERDL6 and as putative candidate for being transported in a Golgi-independent manner.

By constitutively expressing AHA10 ($P_{3A}$-ATPase; Baxter et al., 2005) under the UBQ10 promotor, AHA10-mVenus localized to the tonoplast in root cells (Figure 7 E). After 6 hr of Dex induction, AHA10-mVenus was found at the tonoplast and additionally in the ER and in punctae, which colocalized with Sar1b-GTP-CFP (Figure 7 F). This result indicates that the transport of AHA10 to the vacuole is COPII-dependent.

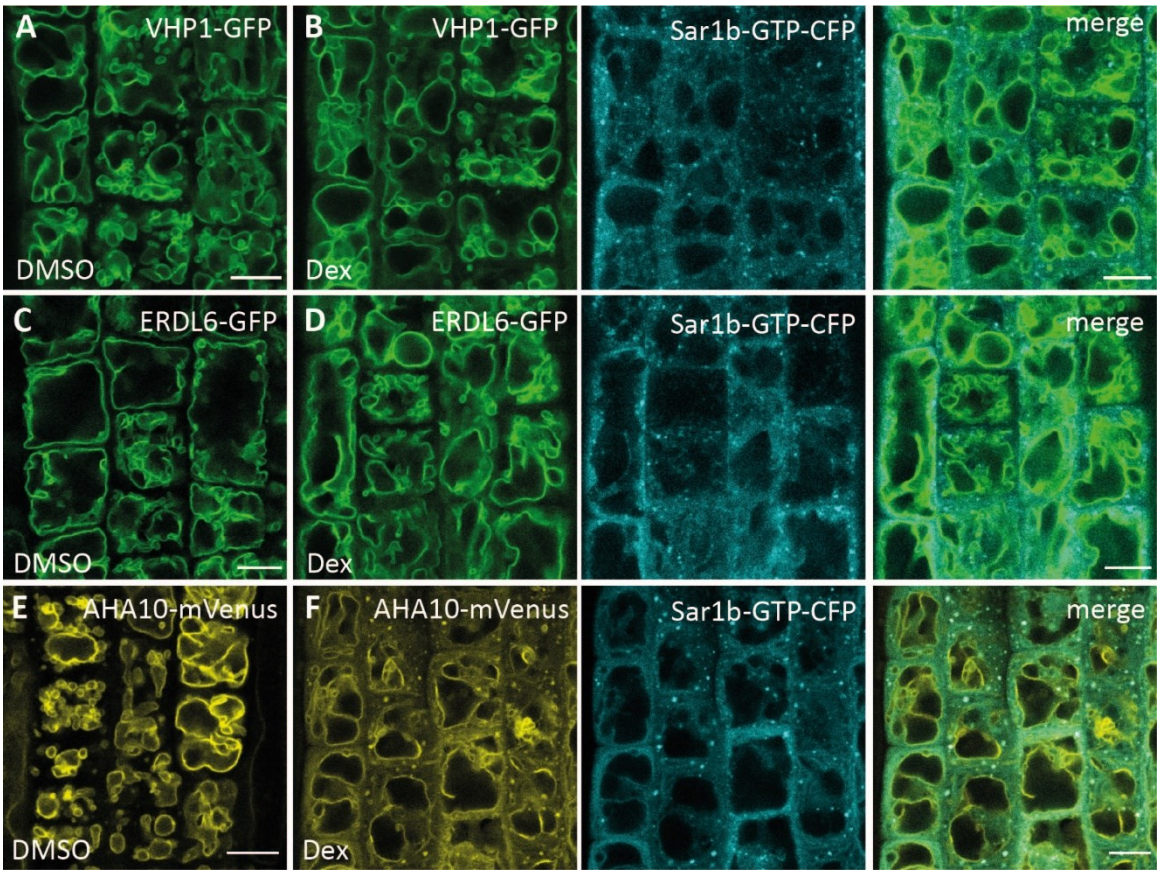


**Figure 7: Blocking COPII-mediated ER export to investigate the trafficking of tonoplast-localized proteins.** 6-days-old Arabidopsis seedlings were treated with DMSO or 60 µM Dex for 6 hr. VHP1-GFP (A), ERDL6-GFP (C), and AHA10-mVenus (E) localized to the tonoplast in DMSO treated roots. After Dex-induced expression of Sar1b-GTP-CFP or Sar1b-GTP-mVenus, no ER retention was observed for VHP1-GFP (B) and ERDL6-GFP (D). AHA10-mVenus colocalized with Sar1b-GTP-CFP at the ER and in punctae after Dex treatment (F). Images in (E) and (F) were taken by Upendo Lupanga. Scale bars are equal to 10 µm.

Next it was examined whether the localization of tonoplast proteins passing through the Golgi and post-Golgi compartments have a similar appearance to AHA10 in the presence of Dex-induced Sar1b-GTP.

The vacuolar Qb-SNARE VTI11 (Vesicle Transport V-SNARE11) was shown to mediate trafficking between the TGN/EE and the vacuole in Arabidopsis (Ebine et al., 2008; Uemura et al., 2004). In the DMSO control, pHGFP-VTI11 localized to the tonoplast (Figure 8 A). Besides the bright tonoplast labeling, a faint GFP signal in the ER was visible in the presence of Dex. The ER-localized pHGFP-VTI11 was best recognized in cell edges (Figure 8 B). The faint GFP signal was unlikely to be caused by a bleeding of mVenus as the brighter Sar1b-GTP-mVenus punctae were not observed in the detection range for GFP (Figure 8 B). Therefore, VTI11 is likely to be dependent on COPII-mediated ER export but is not specifically recognized by the Sar1b isoform. The low fluorescent signal in the ER might indicate that VTI11 accumulates in the ER to a lesser extent than AHA10 after ER-to-Golgi transport is blocked. The low ER retention might also be caused by increased degradation in the ER, low amount of protein biosynthesis or variations in Dex induction.

The R-SNARE VAMP711 (Vesicle Associated Membrane Protein 711) and the vacuolar sucrose transporter SUC4 (Sucrose Transporter 4) are both transported along the AP-3 pathway to the vacuole (Ebine et al., 2014; Wolfenstetter et al., 2012). In the DMSO control, mCherry-VAMP711 (Geldner et al., 2009) localized to the tonoplast. After 6 hr of Dex induction, tonoplast labeling remained unaltered (Figure 8 C and D).

SUC4-GFP (Wolfenstetter et al., 2012) localized to the tonoplast in the DMSO control and showed a slight ER-localized background in atrichoblast cells, likely caused by an overexpression artefact as the result of expression under the 35S promotor (Figure 8 E). The observed ER signal did not increase appreciably in the presence of Sar1b-GTP-CFP (Figure 8 F).

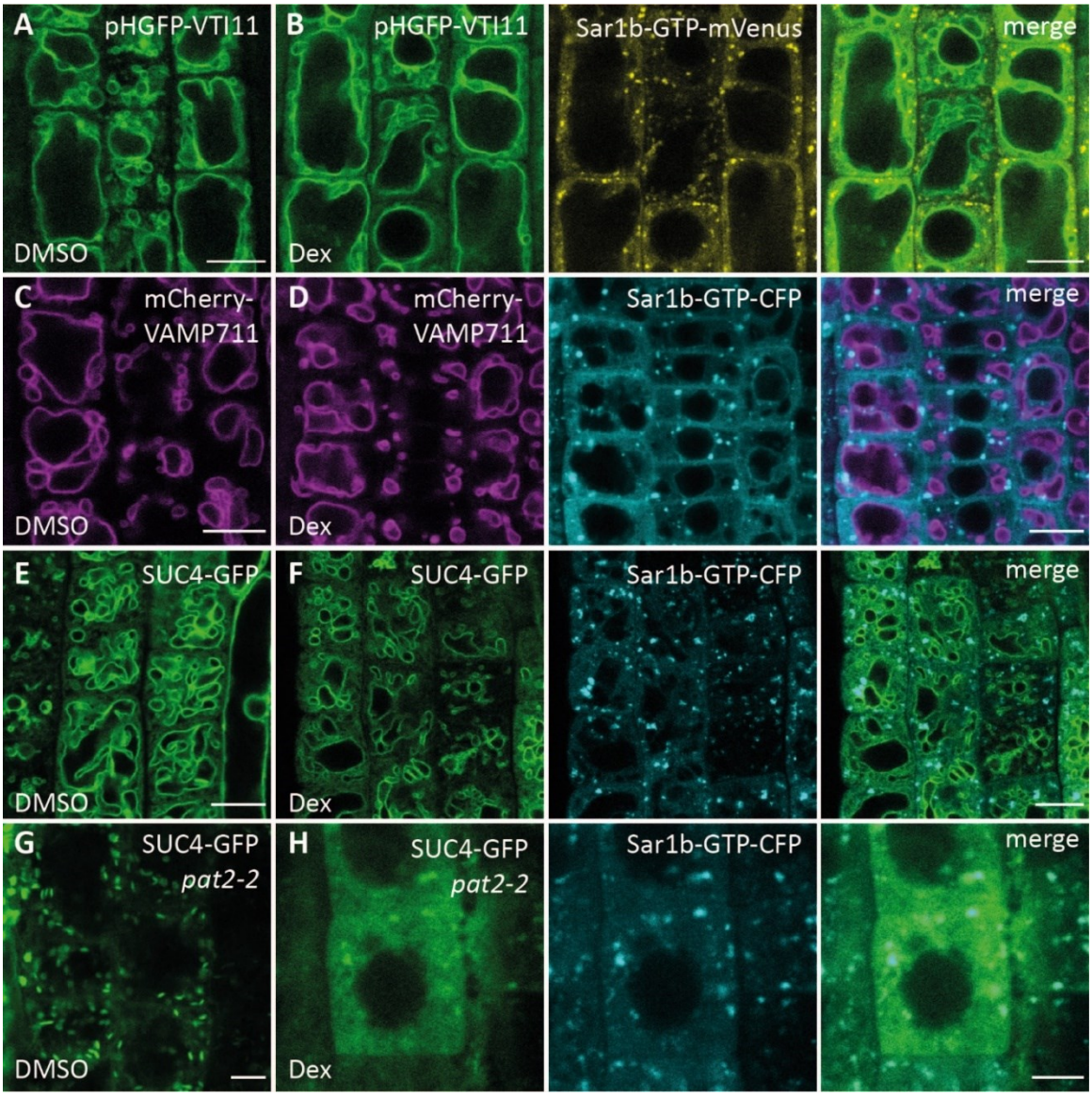


**Figure 8: VAMP711 and SUC4-GFP, both cargo of the AP-3 pathway, are not retained in the ER after Dex-induced expression of Sar1b-GTP.** Plants expressing tonoplast-localized proteins being transported through the Golgi or post-Golgi compartments were transformed with Sar1b-GTP-CFP/mVenus. 6-days-old seedlings were treated with DMSO or 60 µM Dex for 6 hr. (A) pHGFP-VTI11 localized to the tonoplast in the DMSO control. (B) After Dex treatment, a faint ER signal but no punctae were visible. (C and D) The tonoplast localized mCherry-VAMP711 did not accumulate in the ER after Dex-induced expression of Sar1b-GTP-CFP. (E) SUC4-GFP localized to the tonoplast and showed slight signal at the ER in the DMSO control. (F) After the application of Dex, the ER signal of SUC4-GFP did not increase. (G and H). In the *pat2-2* mutant, SUC4-GFP localized to the Golgi in the DMSO control and accumulated in the ER and in punctae, which overlapped with Sar1b-GTP-CFP. Scale bars are equal to 10 µm in (A) to (D) and 5 µM in (E) to (H).

The conditional expression of Sar1b-GTP-CFP did not lead to a retention of VAMP711 or SUC4 in the ER, which conflicts with the finding that R-SNAREs of the VAMP7 family and SUC4 are localized to the Golgi and cannot be transported to the tonoplast in mutants impaired in the AP-3 pathway (Feng et al., 2017a; Wolfenstetter et al., 2012).

To evaluate whether SUC4-GFP is degraded in the ER or whether the amount of newly synthesized protein is too low for the detection with CLSM, crosses were performed with the *pat2-2* mutant (*protein affected trafficking 2-2*; Feraru et al., 2010), which lacks the AP-3 β subunit.

In the DMSO control, SUC4-GFP localized to the Golgi in the *pat2-2* mutant (Figure 8 G). In the presence of Dex, SUC4-GFP accumulated in the ER and localized to punctae, which overlapped with Sar1b-GTP-CFP (Figure 8 H). This shows that the ER export of SUC4 depends on COPII vesicles in the *pat2-2* mutant. Notably, SUC4-GFP acts like a Golgi-resident protein in the *pat2-2* mutant, similar to ST-GFP. It might be that VAMP711 and SUC4 are sorted into a Golgi-independent trafficking pathway in Col-0 when COPII trafficking is disrupted. On the other hand, it cannot be excluded that a low biosynthesis rate or a degradation process causes the absent ER retention in Col-0 after COPII-mediated ER export is blocked. However, these possibilities were tested for VHA-a3 and the results supported the finding that VHA-a3 is able to exit the ER via a COPII-independent route.

## 3.2 In vivo imaging of provacuoles

### 3.2.1 Provacuoles likely appear as punctae and fine tubules in vivo.

To learn more about the Golgi-independent trafficking to the vacuole, the morphological structure of provacuoles is of special interest. To further investigate the structure and morphology of provacuoles *in vivo,* a genetic piggyback system (Krüger, 2017) was used. Here, the V-ATPase Associated Protein 2 (VHA-AP2), which colocalizes with the V-ATPase at the TGN/EE and the tonoplast (Fink, 2012; Krüger, 2017), proved to be of particular benefit (Krüger, 2017).

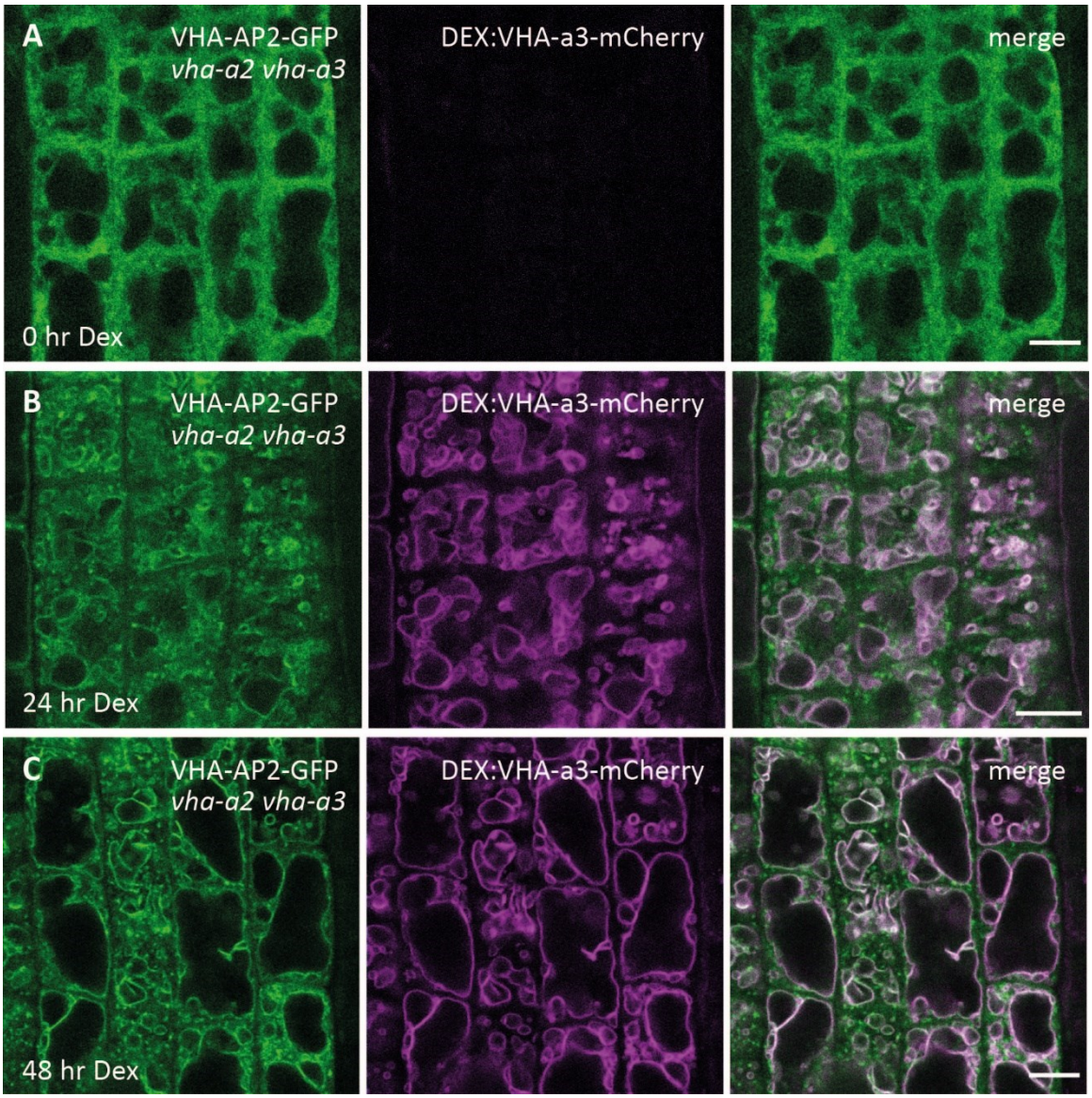


**Figure 9: VHA-AP2-GFP is transported to the vacuole after Dex-induced expression of VHA-a3-mCherry.** (A) Without Dex VHA-AP2-GFP localized to the ER and TGN/EE in the *vha-a2 vha-a3* mutant. (B) After 24 hr Dex induction, VHA-a3-mCherry localizes to the

tonoplast. The localization of VHA-AP2-GFP shifted from the ER to the tonoplast overlapping with VHA-a3-mCherry. (C) After 48 hr Dex treatment, the tonoplast labeling of VHA-AP2-GFP was not enhanced. Scale bars are equal 10 µm.

VHA-AP2-GFP localized to the ER and the TGN/EE in the *vha-a2 vha-a3* double mutant at time point 0 hr. No signal was observed for the uninduced VHA-a3-mCherry (Figure 9 A). After 24 hr Dex treatment, induced VHA-a3-mCherry localized to the tonoplast and the subcellular localization of VHA-AP2-GFP changed from ER and TGN/EE to tonoplast and TGN/EE (Figure 9 B). The tonoplast signal of VHA-AP2-GFP did not further increase after 48 hr Dex induction (Figure 9 C). These observations are the same as in previous experiments (Krüger, 2017).

Next, single-cell images were checked for VHA-AP2-GFP signal, which did not overlap with VHA-a3-mCherry at the tonoplast as these independent VHA-AP2-GFP structures may represent putative provacuoles *in vivo*. I found bright punctae and tubular stretches of VHA-AP2-GFP that did not overlap with VHA-a3-mCherry at the tonoplast after 24 hr Dex treatment (Figure 10 A).

As part of VHA-AP2 colocalizes with VHA-a1 containing V-ATPase complexes at the TGN/EE (Fink, 2012; Krüger, 2017), FM4-64 was used to stain the TGN/EE. Thereby, the punctae could be separated in TGN/EE and putative provacuoles. However, it was not possible to simultaneously detect VHA-a3-mCherry due to low fluorescence intensity and different emission spectrum. A population of VHA-AP2-GFP punctae colocalized with FM4-64 (Figure 10 B) marking the subcellular fraction of VHA-AP2-GFP residing at the TGN/EE together with VHA-a1. By imaging Col-0 roots stained with FM4-64 as a control treatment, autofluorescence (AF) present in punctae and small tubules excited by the 488 nm laser line (GFP AF) was observed, which did not colocalize with FM4-64 (Figure 10 C). There seem to be different populations of VHA-AP2-GFP punctae and tubules: TGN/EE, autofluorescent structures and putative provacuoles.

In summary, subcellular structures that are likely to be provacuoles were observed, but with the microscope setup used, it is not possible to distinguish between autofluorescence emitted from endogenous plant components or the fluorescent protein under investigation. Thus, time-gated fluorescence lifetime imaging could

help to distinguish between GFP autofluorescence and VHA-AP2-GFP fluorescence marking provacuoles. The discrimination between FM4-64 and mCherry would also be possible with fluorescence lifetime gating to exclude the fraction of VHA-AP2-GFP at the TGN/EE and tonoplast by colocalization.

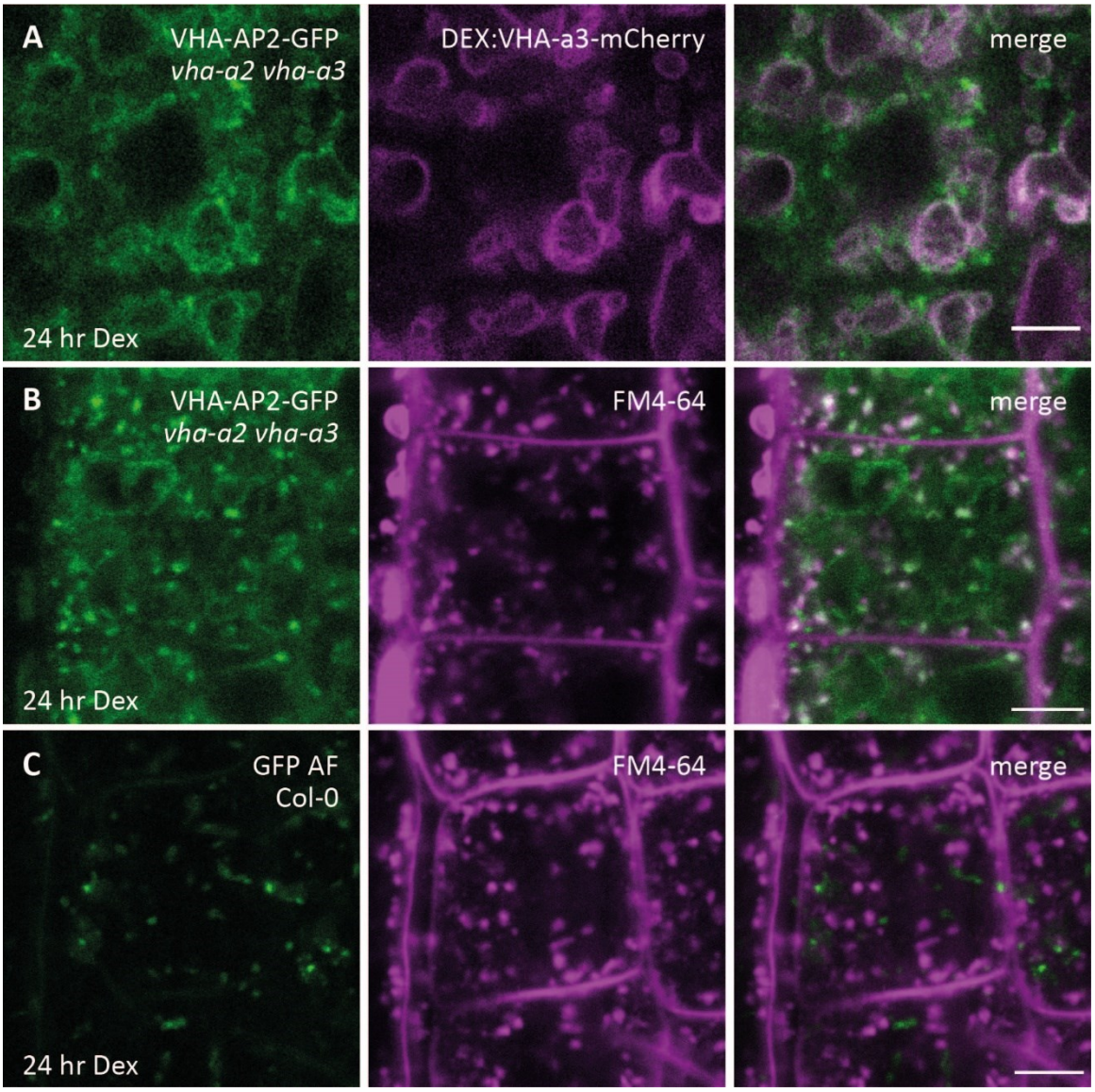


**Figure 10: Independent structures marked with VHA-AP2-GFP, which may resemble provacuoles, cannot be distinguished from GFP autofluorescence by standard CLSM.** (A) VHA-AP2-GFP showed bright punctae and stretches referred to as independent VHA-AP2-GFP structures as they do not overlap with VHA-a3-mCherry. (B) The independent structures of VHA-AP2-GFP did not localize to the TGN/EE stained with FM4-64. (C) Col-0 roots examined with the same imaging settings showed GFP autofluorescence (GFP AF) in structures similar in size and shape to the independent structures of VHA-AP2-GFP. Scale bars are equal to 5 µm.

### 3.2.2 Using inducible expression of VHA-a3 to investigate the trafficking of the tonoplast-localized V-ATPase

Tandem fluorescent protein timers (tFTs) are composed of two fluorophores with different maturation kinetics and are used to measure promotor activity or degradation of a protein by calculating the ratio of the fluorescence intensities (Khmelinskii and Knop, 2014).

By attaching two fluorophores with different maturation times to VHA-a3, different time points after protein biosynthesis may relate to different subcellular distributions of VHA-a3. In this way, VHA-a3 trafficking along subcellular compartments may be traceable from the ER, the place of protein biosynthesis, to the tonoplast. Of special interest were subcellular structures different from tonoplast likely resembling provacuoles.

Here, it was decided for mCherry (monomeric Cherry) and eGFP (enhanced GFP) (Balleza et al., 2018; Cormack et al., 1996). To follow the subcellular localization of VHA-a3-mCherry-eGFP over time, the fusion protein was expressed under the control of the Dex-inducible expression system (DEX:VHA-a3-mCherry-eGFP).

In the absence of Dex, VHA-a3-mCherry-eGFP was not detectable (Figure 11 A). After applying Dex, epidermal root cells were imaged in a cortical plane close to the cell surface and in a median plane through the cell nucleus to achieve a detailed examination of the subcellular distribution of the fluorescence emitted by VHA-a3-mCherry-eGFP. After 4 hr of transfer to medium supplemented with Dex, eGFP was detected in the ER. However, the mCherry fluorescence was faint making it difficult to determine a distinct subcellular localization. (Figure 11 B and C).

After 6 hr of treatment with Dex, eGFP was found in punctae, short tubules and at the tonoplast. The tonoplast signal colocalized with a slightly increased mCherry signal, which was still weaker than the eGFP signal. The mCherry fluorescence was only detected at the tonoplast (Figure 11 D). In the median plane, the fluorescence of eGFP was not evenly distributed over the whole tonoplast but showed brighter areas close to the cell nucleus (Figure 11 E). These sites may mark fusion areas between provacuoles and the vacuole.

As VHA-a3 can be transported to the TGN/EE (Lupanga et al., 2020), roots expressing VHA-a3-mCherry-eGFP were stained with FM6-43 to label the TGN/EE. A population of the eGFP punctae colocalized with punctae labeled with FM4-64 (Figure 11 F). This population of VHA-a3-mCherry-eGFP localized to the TGN/EE after 6 hr of Dex treatment. The other population of punctae may resemble provacuoles.

Notably, also roots, which only showed eGFP and mCherry fluorescence at the tonoplast, were observed after 6 hr of Dex induction (Figure 11 G and H).

Taken together, one population of roots expressing VHA-a3-mCherry-eGFP showed eGFP fluorescence exclusively at the tonoplast (Figure 11 G and H). Whereas a second population exhibited eGFP fluorescence in punctate and tubular structures, which did not colocalize with mCherry fluorescence. However, part of the punctae overlapped with FM4-64 staining the TGN/EE (Figure 11 D to F). Thus, inducibly expressed VHA-a3 localized to the tonoplast, TGN/EE and provacuoles.

To identify provacuoles in vivo with seedlings expressing Dex-inducible VHA-a3-mCherry-eGFP the use of time-gated fluorescence lifetime imaging would be needed to discriminate between FM4-64 and mCherry. Thereby, the fluorescence from FM4-64 (VHA-a3 at the TGN/EE) and from mCherry (VHA-a3 at the tonoplast) could be subtracted to identify provacuoles in vivo. Interestingly, the areas at the tonoplast labeled with higher eGFP fluorescence intensity may be sites, at which provacuoles fuse with the tonoplast.

eGFP seems to mature faster and fluoresce brighter than mCherry in planta, which is in accordance with the Dex-inducible VHA-a3-mCherry being detected exclusively at the tonoplast in the genetic piggyback system (Figure 9 and Figure 10). However, by combining the conditional expression of VHAa3 with a rapidly maturing green fluorophore it was possible to detect VHA-a3 in tubular and punctate structures likely being provacuoles (6 h Dex treatment, Figure 11 D and E).

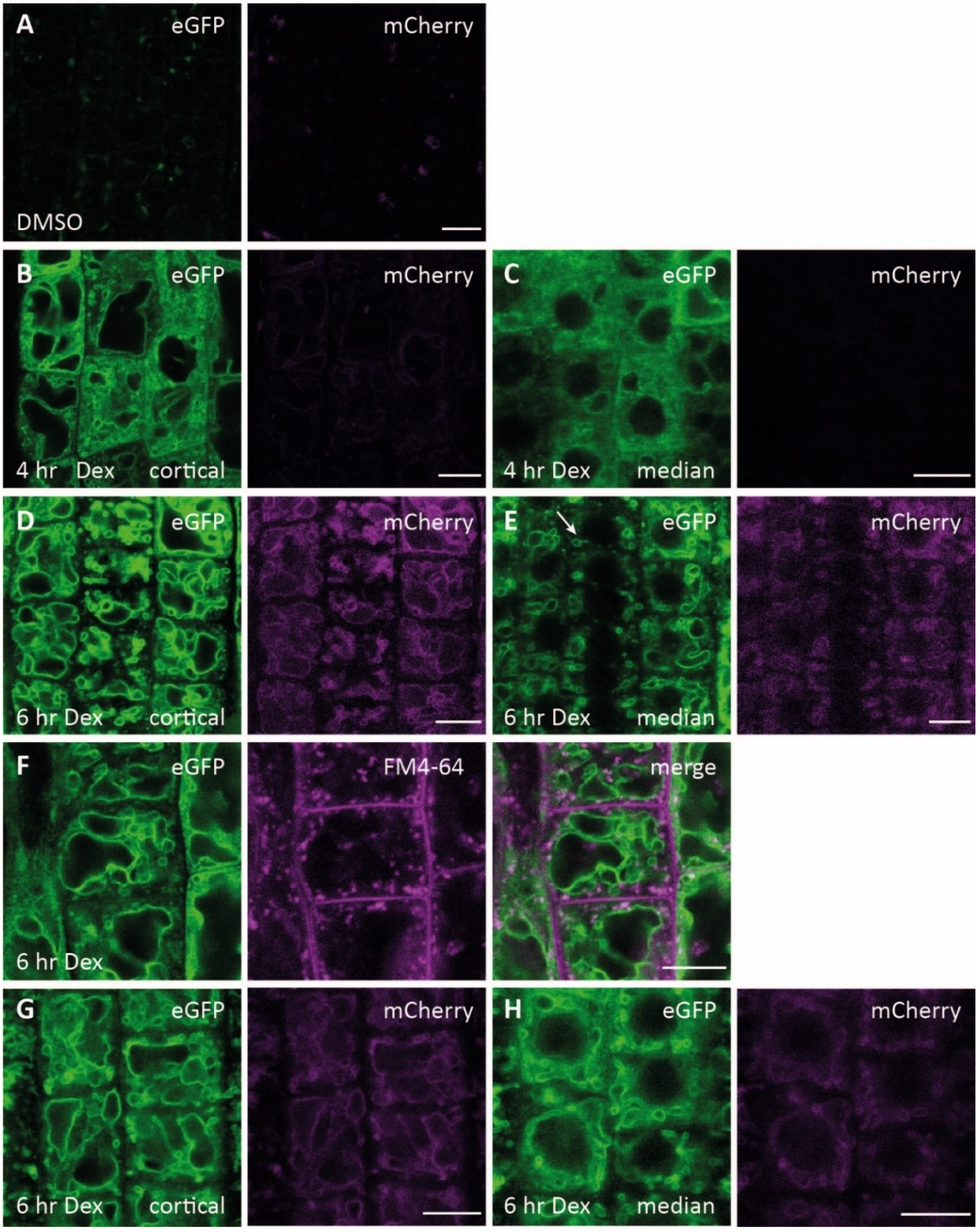


**Figure 11: VHA-a3-mCherry-eGFP localizes to undefined structures, the TGN/EE and the tonoplast when controlled by conditional expression.** (A) Dual fluorescent labeling with eGFP and mCherry under the control of the Dex-induced expression system was used to follow the trafficking of VHA-a3 over time. (A) Autofluorescence in the DMSO control showing that VHA-a3-mCherry-eGFP is not expressed in the absence of Dex. (B and C) After 4 hr Dex treatment, eGFP was detected in the ER, whereas for mCherry no clear signal was recorded. Root cells were imaged in the cortical plane (B, D, G) and in the median plane (C, E, H) to distinguish subcellular localization. (D and E) After 6 hr Dex induction, eGFP was detected in punctae and at the tonoplast. mCherry signal was faintly

detected only at the tonoplast. (F) eGFP punctae colocalized partially with FM4-64 staining the TGN/EE. (G and H) After 6 hr Dex treatment, a population of roots showed fluorescence exclusively at the tonoplast. Scale bars are equal to 10 µm.

In addition, VHA-a3-mCherry-eGFP localized to the TGN/EE strengthening the hypothesis that the trafficking of VHA-a3 is preferably executed independent of the Golgi via provacuoles, but that VHA-a3 can enter the secretory trafficking pathway (Lupanga et al., 2020). However, roots with conditional expression of VHA-a3 that did not exhibit punctate or tubular structures were also observed. These roots showed exclusive labeling of the tonoplast, similar to constitutively expressed VHA-a3-GFP under the endogenous promotor (Dettmer et al., 2006). Here, the amount of fluorescent protein in the putative provacuoles may be too low to be detected by CLSM. This points to the importance of examining different transgenic lines for induction of gene expression.

The conditional expression of VHA-a3 allowed to record the localization of the tonoplast-localized V-ATPase over time and to detect structures unlikely being ER or tonoplast, thereby marking putative provacuoles.

Next, the sites of the tonoplast in close contact to the cell nucleus with higher fluorescence intensity were examined in more detail. Therefore, VHA-a3-LinkerGFP under the control of the estradiol-induced expression system (Denninger et al., 2019) was used to test whether newly synthesized VHA-a3-LinkerGFP appears in sites at the tonoplast with brighter fluorescence. To compare the fluorescence of VHA-a3-LinkerGFP at the tonoplast, constitutively expressed VHP1-mCherry was used as reference.

VHP1-mCherry expressed under the control of the UBQ10 promotor localized to the ER and the tonoplast (Supplementary Figure 5). Neither punctate nor tubular structures were observed indicating that either the trafficking of VHP1-mCherry occurs too fast to image provacuoles or that too few molecules are transported to generate a sufficient fluorescent signal. The fluorescence intensity of the constitutively expressed VHP1-mCherry was not evenly distributed along the whole vacuolar membrane, but showed brighter subareas close to the cell nucleus (Figure 12 A; Supplementary Figure 5 C and D).

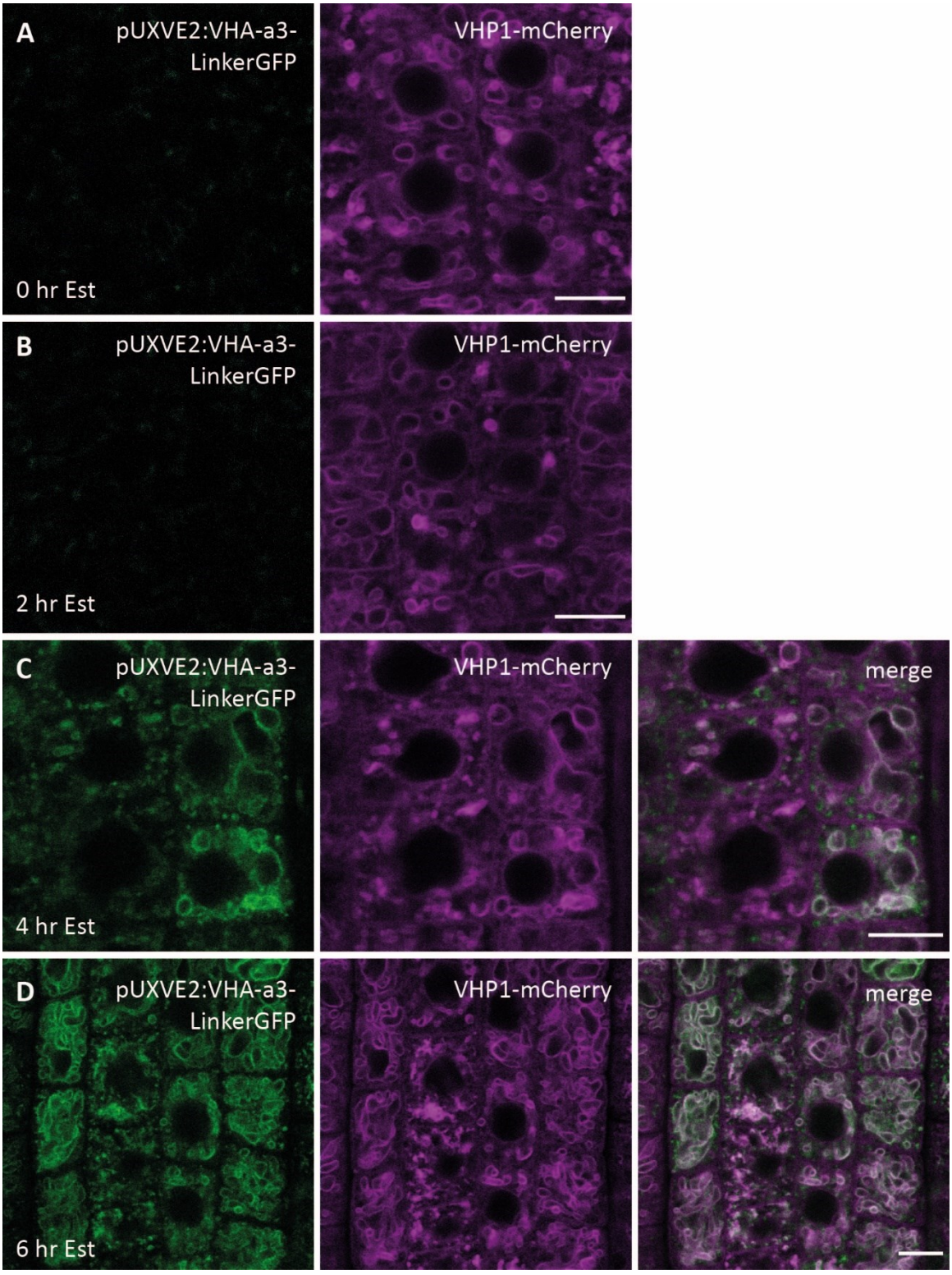


**Figure 12: Areas at the tonoplast with high fluorescence intensity may mark sites of fusion between provacuoles and the vacuole.** (A) In the absence of estradiol (Est), VHA-a3-LinkerGFP under the control of the estradiol-inducible expression system was not detectable. VHP1-mCherry localized to tonoplast and faintly to the ER (B). After 2 hr of estradiol treatment, VHA-a3-LinkerGFP did not exhibit fluorescent signal. (C) After 4 hr of transfer to estradiol, VHA-a3-LinkerGFP colocalized with VHP1-mCherry at the tonoplast. VHA-a3-LinkerGFP was also detected in punctae and tubular structures independent of

VHP1-mCherry. (D) After 6 hr of estradiol induction, tonoplast labeling of VHA-a3-LinkerGPF became more pronounced. Scale bars are equal to 5 µm.

In the absence of estradiol, no signal for VHA-a3-LinkerGFP was recorded (Figure 12 A). Furthermore, estradiol-induced VHA-a3-LinkerGFP could not be detected after 2 hr of estradiol treatment (Figure 12 B). After 4 hr of transfer to estradiol, VHA-a3-LinkerGFP colocalized with VHP1-mCherry at the tonoplast. Here, the brighter sites of VHP1-mCherry at the tonoplast were also labeled with brighter estradiol-induced VHA-a3-LinkerGFP fluorescence. The sites with brighter fluorescence could be observed in close contact with the nuclear envelope. The higher concentration of proton pumps may point to a recent fusion event between a provacuole and the vacuole. Another possibility is that the density of the proton pumps on the tonoplast varies, resulting in membrane stretches with higher fluorescence.

In addition, we found punctae and small tubular structures labeled with VHA-a3-LinkerGFP, which did not colocalize with VHP1-mCherry, after 4 hr of estradiol treatment (Figure 12 C). Some of the punctae labeled with VHA-a3-LinkerGFP resembled the TGN/EE in size and shape, compared with the Dex-induced VHA-a3-mCherry-eGFP localized to the TGN/EE (Figure 11 F). Tonoplast labeling of estradiol-induced VHA-a3-LinkerGFP further increased after 6 hr of estradiol treatment (Figure 12 D). Punctate structures of VHA-a3-LinkerGFP were still visible after 6 hr of estradiol induction.

Overall, areas of the tonoplast characterized by brighter fluorescence from constitutively expressed VHP1-mCherry and conditionally expressed VHA-a3-LinkerGFP were observed. These brighter areas of the tonoplast in close contact to the cell nucleus may resemble fusion sites of provacuoles with the vacuole. However, to detect putative fusion events with quantitative 3D stacks over time, a different microscopic setup such as a Spinning Disk microscope is required. To test whether the vacuolar proton pumps form denser areas at the tonoplast as a result of recent fusion events or whether the bright fluorescence is derived from the overlap of vacuolar membranes in the Z-direction, the distribution of the vacuolar proton pumps at the tonoplast has to be compared to a V-ATPase/V-PPase-independent transmembrane protein in the vacuolar membrane.

## 3.3 A population of tonoplast-localized proton pumps mislocalizes to the TGN/EE under certain conditions

As VHA-a2 and VHA-a3 function redundantly to VHA-a1 in the *vha-a1* knockout mutant during vegetative growth (Lupanga et al., 2020) and VHA-a3 is present at the TGN/EE when expressed with conditional expression systems (Figure 11 and Figure 12), it can be concluded that VHA-a3 can take two routes: a Golgi-dependent trafficking pathway to the TGN/EE and the Golgi-independent route via provacuoles. Therefore, the trafficking of the tonoplast-localized V-ATPase through the Golgi and post-Golgi compartments was further investigated.

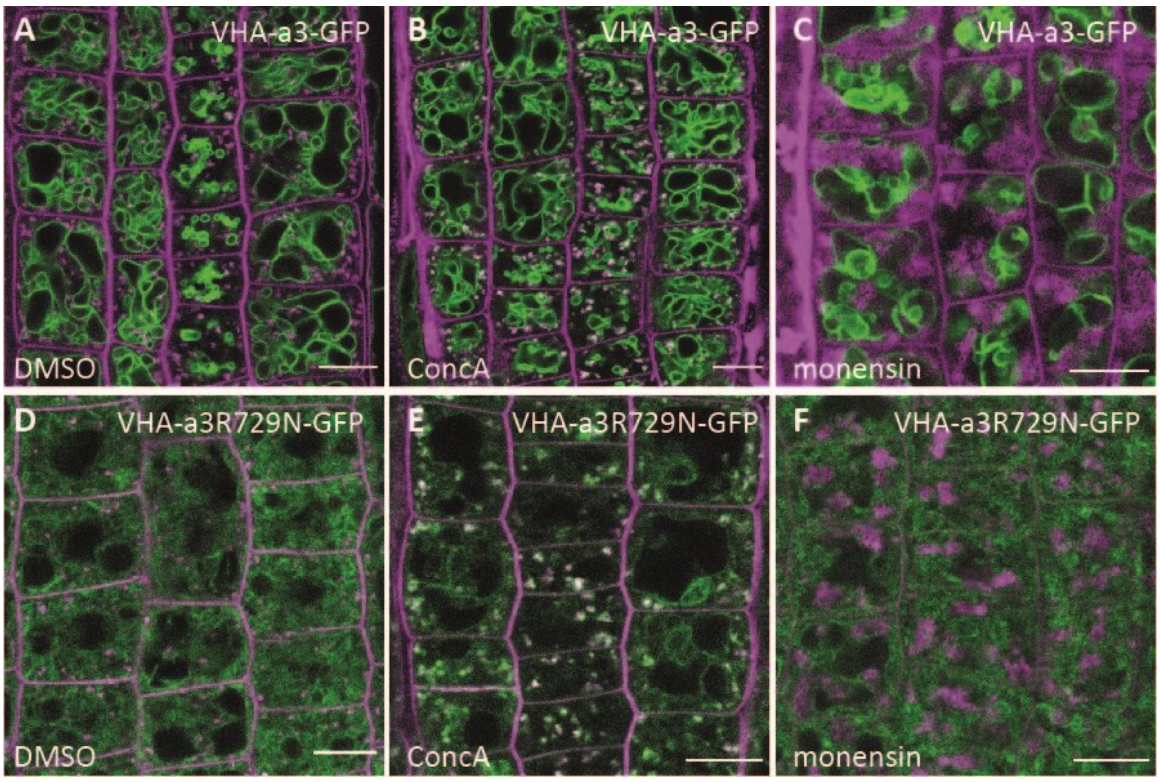


**Figure 13: VHA-a3-GFP and the point-mutated form VHA-a3R729N-GFP localize to the TGN/EE after applying ConcA.** 6-days-old Arabidopsis seedlings were treated with DMSO, 500 nM ConcA for 5 h or 10 µM Monensin for 90 min. The TGN/EE was stained with 1 µM FM4-64 (magenta) for 15 min. (A) VHA-a3-GFP localized to the tonoplast and did not show colocalization with FM4-64 labeling the TGN/EE in the DMSO control. (B) After treatment with ConcA, VHA-a3-GFP localized to the tonoplast and punctae, which overlapped with FM4-64 labeling the TGN/EE. (C) Monensin application led to the formation of aggregates stained with FM4-64 but did not cause a mislocalization of VHA-a3. (D) VHA-a3R729N-GFP localized to the ER in the DMSO control. (E) After treatment with ConcA, VHA-a3R729N-GFP localized to the ER and TGN/EE. (F) Applying monensin did not alter the ER localization of VHA-a3R729N-GFP. Scale bars are equal to 10 µm.

There was no overlap in punctate structures when VHA-a3-RFP and VHA-1-GFP were coexpressed (Supplementary Figure 4) assuring that VHA-a3 does not localize to the TGN/EE under normal circumstances (Viotti et al., 2013).

This could mean that VHA-a3 is preferably transported via provacuoles under normal conditions or that the transport of VHA-a3 through the TGN/EE happens so fast that the amount of fluorescent protein is insufficient for detection with CLSM. If VHA-a3 is transported though the TGN/EE, it can be concluded that VHA-a3 does not contain a TGN/EE retention motif in contrast to VHA-a1. To manipulate protein trafficking at the TGN/EE, either ConcA (Dettmer et al., 2006) or monensin (Zhang et al., 1993) was used and the effects on VHA-a3-GFP and the TGN/EE stained with FM4-64 were observed. VHA-a3-GFP was found exclusively at the tonoplast in the DMSO control (Figure 13 A). After applying ConcA, VHA-a3-GFP localized to the tonoplast and the TGN/EE stained with FM4-64 (Figure 13 B). The monensin treatment was effective as TGN/EEs formed aggregates stained with FM4-64 but did not affect the subcellular localization of VHA-a3-GFP (Figure 13 C). The observation that the application of ConcA causes an accumulation of VHA-a3-GFP at the TGN/EE supports the finding that VHA-a3 can enter the classical route through the Golgi and post-Golgi-compartments (Lupanga et al., 2020).

The point mutation R729N in VHA-a3 is predicted to render the V-ATPase non-functional in pumping protons across the vacuolar membrane. Previous experiments showed that VHA-a3R729N localizes to the ER in Col-0 and the tonoplast in the vha-*a2 vha-a3* mutant. The application of ConcA causes VHA-a3R729N to leave the ER and localize to the TGN/EE (Neubert, 2012). Therefore, the effect of ConcA and monensin on VHA-a3R729N was compared. VHA-a3-R729N-GFP localized to the ER in the DMSO control (Figure 13 D) and overlapped in punctae with FM4-64 labeling the TGN/EE after ConcA treatment. Additionally, the signal of VHA-a3R729N-GFP in the ER after ConcA application appeared to be less bright compared to DMSO treated roots (Figure 13 E) supporting that the application of ConcA induced the ER export of non-functional V-ATPase complexes containing VHA-a3R729N-GFP. The application of monensin led to aggregated TGN/EEs stained with FM4-64 but did not alter the ER localization of VHA-a3R729N-GFP (Figure 13 F).

Taken together, applying monensin did not alter the localization of neither VHA-a3-GFP nor VHA-a3R729N-GFP. In contrast, ConcA treatment caused a fraction of VHA-a3 to accumulate at the TGN/EE. Monensin as well as ConcA induce a less acidic pH in the TGN/EE lumen (Dragwidge et al., 2019; Luo et al., 2015), but the mechanisms are different. ConcA directly inhibits the V-ATPase independent of its subcellular localization. Monensin acts as a cation ionophore meaning that it imports $Na^+/K^+$ and exports $H^+$ across the membrane thereby causing an osmotic swelling of *trans*-Golgi stacks and TGN/EE in plants (Zhang et al., 1993). The different mode of actions could influence protein sorting and vesicle trafficking differently, which could explain the discrepancy why the localization of VHA-a3/VHA-a3R729N is not altered by monensin.

An unknown ER quality control mechanism retains VHA-a3R729N-GFP, which is non-functional, in the ER. As pH homeostasis is crucial for the proper functionality of the TGN/EE (Luo et al., 2015), inhibition of V-ATPase complexes by ConcA may increase the demand of V-ATPase complexes at the TGN/EE thereby overruling an unknown ER-based quality control. This could explain why per se non-functional V-ATPase complexes containing VHA-a3R729N-GFP leave the ER and localize to the TGN/EE after applying ConcA.

This opens the questions whether ConcA enhances the export of VHA-a3 containing V-ATPase complexes to the TGN/EE and whether the fraction of VHA-a3 accumulating at the TGN/EE after ConcA treatment consists of newly synthesized protein or recycled protein derived from the tonoplast. Therefore, the estradiol-inducible expression system (Denninger et al., 2019) was used to investigate the trafficking of newly synthesized VHA-a3 in the presence of BFA or ConcA.

Seedlings treated with 60 $\mu$M estradiol and the appropriate amount of DMSO as control treatment for BFA/ConcA application showed VHA-a3-LinkerGFP fluorescence at the tonoplast and in few punctae colocalizing with FM4-64 staining the TGN/EE (Figure 14 A). Inducing the expression of VHA-a3-LinkerGFP with estradiol for 1 hr and adding BFA for another 6 hr changed vacuole morphology, but not the localization of VHA-a3-LinkerGFP at the tonoplast (Figure 14 B). As BFA did not inhibit the trafficking of newly synthesized VHA-a3 to the vacuole, it

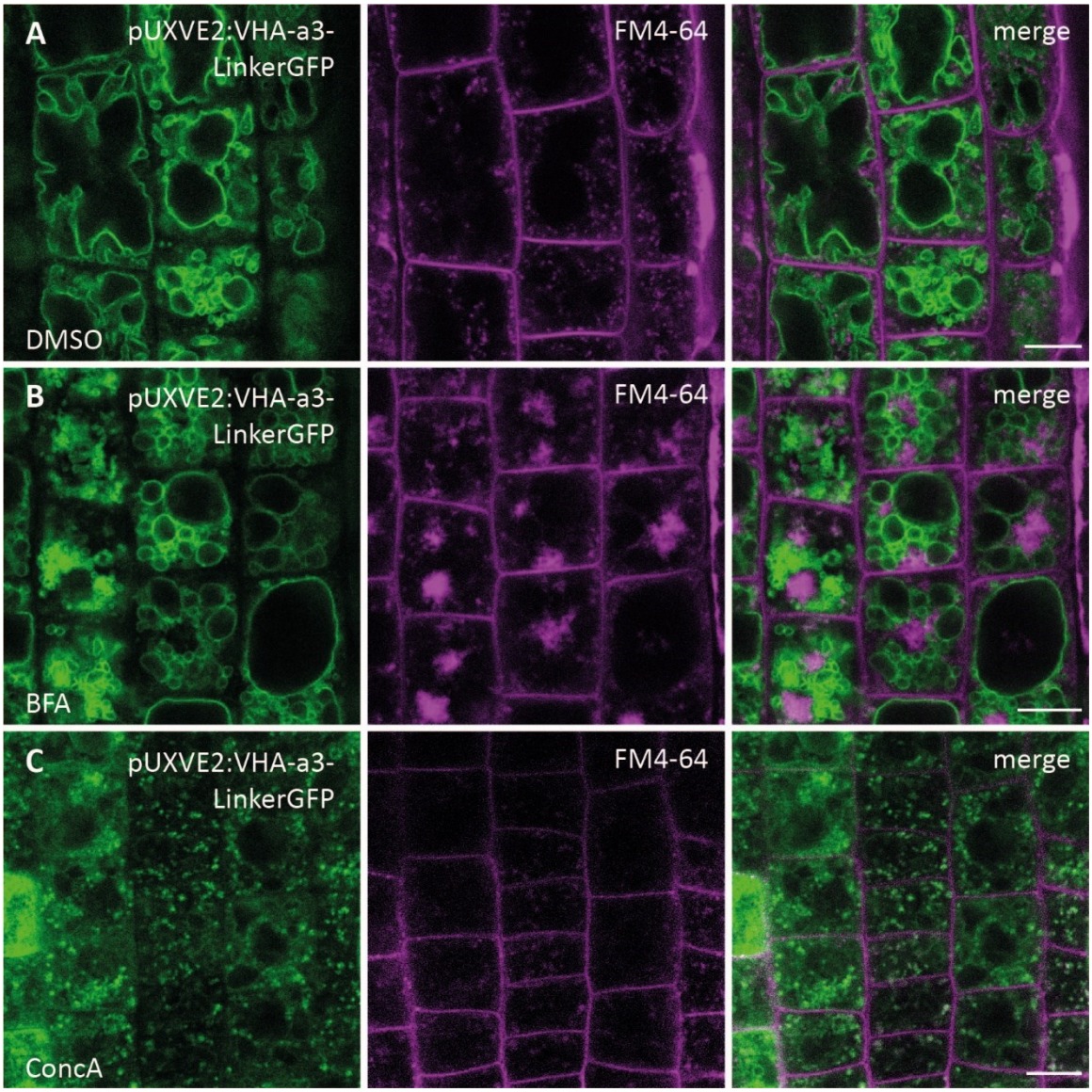


**Figure 14: The trafficking of newly synthesized VHA-a3 is insensitive to BFA, but after adding ConcA VHAa3 localizes to the TGN/EE.** The expression of VHA-a3-LinkerGFP was induced for 1 hr with estradiol prior to the application of either 25 µM BFA, 1 µM ConcA or the equal amount of DMSO. Epidermal root cells were imaged after another 6 hr of incubation and stained with 1 µM FM4-64 to visualize the TGN/EE. (A) After 7 hr VHA-a3-LinkerGFP localized to the tonoplast and showed colocalization with FM4-64 at the TGN/EE. (B) BFA treatment did not alter the tonoplast localization of VHA-a3-LinkerGFP. (C) Applying ConcA caused an accumulation of VHA-a3-LinkerGFP at the TGN/EE. Scale bars are equal to 10 µm.

can be concluded that VHA-a3 is transported to the vacuole via provacuoles in the presence of BFA. A complete sorting of VHA-a3 to provacuoles also explains that VHA-a3 is not retained, when COPII-mediated ER-to-Golgi transport is inhibited with Sar1b-GTP. Adding ConcA while gene expression of VHA-a3-LinkerGFP was

induced with estradiol led to the accumulation of VHA-a3-LinkerGFP at the TGN/EE (Figure 14 C).

Trafficking of newly synthesized VHA-a3 being sensitive to ConcA shows that the population of VHA-a3 at the TGN/EE consists of newly produced protein. Therefore, ConcA inhibits the trafficking of the VHA-a3 population sorted into the Golgi and post-Golgi pathway, but it might as well enhance the sorting of VHA-a3 into this pathway at the ER. Thus, protein trafficking at the TGN/EE was manipulated without using chemical inhibitors.

By expressing the inactive, GDP-locked form of the RAB5 GTPase ARA7 (ARA7-GDP or ARA7S24N) trafficking processes at the TGN/EE to the vacuole are inhibited (Kotzer et al., 2004). The dominant-negative form ARA7-GDP binds to the interaction partners of ARA7 rendering them unavailable for the endogenous ARA7 thereby generating an inhibitory situation. In contrast to ConcA, ARA7-GDP does not directly alter the function of the V-ATPase.

Estradiol-inducible mCherry-ARA7-GDP (EST:mCherry-ARA7S24N) was coexpressed with VHA-a3-GFP to investigate the effects of inhibited trafficking processes at the TGN/EE on the subcellular localization of VHA-a3-GFP without using chemical inhibitors. After applying estradiol no fluorescence of mCherry-ARA7-GDP was detected (Supplementary Figure 6 A). This might be caused by a compromised fluorophore or only few molecules were synthesized, which is not sufficient to be detected with CLSM. Regardless of the lacking fluorescence of induced mCherry-ARA7-GDP, VHA-a3-GFP localized to the tonoplast and punctae resembling the TGN/EE. This suggests that the GDP-locked form of ARA7 was expressed regardless of the non-detectable fluorescence and inhibited the trafficking of VHA-a3-GFP at the TGN/EE (Supplementary Figure 6 B).

In summary, the experiment with ARA7-GDP showed that a population of VHA-a3 relies on the trafficking between the TGN/EE and the vacuole. With using ARA7-GDP it can also be excluded that only non-functional VHA-a3 containing V-ATPases are sorted to the TGN/EE. It rather seems as if VHA-a3 can be transported through the TGN/EE, but that the amount of VHA-a3 varies.

The experiments with conditional expression of VHA-a3, ConcA and ARA7-GDP provide evidence for the trafficking of a VHA-a3 population along post-Golgi compartments. So far, no trafficking pathway from the ER to the TGN/EE was described, which does not depend on the Golgi. Therefore, it can be assumed that the population of VHA-a3, which accumulated at the TGN/EE, also passed through the Golgi, and therefore relies on Golgi-dependent trafficking processes.

To examine whether VHP1, the second proton pump at the vacuole, is also able to be sorted into a Golgi-dependent pathway, ConcA was applied to inhibit V-ATPase activity and trafficking processes at the TGN/EE.

VHP1-GFP was found at the tonoplast in root cells with the only exception of localizing faintly to the plasma membrane in very young meristematic root cells close to the QC (Figure 15 A and B). This indicates that the expression of VHP1-GFP in Col-0 leads to an overflow of the V-PPase into the secretory pathway of root cells in an early developmental stage.

Treatment with ConcA led to the mislocalization of VHP1-GFP to the TGN/EE and the plasma membrane (Figure 15 C). Very few TGN/EEs stained with FM4-64 colocalized with VHP1-GFP indicating that VHP1 transits through the TGN/EE in a rapid manner. In contrast, VHA-a3 is retained at the TGN/EE and is not missorted to the plasma membrane (Figure 13 B).

As VHA-a3 and VHP1 were detected in post-Golgi compartments and provacuoles, both tonoplast-localized proton pumps are capable of leaving the ER via two distinct routes to the vacuole (Lupanga et al., 2020; Viotti et al., 2013). As blocking COPII-mediated ER-to-Golgi transport did not lead to a retention of tonoplast-localized proton pumps in the ER, it is likely that the sorting of tonoplast-localized proton pumps at the ER is highly adaptable.

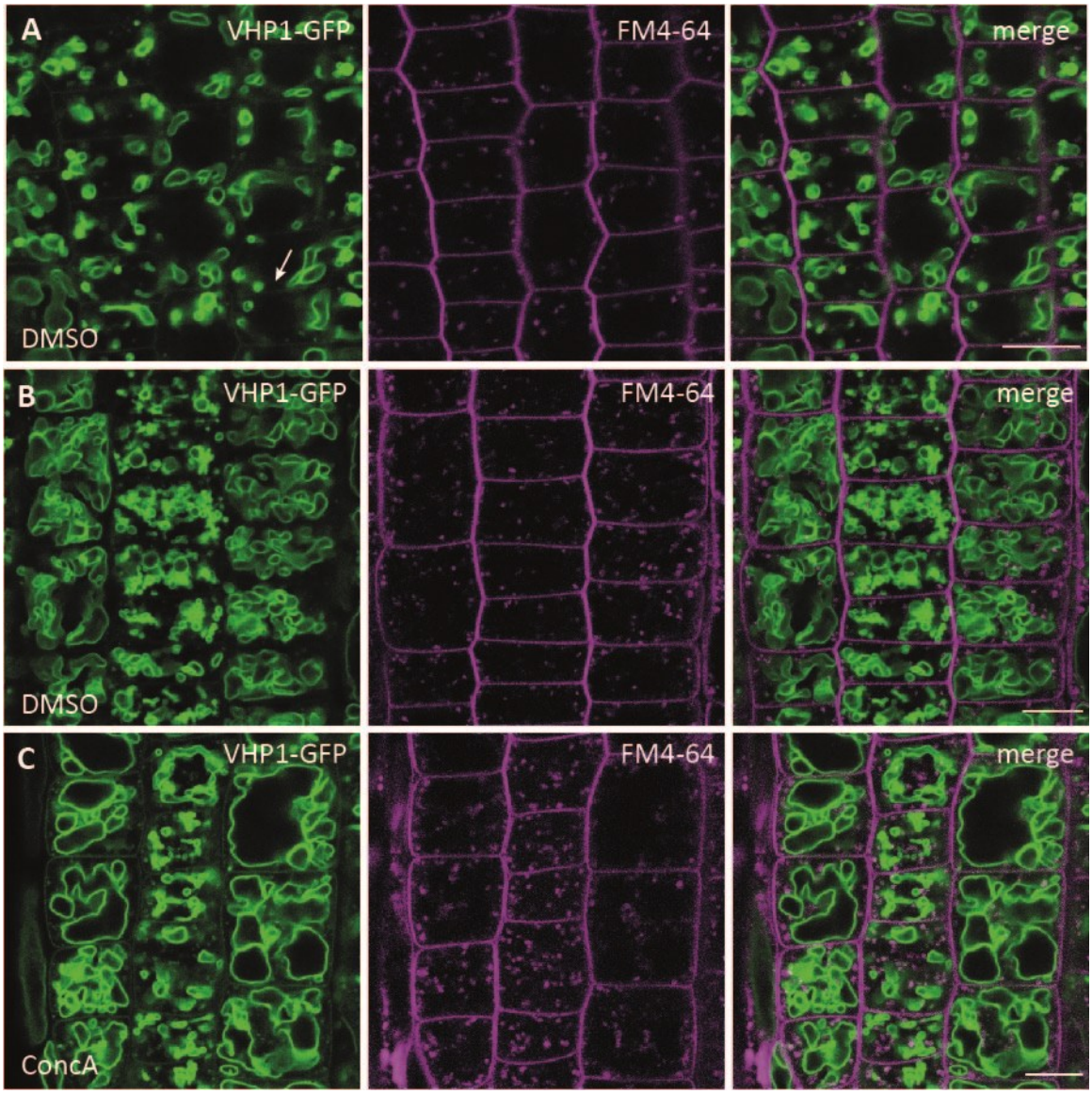


**Figure 15: VHP1-GFP mislocalizes to the TGN/EE and the plasma membrane after ConcA treatment.** 6-days-old seedlings expressing VHP1-GFP were treated with DMSO or 500nM ConcA for 5 hr and stained with 1 µM FM4-64 for 15 to 20 min marking the TGN/EE. (A) In meristematic root cells close to the QC VHP1-GFP exhibited a weak signal at the plasma membrane next to the pronounced labeling of the tonoplast. (B) In root cells of the transition zone VHP1-GFP exclusively labeled the tonoplast and no overlap with FM4-64 was detected. (C) After applying ConcA VHP1-GFP mislocalized to the TGN/EE and the plasma membrane. Scale bars are equal to 10 µm.

## 3.4 HOPS and CORVET mediate distinct trafficking pathways to the vacuole

As both tonoplast-localized proton pumps seem can take two routes to the vacuole, it is necessary to find a way to distinguish between the two populations for further investigations. Here, it might be useful to inhibit the subcellular trafficking before reaching the vacuole. The HOPS and CORVET membrane tethering complexes mediate membrane fusion processes between transport vesicles or compartments along the trafficking pathway of the early endosome (EE) to the vacuole or lysosome in yeast and metazoans (Balderhaar and Ungermann, 2013). Therefore, Dex-inducible amiRNAs were used to study the function of HOPS or CORVET in the trafficking pathways towards the vacuole in Arabidopsis.

### 3.4.1 Loss of HOPS or CORVET impact plant growth and vacuole morphology

First, the Dex-inducible knockdowns against subunits of HOPS and CORVET were tested for root growth phenotypes. Seeds were germinated and grown on Dex-containing vertical ½ MS plates for 6 to 8 days. The knockdown of *VPS16*, as well as the knockdown against the HOPS-specific subunits *VPS39* or *VPS41*, did not show a difference in the overall morphology of the root tip compared to Dex-treated Col-0 seedlings (Figure 16 A to D). However, the root tips of the CORVET-specific knockdown against *VPS3* or *VPS8* showed stunted and deformed root meristems (Figure 16 E and F).

To examine the effects of the Dex-induced knockdowns against HOPS and CORVET on vacuole morphology, the lumen of vacuoles was stained with the dye BCECF-AM (2′,7′-bis-(2-carboxyethyl)-5-(and-6)-carboxyfluorescein) (Krebs et al., 2010). For a first comparison, the zone of the root, at which the late elongation zone merges with the differentiation zone, was imaged. Here, vacuoles in Dex-treated Col-0 roots showed the typical brick-like morphology (Figure 17 A). In the Dex-treated knockdowns against *VPS16*, *VPS39* and *VPS41* root cells possessed multiple round vacuoles (Figure 17 B to D). While the vacuoles of root cells in the induced knockdowns against the CORVET-specific subunits *VPS3* and *VPS8* had a similar morphology to Col-0 (Figure 17 E and F).

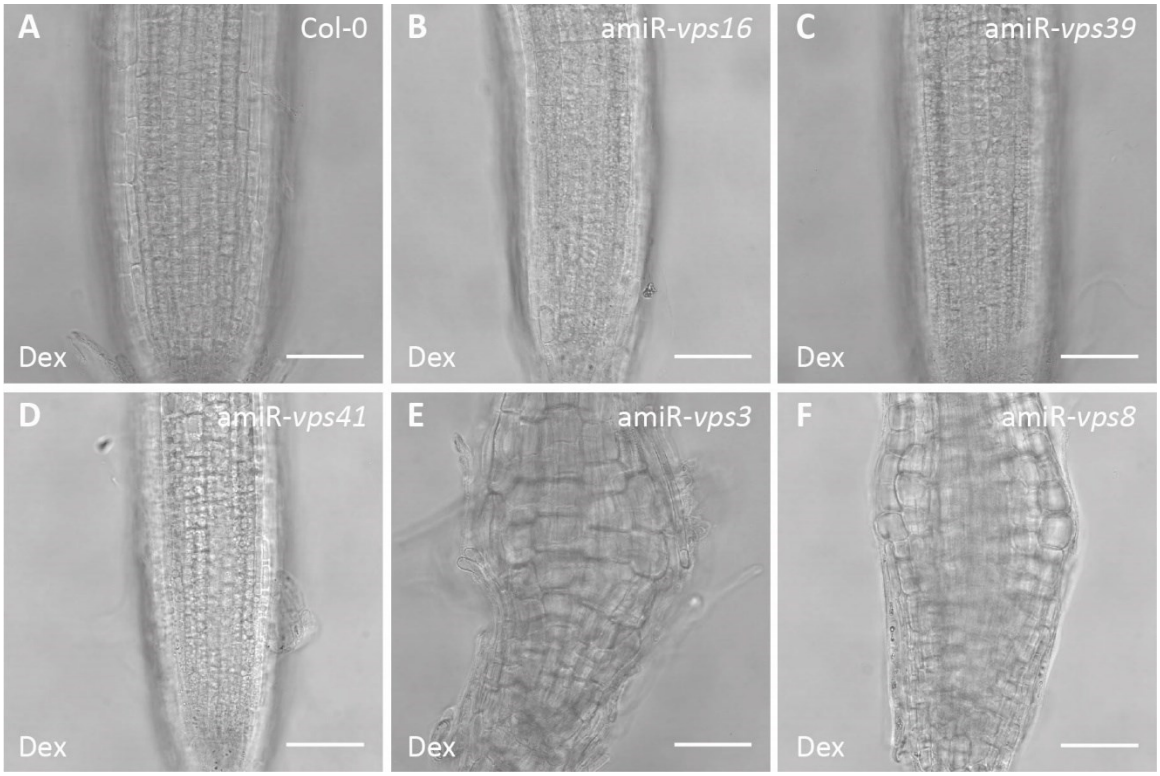


**Figure 16: Knockdown of CORVET-specific subunits *VPS3* and *VPS8* showed deformed root meristems**. Seedlings were grown vertically for 6 to 8 days on ½ MS medium supplemented with 30 µM Dex. Root meristems of amiR-*vps16* (shared subunit of HOPS and CORVET), amiR-*vps39* and amiR-*vps41* (HOPS-specific knock downs) were indistinguishable from Col-0. Root meristems of amiR-*vps3* and amiR-*vps8* (CORVET-specific subunits) show an altered shape compared to Col-0. Scale bars indicate 50 µm. Images of Col-0, amiR-*vps39*, amiR-*vps3* and amiR-*vps8* are published in Takemoto et al., 2018.

In summary, the HOPS-specific knockdown leads to multiple round vacuoles indicating that HOPS is required for homotypic vacuole fusion in Arabidopsis. Previously, the vacuoles in the Dex-induced knockdown against *VPS16* were shown to be fragmented thus representing separated compartments (Dissertation Falco Krüger, 2017). As the fragmentation of vacuoles is characteristic for the loss of HOPS, it can be assumed that vacuoles in root cells of the induced knockdown against *VPS39* and *VPS41* are separated as well. Interestingly, the root meristem and the vacuole morphology of the Dex-induced knockdown against *VPS16*, the shared subunit of HOPS and CORVET, is similar to the phenotypes of the HOPS-specific knockdown indicating that the morphological defects caused by the loss of HOPS overrule the ones of the lacking CORVET complex. The difference in root meristem and vacuole phenotypes by the loss of either HOPS or CORVET indicates that HOPS and CORVET operate different trafficking pathways.

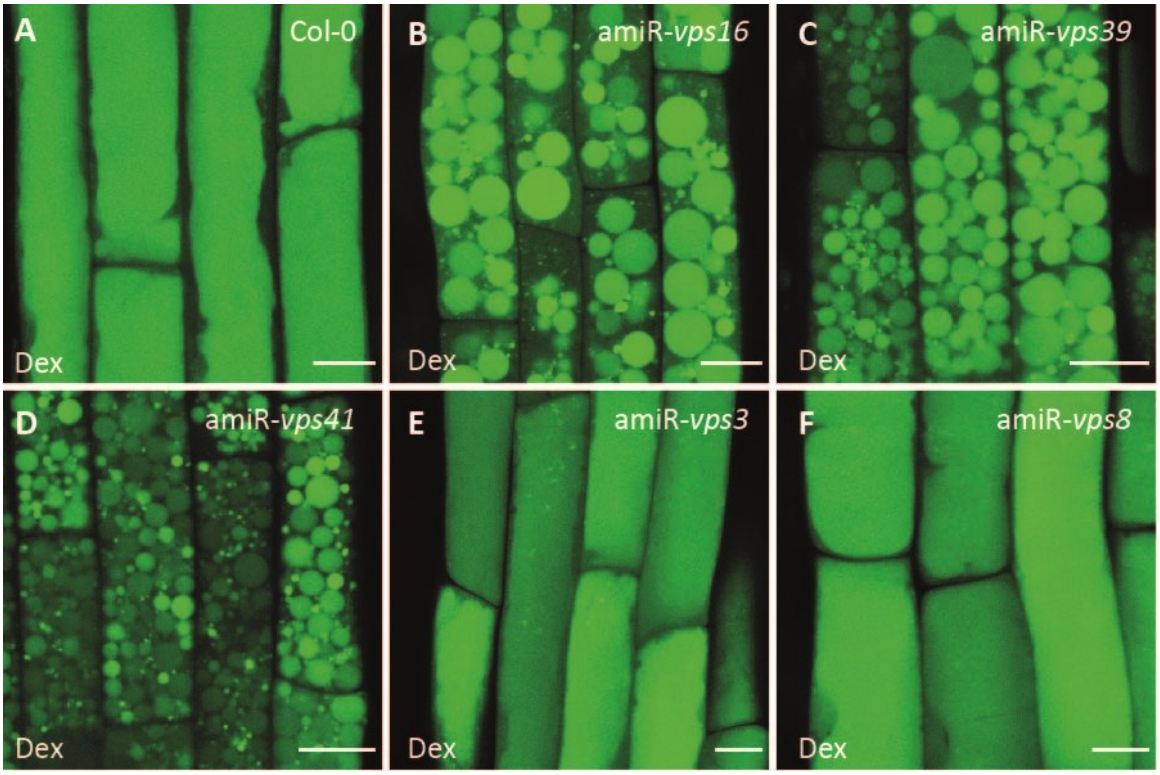


**Figure 17: Vacuole morphology differs in HOPS and CORVET knockdowns indicating different functions for the two membrane tethering complexes.** Seedlings were treated with 30 µM Dex for 72 hr and stained with BCECF-AM to visualize the vacuolar lumen. Images were taken in the late elongation zone of the roots. (A) Vacuoles in Col-0 showed the typical brick-like morphology in elongated root cells. (B) The knockdown of *VPS16* caused multiple, spherical vacuoles similar to the knockdown of the HOPS-specific subunits *VPS39* (C) and *VPS41* (D). (E and F) The vacuoles in the CORVET-specific knockdown against *VPS3* and *VPS8* were similar to Col-0. Scale bars are equal to 10 µm.

### 3.4.2 CORVET mediates a plant specific transport pathway from the TGN/EE to the vacuole

To test whether the HOPS complex is required for fusion of autophagosomes with the vacuole in Arabidopsis similar to its function in yeast, autophagy was induced with ConcA and observed the accumulation of autophagic inclusions inside the vacuole. As these inclusions are not stained with BCECF, they are seen as non-fluorescent, black spots. Autophagic inclusions inside the vacuole were found in Col-0 and the induced knockdown against *VPS8* (Supplementary Figure 7 A and C). In the *VPS16* and *VPS41* knockdown, vacuolar inclusions with autophagic content could not be detected (Supplementary Figure 7 B and D) indicating that the HOPS complex is required for autophagosome-to-vacuole fusion as described in yeast.

In Arabidopsis, four different protein trafficking pathways towards the vacuole are known: RAB5-mediated trafficking from the TGN/EE to the vacuole via LEs, RAB7-mediated fusion of MVBs with the vacuole, AP-3 vesicles from the Golgi or TGN/EE to the vacuole and ER-derived provacuoles (Ebine et al., 2014; Viotti et al., 2013; Wolfenstetter et al., 2012). To investigate whether the HOPS or CORVET membrane tethering complex is involved in membrane fusion events of RAB5-positive LEs, MVBs, AP-3 vesicles or provacuoles, cargo proteins shown to take a distinct route to the vacuole were introduced into the Dex-inducible knockdowns.

To investigate the function of HOPS and CORVET in MVB maturation and MVB-to-vacuole fusion, the subcellular localization of the INOSITOL TRANSPORTER 1 (INT1), whose vacuolar trafficking relies on the subsequent action of RAB5 and RAB7 (Feng et al., 2017a; Wolfenstetter et al., 2012), was examined.

INT1-mTurquoise localized to the tonoplast and the vacuolar lumen of Dex-treated Col-0 roots (Figure 18 A). As mTurquoise is highly pH-stable (Fredj et al., 2012), it accumulates in the vacuole explaining the difference to fusion proteins with GFP, which do not show fluorescence inside the vacuole (Feng et al., 2017a; Wolfenstetter et al., 2012). After Dex treatment, the HOPS-specific knockdown against *VPS39* showed INT1-mTurquoise faintly at the membrane of the round vacuoles and in bright punctae (Figure 18 B; arrow) indicating that MVB-to-vacuole

fusion is inhibited. In the Dex-induced CORVET-specific knockdown against *VPS8* INT1-mTurquoise mislocalized to punctae and the plasma membrane (Figure 18 C).

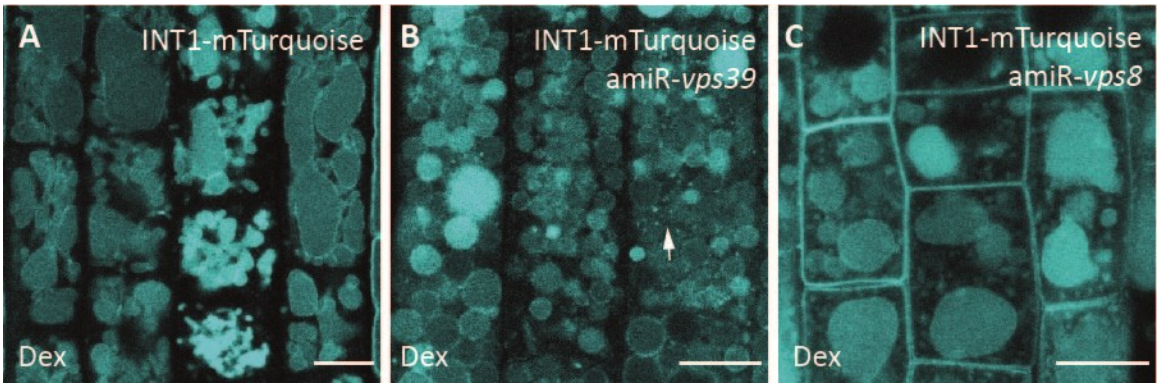


**Figure 18: Trafficking of INT1 depends on HOPS and CORVET.** Seedlings were grown for 5 days on ½ MS medium and then transferred to liquid medium supplemented with 30 µM Dex. (A) INT1-mTurquoise localized to the tonoplast and vacuolar lumen in Col-0 roots. (B) In the induced knockdown against *VPS39* INT1-mTurquoise localized faintly to the tonoplast and to bright punctae (arrow). (C) After the induction of the *VPS8* knockdown, INT1-mTurquoise was mislocalized to punctae and the plasma membrane. Scale bars are equal to 10 µm.

As the vacuolar targeting of INT1 depends on both RAB5 and RAB7 and their RAB conversion on the surface of MVBs, the finding that INT1 requires the action of HOPS as well as CORVET is in accordance with published data (Feng et al., 2017a; Wolfenstetter et al., 2012). The fusion of matured MVBs with the vacuole relies on the HOPS complex in Arabidopsis similar to yeast, whereas the CORVET complex may function at the TGN/EE in MVB formation.

The R-SNARE VAMP711 reaches the vacuole with AP-3 vesicles, whereas the Qb-SNARE VTI11 is transported from the TGN/EE to the vacuole via RAB5-positive LEs that are unique to plants (Ebine et al., 2014; Wolfenstetter et al., 2012). Both SNARE proteins (YFP-VAMP711 or pHGFP-VTI11) were observed in the induced knockdowns against HOPS or CORVET-specific subunits to investigate whether the membrane tethering complexes HOPS or CORVET are involved in the two trafficking routes in Arabidopsis.

Under control conditions YFP-VAMP711 and pHGFP-VTI11 localized to the tonoplast (Figure 19 A and E). In the Dex-induced knockdown against *VPS16* both fluorescent fusion proteins mislocalized to punctae and the plasma membrane and

showed faint residual signal at the tonoplast (Figure 19 B and F). The same subcellular mislocalization was observed for YFP-VAMP711 in the HOPS-specific knockdown against *VPS39* (Figure 19 C). In the induced knockdown against the CORVET-specific subunit *VPS8* YFP-VAMP711 remained unaltered at the tonoplast (Figure 19 D). This finding indicates that the trafficking of the R-SNARE VAMP711 requires the HOPS complex in Arabidopsis. As VAMP711 was shown to be a cargo of AP-3 vesicles, it can be concluded that the fusion of AP-3 vesicles with the vacuole requires the HOPS complex in Arabidopsis.

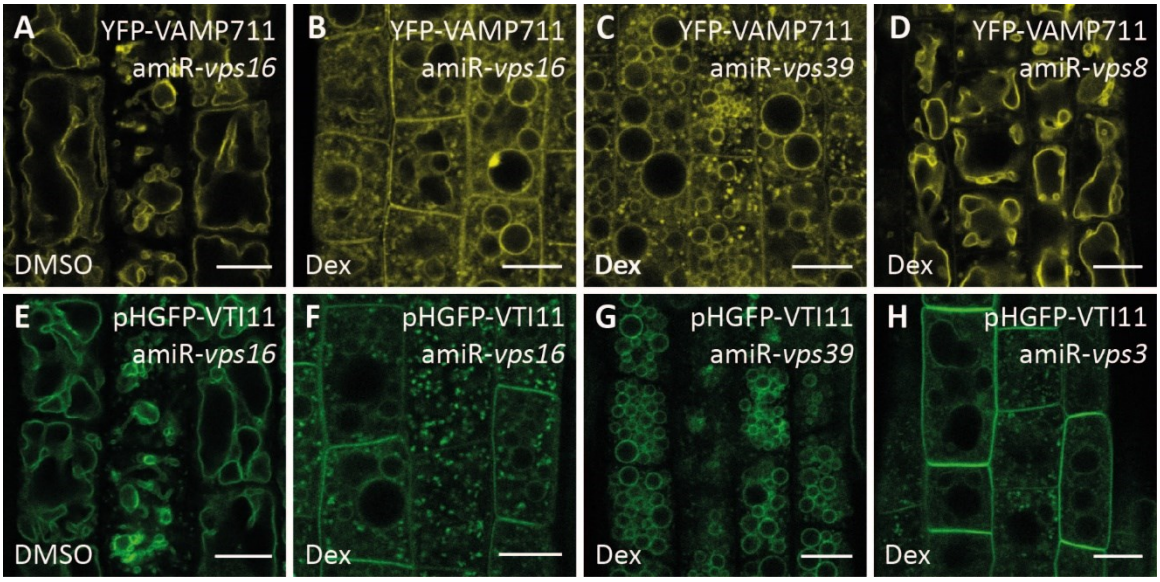


**Figure 19: Vacuolar trafficking of VAMP711 relies on HOPS, whereas VTI11 requires CORVET for tonoplast targeting.** After seedlings were grown for 5 days on ½ MS medium, they were incubated for 72 h in liquid medium containing 30 µM Dex. (A) The R-SNARE YFP-VAMP711 localized to the tonoplast in the DMSO control of the uninduced knockdown against *VPS16*. (B and C) In the induced knockdown against *VPS16* and *VPS39*, the subcellular localization of YFP-VAMP711 was at the tonoplast, in punctae and at the plasma membrane. (D) In the induced CORVET-specific knockdown against *VPS8*, the subcellular localization at the tonoplast remained unaltered. (E) The Qb-SNARE VTI11 was localized to the tonoplast in the DMSO control. (G) In the Dex-induced HOPS-specific knockdown against *VPS39*, the tonoplast localization of pHGFP-VTI11 was not altered. (H) In the induced CORVET-specific knockdown against *VPS3*, pHGFP-VTI11 mislocalized to punctae and the plasma membrane. Scale bars are 10 µm.

In contrast, pHGFP-VTI11 mislocalized in the CORVET-specific knockdown against *VPS3* and showed unaltered tonoplast labeling in the HOPS-specific knockdown against *VPS39* (Figure 19 G and H). This experiment showed that the localization of the vacuolar Qb-SNARE VTI11 depends on the CORVET complex. As VTI11 was shown to be transported with RAB5-positive LEs that do not require

the SAND1/CCZ1 mediated RAB conversion, it can be hypothesized that the CORVET complex mediates the fusion of these RAB5-positive LEs. Moreover, this means that the CORVET complex evolved a new function explicitly at the vacuole in Arabidopsis (Takemoto et al., 2018).

### 3.4.3 The trafficking of tonoplast-localized proton pumps via the Golgi-dependent pathway requires the CORVET complex

To answer the question whether the trafficking of the tonoplast-localized proton pumps requires the action of the conserved membrane tethering complexes HOPS and CORVET, VHA-a3-GFP or VHP1-GFP was crossed with the knockdowns against the HOPS-specific subunit *VPS39* and the CORVET-specific subunit *VPS8*.

VHA-a3-GFP localized to the tonoplast and showed no colocalization with FM4-64 in Col-0 roots treated with 30 µM Dex as control (Figure 20 A). After inducing the knockdown against the HOPS-specific subunit *VPS39*, VHA-a3-GFP did not change its localization at the tonoplast. However, the knockdown against *VPS39* was effective as vacuole morphology was altered to multiple round vacuoles (Figure 20 B). Upon knockdown against the CORVET-specific subunit *VPS8*, VHA-a3-GFP localized to the tonoplast and in punctae, which colocalized with FM4-64 at the TGN/EE (Figure 20 C). As the CORVET complex was shown to mediate fusion between RAB5-positive LEs derived from the TGN/EE and the vacuole, this finding indicates that CORVET is required for the proper trafficking of the population of VHA-a3, which is sorted into the Golgi-dependent pathway. Moreover, this finding indicates that the Golgi-dependent population of VHA-a3 may be transported via RAB5-positive LEs from the TGN/EE to the vacuole, which is a plant-specific transport route.

VHP1-GFP localized to the tonoplast in Dex-treated Col-0 and amiR-*vps39* root cells (Figure 21 A and B). After inducing the knockdown against *VPS8*, VHP1-GFP was found at the tonoplast, in punctae reminiscent of the TGN/EE and at the plasma membrane (Figure 21 C) indicating that CORVET is required for proper trafficking of the Golgi-dependent population of VHP1 to the vacuole.

In summary, the loss of HOPS did neither affect the trafficking of VHA-a3 nor of VHP1. However, the tonoplast-localized proton pumps were found in compartments along the secretory pathway in the induced CORVET-specific knockdown indicating that the population of proton pumps sorted into the Golgi and post-Golgi pathway require the CORVET complex for trafficking to the vacuole.

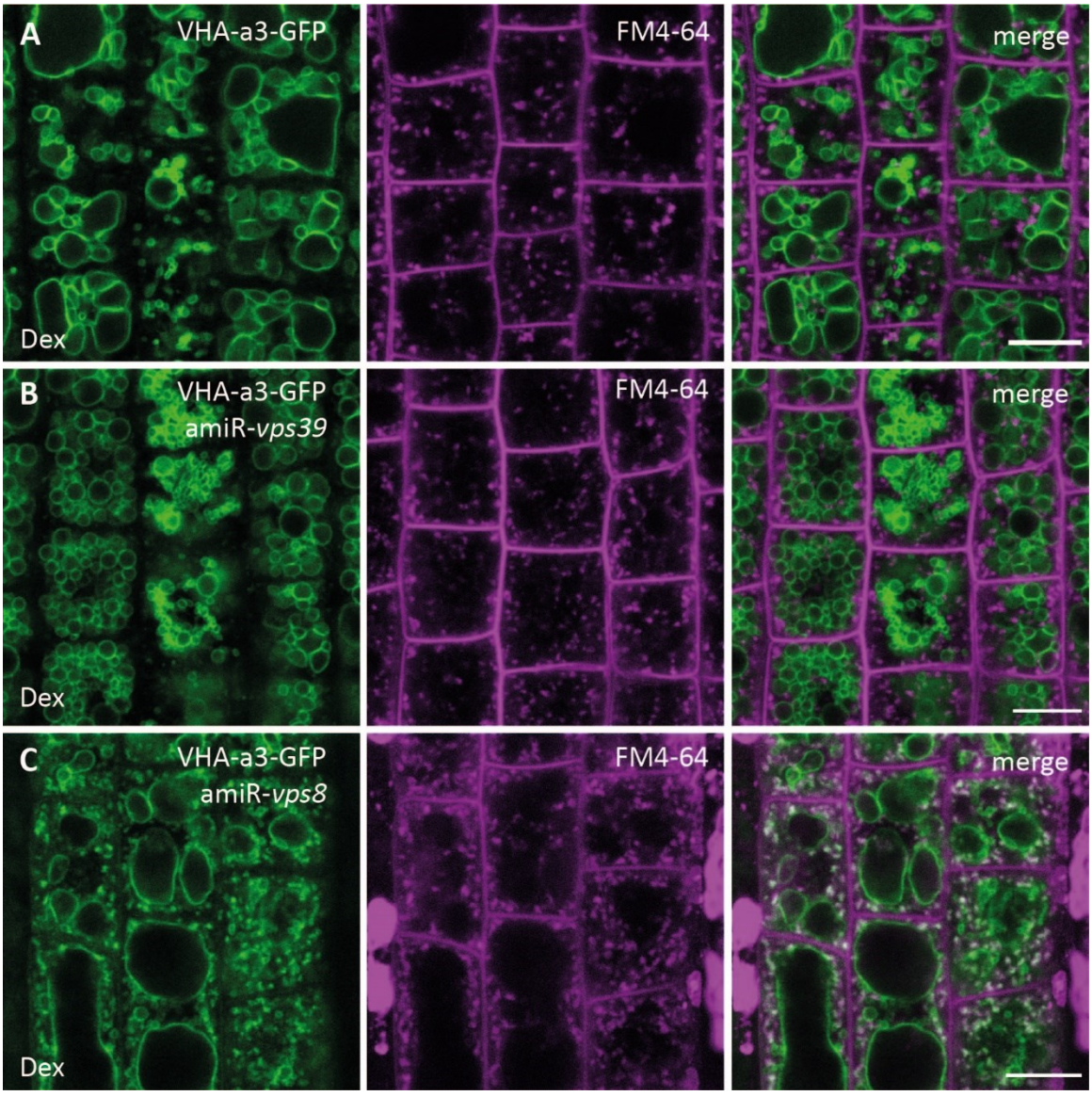


**Figure 20: VHA-a3-GFP localized to the TGN/EE and the tonoplast in the Dex-induced CORVET-specific knockdown.** Seedlings were treated with 30 µM Dex for 72 hr and stained prior to imaging with FM4-64 to label the TGN/EE. (A) VHA-a3-GFP localized to the tonoplast and did not show overlap with FM4-64 staining the TGN/EE in Dex-treated Col-0 roots. (B) After Dex treatment the tonoplast localization of VHA-a3-GFP was not altered in the knockdown against *VPS39*. (C) In the induced knockdown against *VPS8* VHA-a3-GFP mislocalized to punctae colocalizing with FM4-64 at the TGN/EE. Scale bars are equal to 10 µm.

Therefore, the vacuolar trafficking of tonoplast-localized proton pumps via the Golgi-dependent pathway likely occurs via RAB5-positive LEs (Ebine et al., 2014), which mediate protein transport from the TGN/EE to the vacuole and is unique to plants.

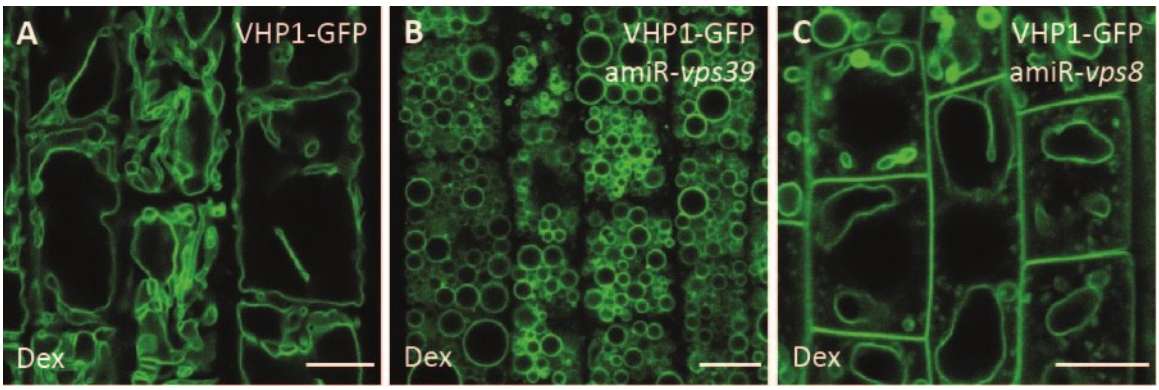


**Figure 21: VHP1-GFP mislocalized to the TGN/EE and the plasma membrane in the CORVET-specific knockdown.** Knockdown of *VPS39* or *VPS8* was induced with 30 µM Dex for 72 hr. (A) VHP1-GFP in the Col-0 treated with Dex as control localized to the tonoplast. (B) In the induced knockdown against the HOPS-specific subunit *VPS39* VHP1-GFP localized to the membrane of the round vacuoles. (C) VHP1-GFP mislocalized to punctae resembling TGN/EE and the plasma membrane in the Dex-induced loss of the CORVET-specific subunit *VPS8*. Scale bars are equal to 10 µm.

As HOPS did not impair the localization of VHA-a3 or VHP1, fusion events between provacuoles and the vacuole seem to not require the HOPS complex. However, a lack of missorting of VHA-a3 or VHP1 or a lack of accumulation of both proteins in punctae likely representing provacuoles could also be explained with an increased sorting of VHA-a3 or VHP1 into the Golgi-dependent pathway. This scenario seems plausible as the ER export of VHA-a3 or VHP1 is shifted towards provacuoles, when COPII-mediated ER-to-Golgi transport is blocked upon the expression of Sar1b-GTP. Nonetheless, an enhanced rerouting into the Golgi-dependent pathway may lead to a subcellular localization at the TGN/EE as seen with the conditional expression of VHA-a3. Therefore, it is unlikely that HOPS facilitates fusion events between provacuoles and the vacuole.

Next, it was investigated whether the CORVET complex might facilitate fusion events between provacuoles and the vacuole. Inhibited fusion events may lead to an altered structure of provacuoles. Therefore, high pressure freezing (HPF) and freeze substitution to perform transmission electron microscopy (EM) was used to examine the morphology of provacuoles in the CORVET-specific knockdown.

Circular structures composed of a double membrane enclosing cytosolic content, which resemble early stages of provacuoles, were observed. This indicates that provacuole formation is not altered in the CORVET-specific knockdown against *VPS8*. Together with the finding that VHA-a3 did not accumulate in other subcellular compartments other than the TGN/EE, the CORVET complex is most likely not required for facilitating the fusion between provacuoles and the vacuole.

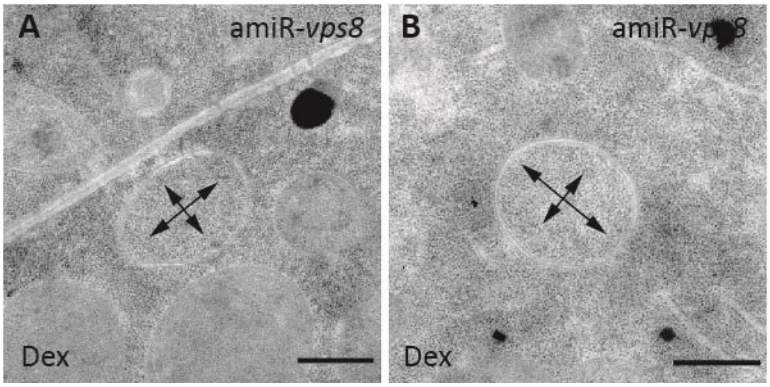


**Figure 22: Circular double-membrane structures reminiscent of provacuoles formed in the Dex-induced CORVET-specific knockdown.** EM images of high-pressure frozen and freeze-substituted Arabidopsis root tips of the Dex-induced CORVET-specific knockdown against *VPS8*. Scale bars are equal to 500 nm. EM images were obtained by Stefan Hillmer.

In summary, the HOPS complex orchestrates membrane fusion events of MVBs and AP-3 vesicles with the vacuole and the CORVET complex serves as a mediator of a plant-specific trafficking pathway from the TGN/EE to the vacuole. In Arabidopsis, the population of tonoplast-localized proton pumps sorted into a Golgi-dependent pathway are transported via this novel trafficking pathway to the vacuole. The fusion between provacuoles and the vacuole does neither require the HOPS nor CORVET complex.

## 3.5 The regulation of vacuolar membrane fusion is required for proper vacuole morphology

### 3.5.1 The cytoskeleton does not influence vacuolar fragmentation in the HOPS-specific knockdown

The depolymerisation of actin filaments changes vacuole morphology and leads to the occurrence of multiple round vacuoles in meristematic root cells (Scheuring et al., 2016). This vacuole phenotype is similar to the multiple spherical vacuoles in the Dex-induced knockdown against *VPS16* and HOPS-specific subunits (Figure 17). To test whether a disturbed actin cytoskeleton causes the altered vacuole morphology, the actin organization in root cells of the knockdown mutants against HOPS or CORVET subunits was examined.

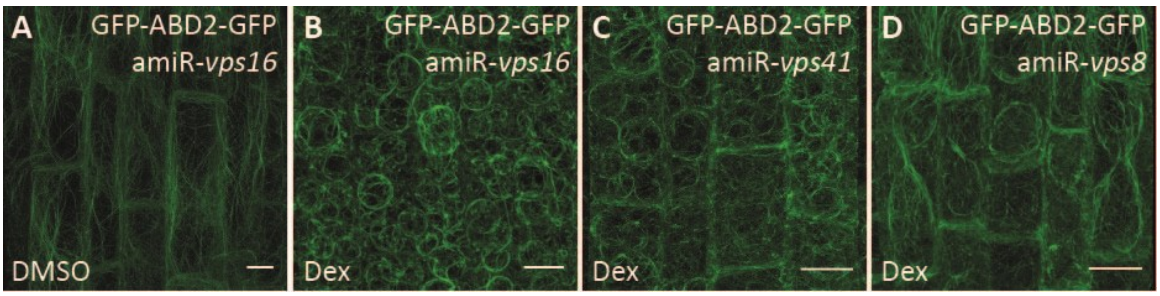


**Figure 23: Actin filaments traverse through root cells in close contact to the vacuolar membrane.** GFP-ABD2-GFP was used to label actin filaments in root cells. Seedlings were treated with DMSO or 30 µM Dex for 72 hr. (A) In DMSO-treated root cells the actin filaments traverse along the vacuole in a longitudinal manner. (B) In the Dex-induced knockdown against *VPS16* the actin filaments were aligned in spirals around the spherical vacuoles. (C) The same spiral distribution of actin filaments at spherical vacuoles was observed in the Dex-induced HOPS-specific knockdown against *VPS41*. (D) Actin filaments projected along the vacuole in a longitudinal direction in the CORVET-specific knockdown against *VPS8*. Scale bars are equal to 10 µm.

The fluorescent marker GFP-ABD2-GFP was used to label actin filaments (Actin Binding Domain 2; Dyachok et al., 2014). The filament arrangement in epidermal root cells was observed by taking Z-stacks, which were projected to 2D images afterwards. Actin filaments in DMSO-treated root cells of the uninduced knockdown against *VPS16* showed a longitudinal orientation and outlined the shape of the vacuole (Figure 23 A). After Dex treatment, the actin filaments formed spirals around the spherical vacuoles of the induced knockdown against *VPS16* (Figure 23 B). The same spiral arrangement was observed in the Dex-induced HOPS-

specific knockdown against *VPS41* (Figure 23 C). This shows that the actin filaments are intact in cells of the HOPS knockdown mutants in which multiple, spherical vacuoles are present. In the CORVET-specific knockdown against *VPS8*, the actin filaments were oriented in a longitudinal manner and outlined the vacuole similarly to the control treatment (Figure 23 D). In summary, the actin cytoskeleton is not affected by the loss of HOPS or CORVET and the actin filaments remain in close contact with the vacuolar membrane. In addition, the actin cytoskeleton was analyzed in two other mutants showing a spherical vacuole morphology: *gfs9-3* (Ichino et al., 2014) and *zig-1* (Kato, 2002) (Supplementary Figure 8). The actin filaments aligned in circles around the spherical vacuoles (Supplementary Figure 9) resembling the organization in the Dex-induced knockdown against *VPS16* and *VPS41*. This finding shows that vacuolar fragmentation occurs independently of the actin cytoskeleton in the examined vacuolar mutants.

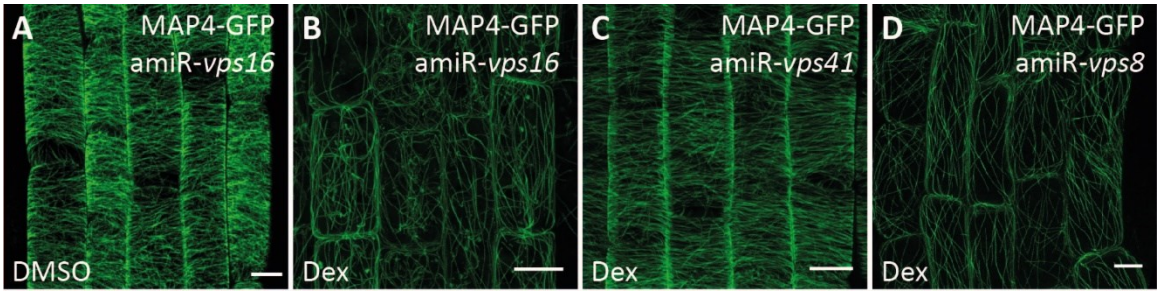


**Figure 24: Microtubule misalign in the Dex-induced knockdown against *VPS16* and the CORVET-specific subunit *VPS8*.** MAP4-GFP labeled microtubule filaments in seedlings with conditional knockdown treated with DMSO or 30 µM Dex for 72 hr. (A) Microtubule filaments aligned in the transversal direction to the root axis in DMSO treated roots of the knockdown against *VPS16* as control treatment. (B) In the Dex-treated knockdown against *VPS16* the microtubule filaments projected through the cell in an unordered manner. (C) Microtubule filaments in the Dex-induced knockdown against the HOPS-specific subunit *VPS41* aligned in the transversal direction similar to the DMSO control. (D) Microtubule alignment was disturbed in the Dex-induced knockdown against the CORVET-specific subunit *VPS8*. Scale bars are equal to 10 µm.

To test whether a disturbed microtubule alignment caused the spherical vacuole phenotype in HOPS knockdown mutants, the orientation of microtubules in the knockdown mutants was checked. Microtubule filaments labeled with MAP4-GFP (Microtubule Associated Protein 4; Marc et al., 1998) were aligned in parallel arrays perpendicular to the growth axis in the elongation zone of the DMSO treated knockdown against *VPS16* as control (Figure 24 A). A similar orthogonal alignment of microtubules was observed in root cells of the Dex-induced knockdown against

*VPS41* (Figure 24 C) indicating that a loss of the HOPS complex does not influence the microtubule arrangement. Also, the microtubule organization in the *gfs9-3* and *zig-1* mutants displaying a similar spherical vacuole phenotype in meristematic root cells was examined. Microtubules aligned properly in parallel filaments perpendicular to the direction of growth in root cells of *gfs9-3* and *zig-1* mutants (Supplementary Figure 10).

Upon Dex-induced knockdown against *VPS16*, the microtubule filaments lost their parallel arrangement and projected through the root cells in a disorganized manner (Figure 24 B). A similar disturbed arrangement of microtubules appeared in root cells of the Dex-induced CORVET-specific knockdown against *VPS8* (Figure 24 D). This observation indicates that the CORVET complex may play a role in microtubule orientation. However, radial swelling of root cells was not observed in the Dex-induced knockdown against *VPS16* or *VPS8* (Figure 24 B and D).

Inhibition of cell expansion was shown to result in microtubule redistribution (Panteris et al., 2013). Col-0 roots expressing MAP4-GFP treated for 20 hr with a high concentration of the auxin IAA (indole-3-acetic acid) , which inhibits root cell expansion and root growth (Sauer et al., 2013), showed an unordered orientation of microtubule filaments (Supplementary Figure 11) similar to the phenotype in the *VPS16* and *VPS8* knockdown.

Remarkably, the microtubule arrangement in young meristematic cells of the Dex-induced knockdown against *VPS16* exhibited parallel filaments similar to the DMSO control. The microtubule orientation became unordered and rather longitudinal in the transition zone from the meristematic to the elongation zone of the root (Supplementary Figure 12) indicating that the proper microtubule alignment is lost over time. Taken the reduced root growth of knockdowns against *VPS16* and *VPS8* into account, the microtubule misalignment is rather caused by the inhibition of root growth and does likely not result from a function of the CORVET complex in coordinating the microtubule cytoskeleton with subcellular trafficking.

In summary, the loss of HOPS does not lead to disruption of the actin cytoskeleton, which could have been the cause for the formation of multiple, spherical vacuoles.

Upon knockdown of HOPS, the actin filaments align spirally around the spherical vacuoles and seem to follow the shape of the fragmented vacuoles. The fragmentation of the vacuoles is the primary event followed by the disruption of an unknown mechanism that forms the vacuolar tubules. The disturbed microtubule alignment in the CORVET-specific knockdown occurs independent of vacuole morphology and likely is a secondary consequence of arrested root growth. The subcellular distribution of other factors that influence vacuole morphology remain to be examined, e.g., SNAREs (Löfke et al., 2015).

### 3.5.2 HOPS is required for maintaining the vacuolar network in the root meristem

To investigate the role of the HOPS and CORVET complex on vacuole development in more detail, vacuole morphology of Col-0 roots and the Dex-induced knockdowns was compared. Vacuolar lumen was stained with BCECF-AM and the lipophilic dye FM4-64 was used to simultaneously visualize the plasma membrane. The different developmental root zones, i.e., meristematic zone, elongations zone and differentiation zone, were observed to compare vacuole morphology.

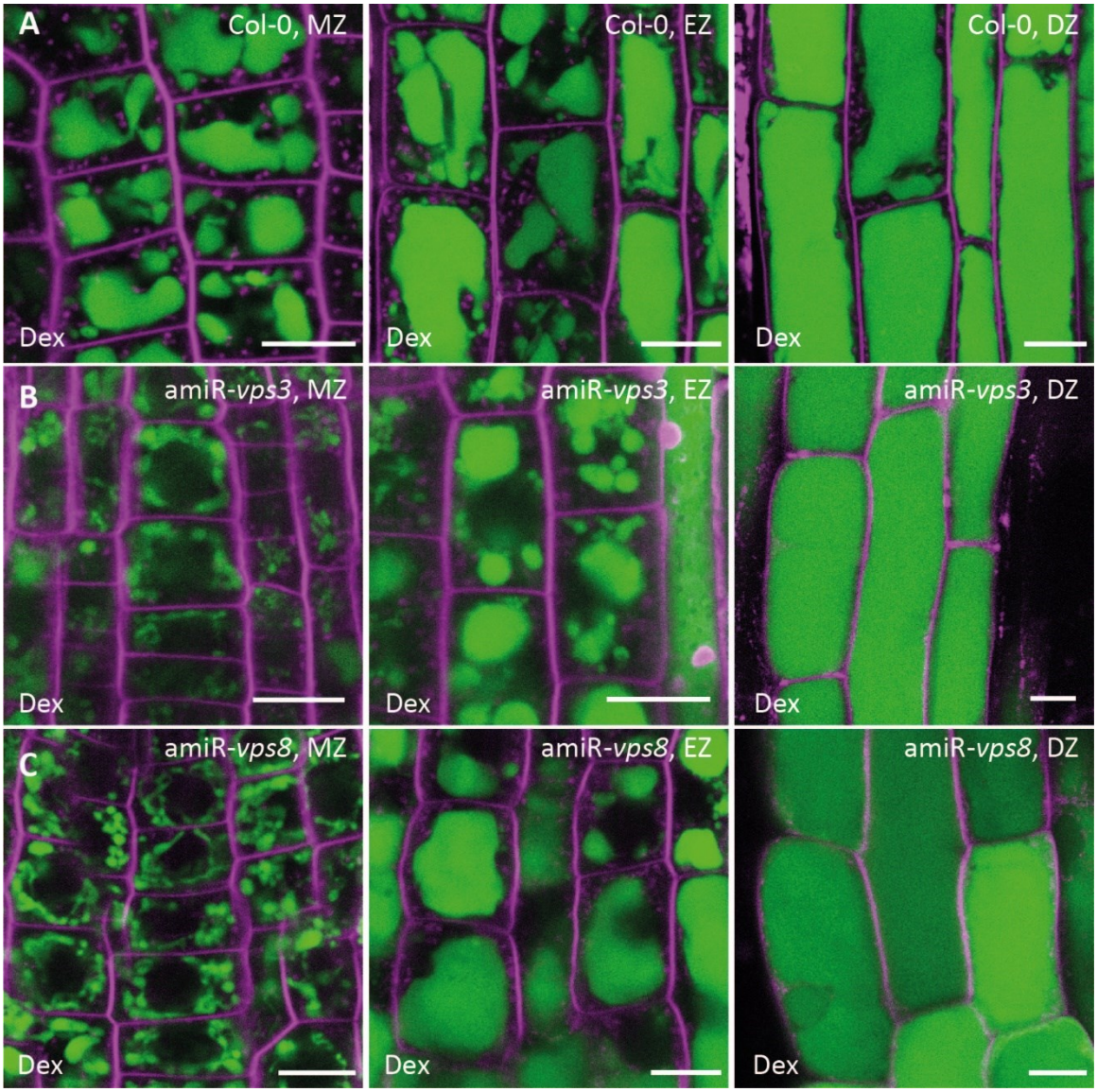


**Figure 25: The knockdown of CORVET-specific subunits leads to fine vacuolar tubules in the meristematic root zone and less constricted vacuolar subvolumes in the elongation zone of the root.** Seedlings were treated with 30 µM Dex for 72 hr and stained with 10 µM BCECF-AM and 1 µM FM4-64. Images were taken in different zones of the root:

meristematic zone (MZ), elongation zone (EZ) and differentiation zone (DZ). (A) Images show the vacuolar lumen of Col-0 root cells. (B) and (C) show the vacuole morphology after Dex-induced knockdown against the CORVET-specific subunits *VPS3* (B) or *VPS8* (C). Scale bars are equal to 10 µm.

In the meristematic root zone, vacuoles were composed of fine, convoluted tubules in the Dex-induced knockdown against the CORVET-specific subunits VPS3 and VPS8 (Figure 25 B and C). These tubules appeared to be thinner than the vacuoles in Col-0 (Figure 25 A). In the elongation zone, the vacuoles in the knockdown against VPS3 and VPS8 showed large subvolumes, which filled the cell volume as brick-like structures in the differentiation zone. However, cells in the differentiation zone were shorter than Col-0 cells in a comparable region (Figure 25).

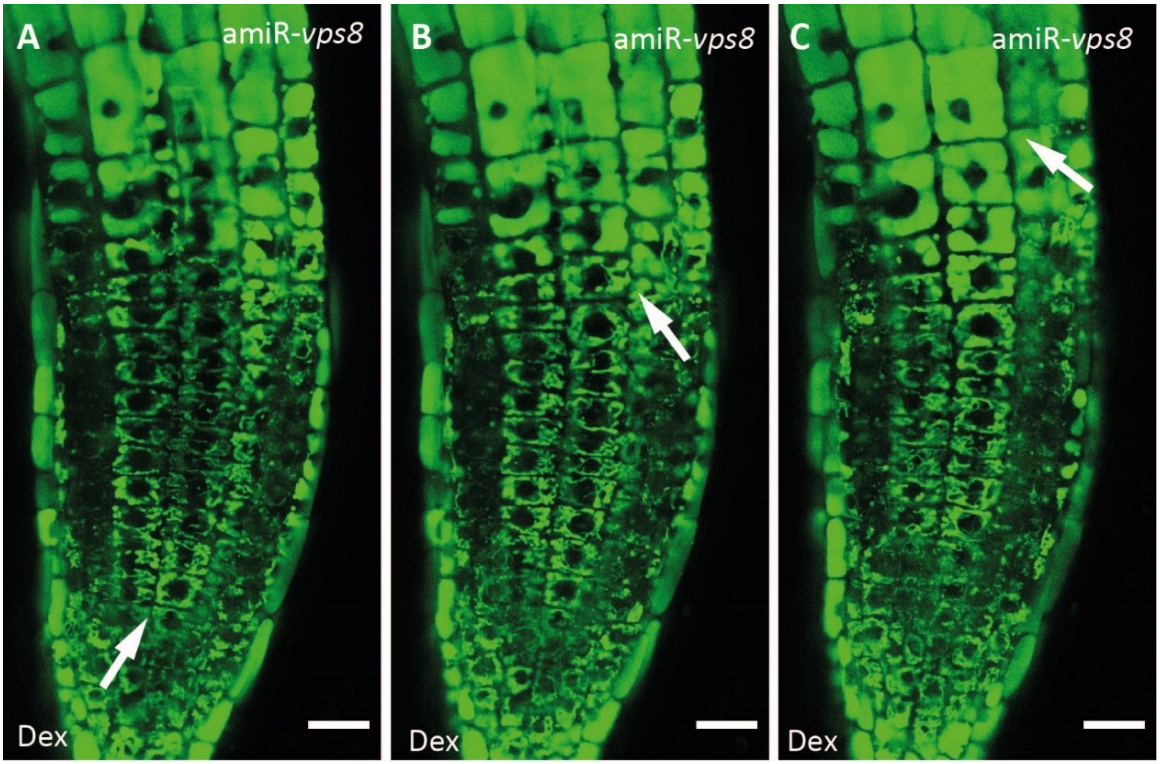


**Figure 26: The transition from highly convoluted to unconstrained vacuolar morphology occurs rapidly within a few cells in roots of the knockdown against the CORVET complex.** Seedlings were treated with 30 µM Dex for 72 hr. Images were taken in a distance of 0.17 µm in Z-direction to record the vacuolar volume of epidermal root cells. (A) Vacuoles close to the quiescent center in the CORVET-specific knockdown were composed of convoluted and constricted fine tubules. (B) In the beginning of the elongation zone, the vacuolar shape was altered to larger constricted subvolumes. (C) In the elongation zone, vacuoles form brick-like compartments filling the cell volume. Scale bars are equal to 20 µm.

To investigate the abrupt transition from narrow constricted tubules to a large, unconstrained vacuole volume in more detail, a Z-stack of a complete root tip of

the induced knockdown of *VPS8* was recorded (Figure 26). By observing single cell files, it became apparent that the change from fine tubules to brick-like vacuoles was accomplished within circa three cells. Thereby, vacuoles with the morphology of a differentiated state harbor cells, whose size is typical for the elongation zone (Figure 26).

The vacuole morphology upon knockdown of the CORVET-specific subunits is reminiscent of the effect of auxin (Löfke et al., 2015). This indicates that the effect on vacuole morphology after the knockdown of CORVET is not a direct consequence but rather a secondary effect of inhibited growth processes.

Sphere-like vacuoles in the Dex-induced knockdown against *VPS16* were shown to be fragmented (Dissertation Falco Krüger 2017). Sphere-like vacuoles were observed in the meristematic root zone, the elongation zone and in the early part of the differentiation zone of the knockdown against *VPS16*, *VPS39* and *VPS41* (Figure 27 B, C and D). As the spherical vacuole phenotype was observed in the HOPS-specific knockdown against *VPS39* and *VPS41* (Figure 17 and Figure 27), it can be concluded that the vacuolar fragmentation is caused by a lack of the HOPS complex.

Within the differentiation zone of the root, the shapes of the vacuoles appeared to be less round and more oval or egg-shaped (Figure 27 B, C and D; white arrows). As vacuolar fragmentation was most prominent in the meristematic and elongation zone, it was investigated whether the HOPS knockdown is only active in this part of the root. Therefore, the R-SNARE YFP-VAMP711, whose trafficking was shown to require the HOPS complex, was observed in the induced knockdown against *VPS16*. Here, the subcellular localization of YFP-VAMP711 was compared in the elongation zone (EZ) and late differentiation zone (Late DZ; which was marked by emerged root hairs) of individual roots.

In the DSMO control, YFP-VAMP711 localized to the tonoplast in the elongation zone as well as in the late differentiation zone (Figure 28 A, C and D). After inducing the knockdown against *VPS16*, YFP-VAMP711 mislocalized to punctae and the plasma membrane in the elongation zone (Figure 28 B). In the late differentiation zone, root cells with fragmented vacuoles could be found next to root cells with a

brick-like vacuole morphology. Also, fragmented vacuoles ranged from round to oval and egg-shaped in appearance (Figure 28 E).

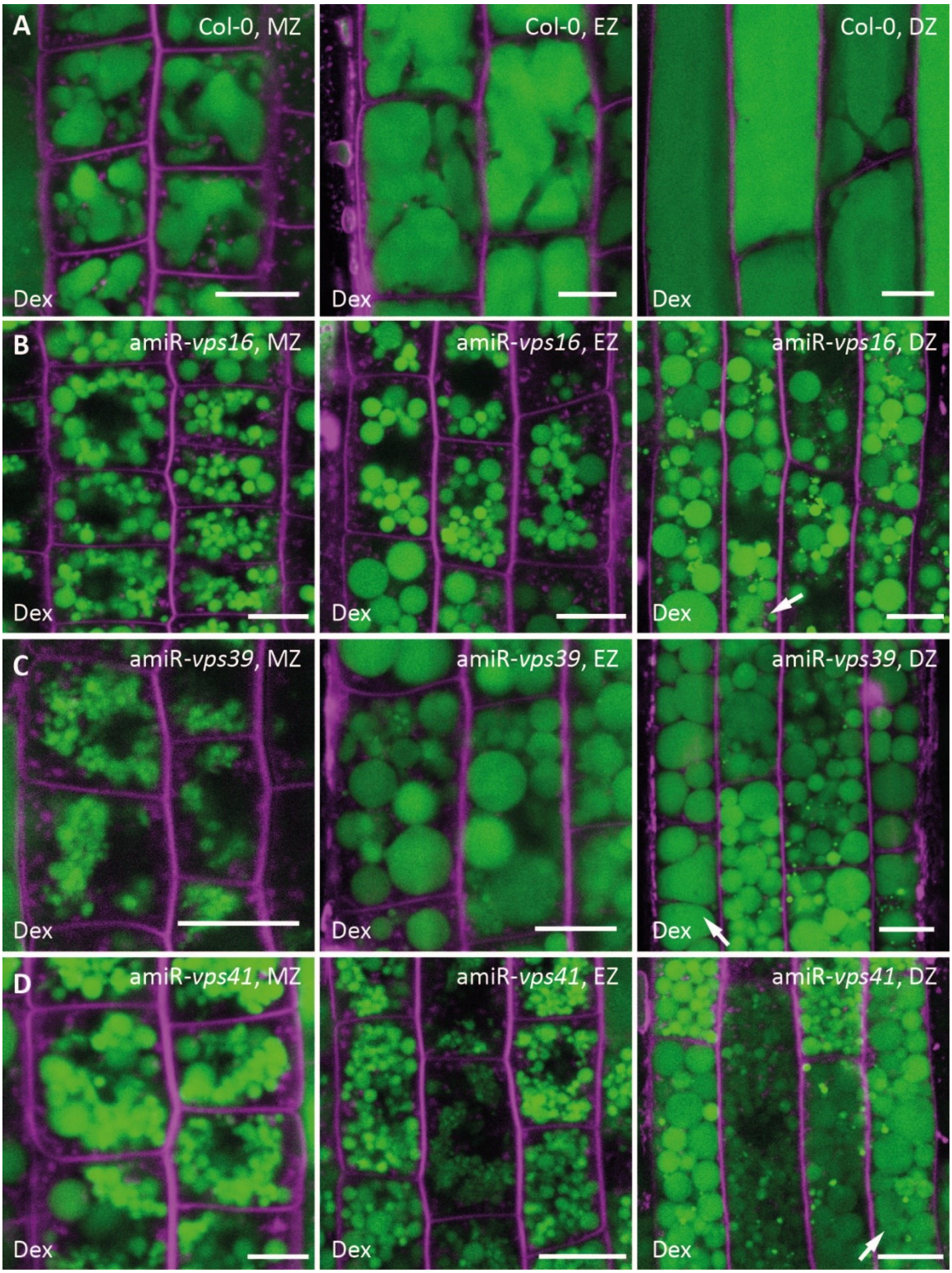


**Figure 27: The HOPS complex is required for homotypic vacuole fusion in Arabidopsis.** Seedlings were treated with 30 µM Dex for 72 hr and stained with BCECF and FM4-64. Images were taken in different zones of the root: meristematic zone (MZ), elongation zone (EZ) and differentiation zone (DZ). (A) Vacuole morphology in Col-0 root cells showed

constricted subvolumes. (B) Induced knockdown against the common subunit of HOPS and CORVET *VPS16* caused multiple spherical vacuoles. (C) and (D) After knockdown of the HOPS-specific subunits *VPS39* and *VPS41*, root cells showed multiple, spherical vacuoles. White arrows indicate the occurrence of oval and egg-shaped vacuoles in the differentiation zone of induced knockdowns. Scale bars are equal to 10 µm.

YFP-VAMP711 was mislocalized to punctae in root cells with fragmented vacuoles as well as in root cells with unaltered vacuole morphology in the late differentiation zone (Figure 28 E and F). Moving further towards the shoot, the cells were shorter compared to the DMSO control, but exhibited an unaltered, brick-like vacuole morphology (Figure 28 G). Even in these cell, YFP-VAMP711 was mislocalized to punctae (Figure 28 G and H) indicating that the knockdown of HOPS is functional even in root cells that do not show vacuolar fragmentation. Therefore, the occurrence of fragmented, spherical vacuoles seems to happen in undifferentiated root cells, in which the vacuole is subject to constant rearrangement processes likely caused by cytoplasmic streaming. Time-lapse recordings showed that vacuolar subvolumes are pinched off and fused again (Dissertation Falco Krüger 2017). These fission processes seem to rarely happen in differentiated root cells. This could explain the brick-like vacuole morphology in the late differentiation zone of the root after the knockdown of the HOPS complex. A second possible explanation is that meristematic root cells harbor separated, small vacuoles as described in Cui et al., 2018, which cannot fuse after the knockdown of the HOPS complex.

To investigate whether the fragmentation of the vacuole is the result of processes, in which subvolumes are pinched off from a connected, tubular network or whether separated small vacuoles cannot fuse, Z-stacks of the vacuoles in the epidermal cell layer over the complete root tip were recorded (Figure 29).

After the Dex-induced knockdown against *VPS16*, vacuoles in the quiescent center and close to the quiescent center showed the typical vacuolar network of constricted tubules as seen in Col-0 (Figure 29 A; white arrow). Based on this observation it can be concluded that the knockdown of VPS16 is likely not functional in and close to the quiescent center. In cells closely above the quiescent center, the vacuolar network slightly changed to a more rounded morphology

(Figure 29 B; white arrow). Circa 9 cells above the quiescent center, vacuoles were fragmented, spherical vacuoles (Figure 29 C; white arrow).

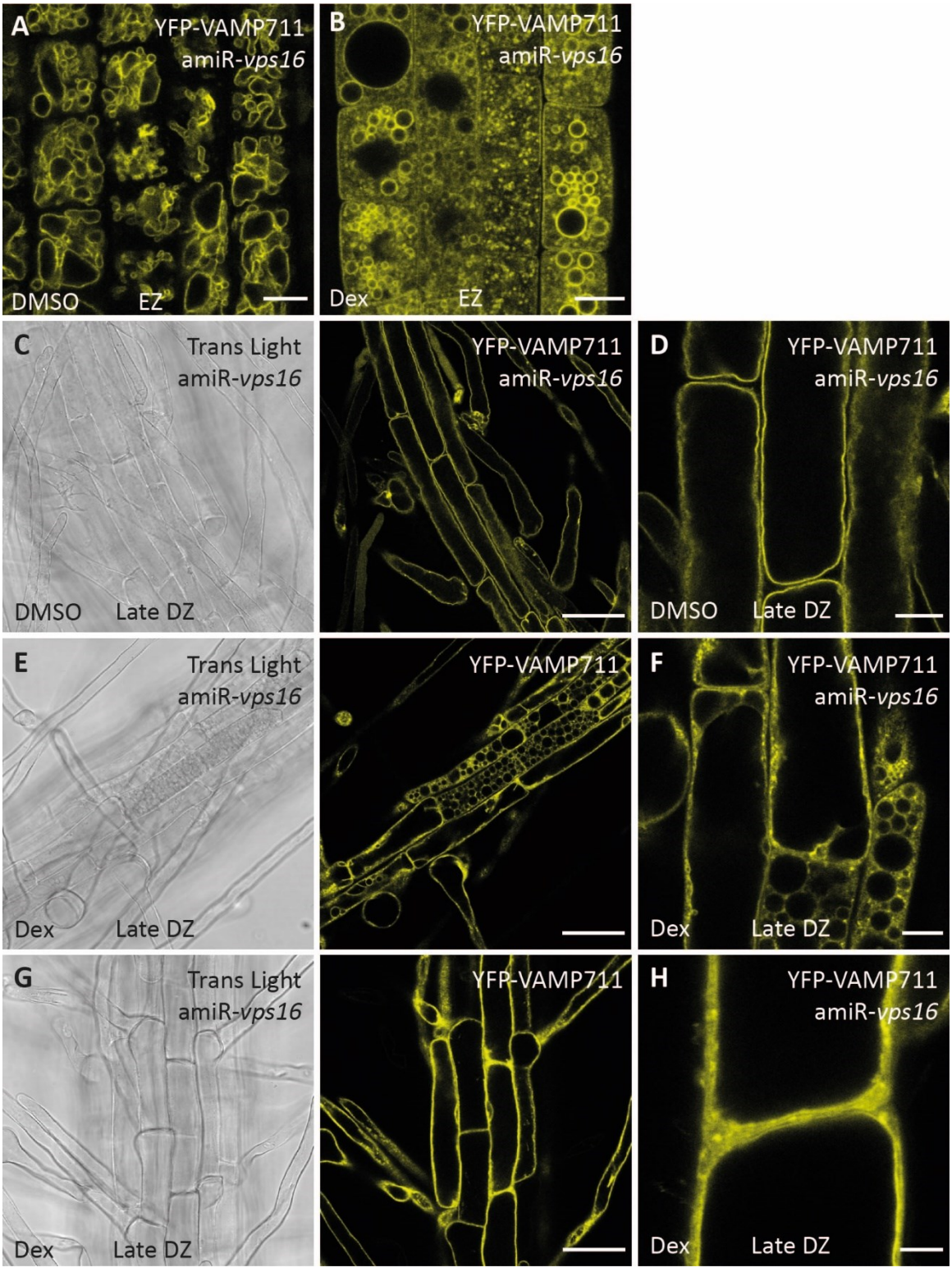


**Figure 28: The Dex-induced HOPS knockdown is not restricted to the root meristem.** After seedlings were grown for 5 days on ½ MS medium, they were incubated for 72 h in

liquid medium containing DMSO or 30 µM Dex. (A) + (B) show the elongation zone of roots expressing the R-SNARE YFP-VAMP711 in the DMSO control and Dex-induced knockdown against *VPS16*. (C) – (H) show the differentiation zone of the roots examined in (A) and (B) respectively in transmitted light (Trans Light) and YFP. (G) and (H) were taken in the late differentiation zone, in which no fragmented vacuoles could be observed. After Dex induction, the localization of YFP-VAMP711 is disturbed even in cells without vacuolar fragmentation. Scale bars in (C), (E), (G) are equal to 50 µm, in (A), (B), (D), (F) to 10 µm and in (H) to 5 µm.

According to Cui et al., 2018, cells in and close to quiescent center possess separated, small vacuoles. These vacuoles should be identifiable as fragmented vacuoles when stained with BCECF-AM, as BCECF-AM does not alter vacuole properties or morphology as shown with FRAP experiments and 3D renderings (Minina et al., 2021). However, vacuoles in and close to the quiescent center were constricted, tubular structures. This observation supports the assumption that the vacuole is a constricted network of tubules in meristematic root cells and that the fragmented vacuoles in the HOPS knockdown are the consequence of detached subvolumes, which cannot fuse back to the vacuolar network. Thus, the HOPS complex maintains vacuolar integrity.

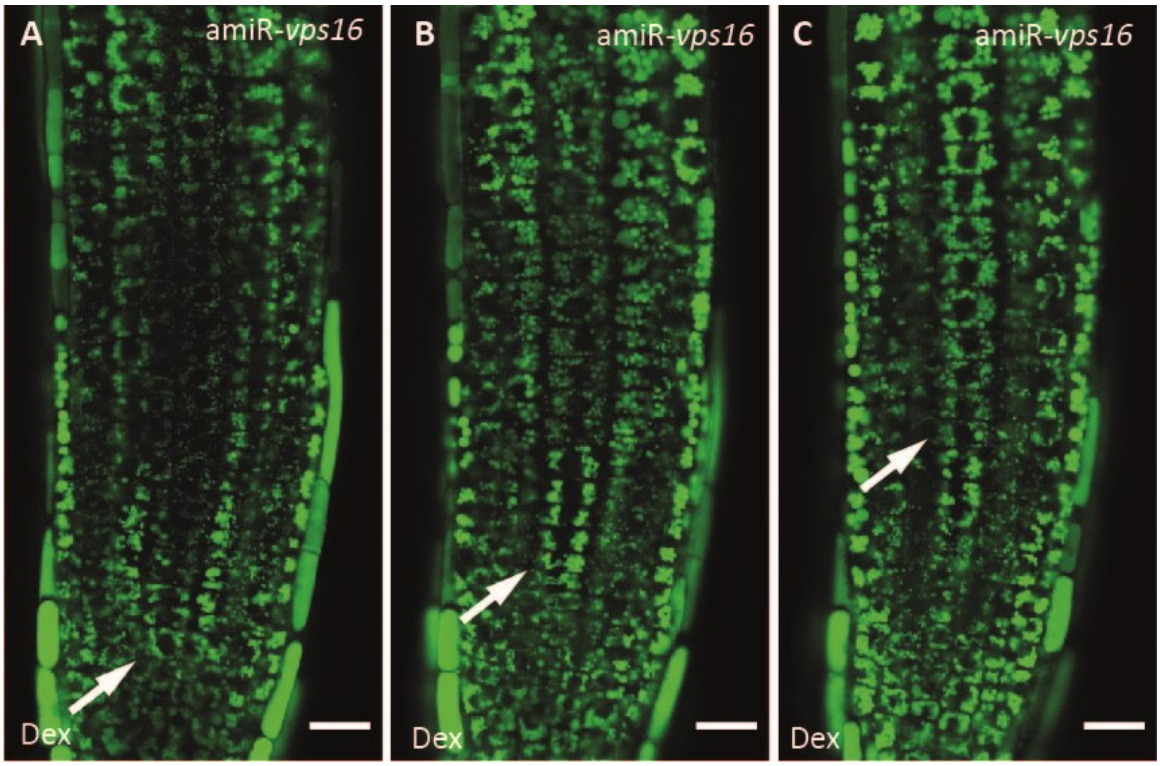


**Figure 29: Vacuoles in the root meristem are composed of a tubular network, whose integrity is maintained by the HOPS complex.** Seedlings of the Dex-induced knockdown against *VPS16* were stained with BCECF-AM to visualize the vacuolar lumen. Consecutive sections in the Z direction were taken to record vacuole morphology of single cell files

from the quiescent center along the developmental gradient of the root meristem. (A) After the knockdown of *VPS16*, vacuoles close to the quiescent center consisted of a network of constricted tubules. (B) The vacuolar network slightly changed shape in cells closely above the quiescent center. (C) Vacuoles were fragmented and showed the typical spherical shape caused by the loss of HOPS. Scale bars are equal to 20 µm.

### 3.5.3 Homotypic vacuole fusion occurs via vertex ring formation in Arabidopsis

To further investigate homotypic vacuole fusion, the localization of GFP-VPS16 was observed at the tonoplast labeled with VHA-a3-RFP or VHP1-mCherry. GFP-VPS16 accumulated at short stretches at the tonoplast, which colocalized with VHA-a3-RFP or VHP1-mCherry (Supplementary Figure 13). These short stretches may resemble fusion sites at the vacuole.

In yeast, fusion sites at the vacuolar membrane are marked with the signaling lipid phosphatidyl 3-phosphate (PI3P) (Wickner, 2010). In Arabidopsis, fusion sites in the HOPS knockdown could be initiated and arrested in the stage before SNARE tethering, which is controlled by the HOPS complex. Due to that, the localization of the PI3P marker 2xFYVE-GFP was analyzed. In DMSO treated seedlings of the *VPS16* knockdown, the PI3P marker 2xFYVE-GFP localized to punctae, which resemble MVBs, and faintly to the tonoplast (Supplementary Figure 14 A). After Dex-induced knockdown of *VPS16*, 2xFYVE-GFP accumulated at the tonoplast (Supplementary Figure 14 B), indicating that the signaling lipid PI3P is enriched at the tonoplast of fragmented vacuoles. As the distribution of the PI3P marker at the tonoplast was equally, no specific putative fusion sites could be determined.

In yeast, another factor necessary for fusion is the Rab7 GTPase, which binds to PI3P and acts an effector for the HOPS complex (Wickner, 2010). In Arabidopsis, the HOPS-specific subunit VPS39 was shown to colocalize with the RAB7 GTPase RABG3f at contact sites between two vacuoles (Takemoto et al., 2018). Therefore, the localization of mCherry-RABG3f and VHA-a3-GFP labeling the tonoplast was observed. In the uninduced knockdown against *VPS16*, mCherry-RABG3f mainly localized to punctae, which resembled MVBs, and faintly to the tonoplast (Figure 30 A). After Dex induction, mCherry-RABG3f accumulated at the tonoplast of the fragmented spherical vacuoles (Figure 30 B). As the accumulation of mCherry-RABG3f was equally distributed over the tonoplast, no specific fusion sites could be determined.

Since vacuole morphology changed to rounded, oval and egg-shaped structures at some point in the differentiation zone of the induced HOPS knockdown (Figure 27 and Figure 28), it could be assumed that membrane fusion events were initiated and arrested. To investigate putative fusion phenotypes, VHA-a3-GFP and mCherry-RABG3f were imaged in the differentiation zone of the Dex-induced knockdown against *VPS16*.

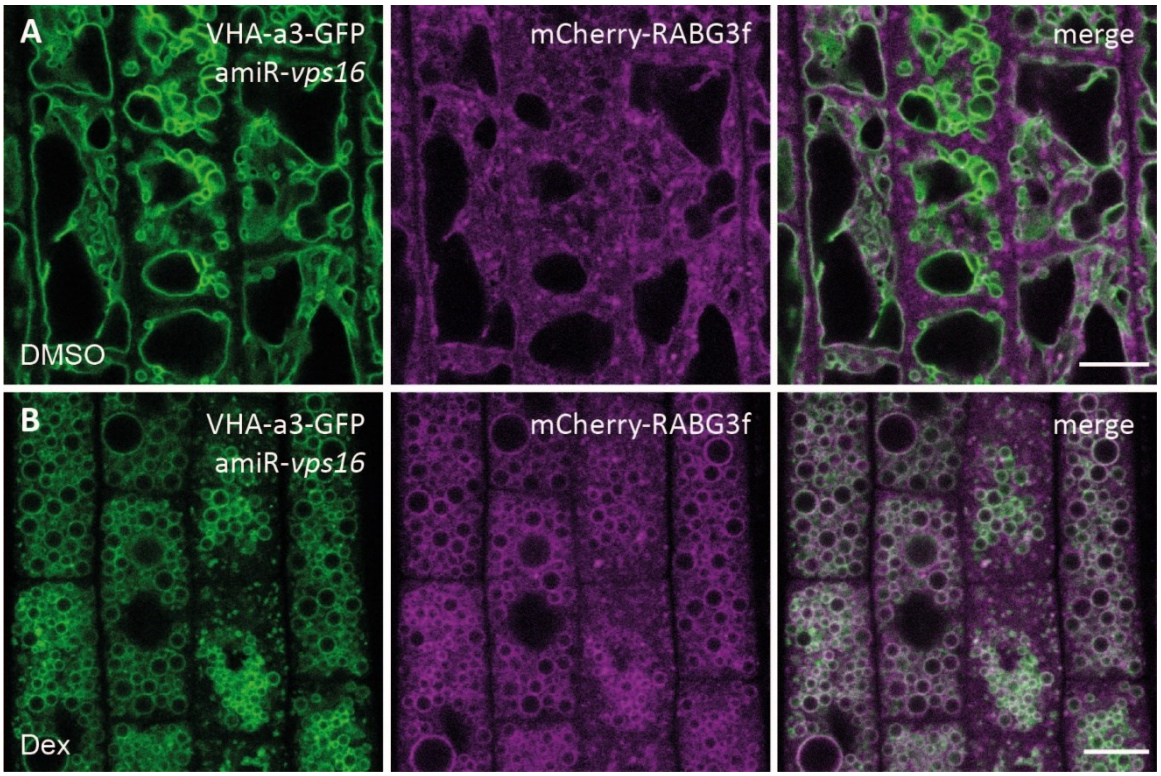


**Figure 30: The RAB7-GTPase mCherry-RABG3f accumulates at the tonoplast of fragmented vacuoles in the *VPS16* knockdown.** Seedlings were treated with DMSO or 30 µM Dex for 72 hr. (A) Under control conditions, the RAB7-GTPase mCherry-RABG3f localized to punctae representing MVBs and faintly to the tonoplast. (B) In the Dex-induced knockdown against *VPS16*, mCherry-RABG3f accumulated at the tonoplast of fragmented, spherical vacuoles. Scale bars are equal to 10 µm.

In the late differentiation zone of the root in the induced knockdown against *VPS16*, in which oval vacuoles can be observed, mCherry-RABG3f accumulated along stretches at contact sites between vacuoles. Within these stretches a decreased fluorescent signal from VHA-a3-GFP was recorded (Figure 31 A and B). Z-stacks were recorded to examine the distribution of mCherry-RABG3f and VHA-a3-GFP along these contact sites in more detail. Orthogonal views in XZ direction at two different contact sites showed that mCherry-RABG3f formed leaflets, which were surrounded by a ring-like structure labeled with VHA-a3-GFP (Figure 31 B to D).

These structures are reminiscent to the formation of vertex rings in homotypic vacuole fusion in yeast (Wickner, 2010). Therefore, homotypic fusion occurs via the formation of a vertex ring in Arabidopsis.

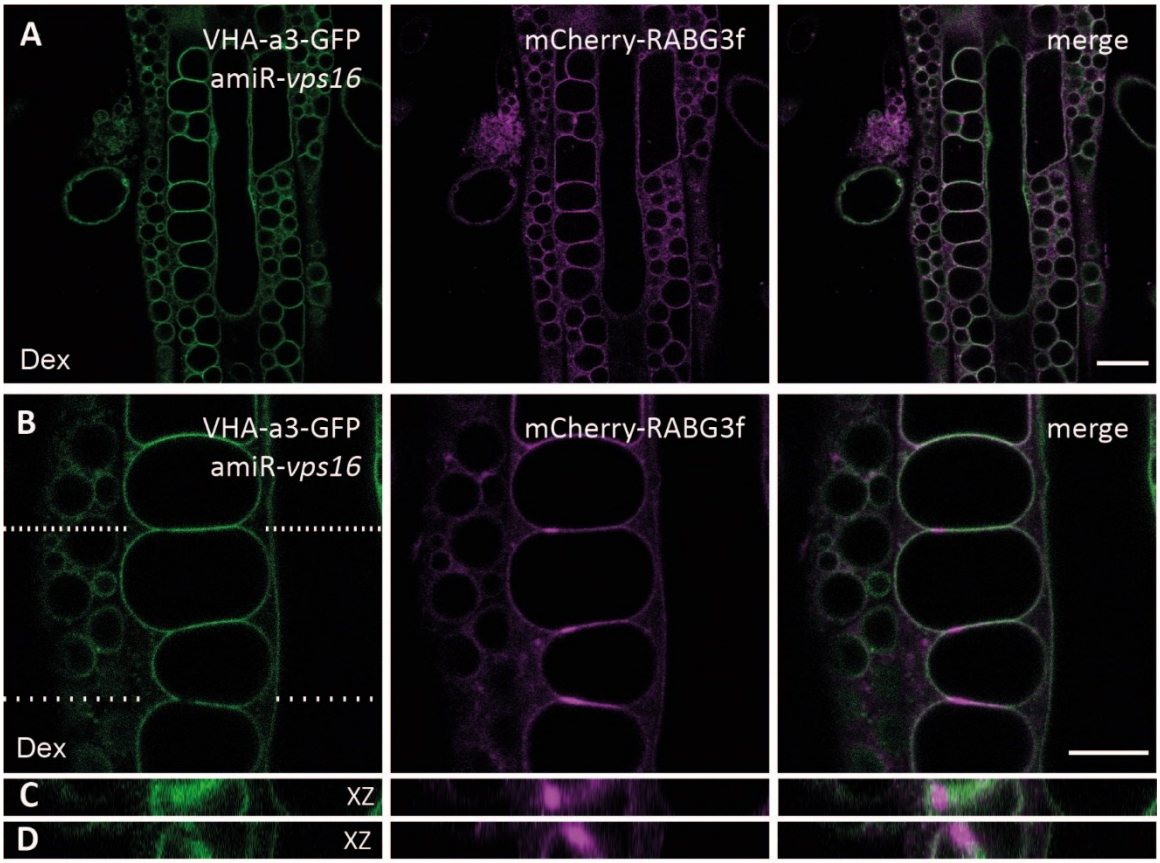


**Figure 31: The V-ATPase is eliminated from sites of vacuolar membrane fusion.** Seedlings were treated with 30 µM Dex for 72 hr to induce the knockdown of *VPS16*. (A) In the differentiation zone (DZ), vacuoles displayed a rounded, oval or elliptic shape. At stretches along the contact sites between two vacuoles, mCherry-RABG3f accumulated. (B) shows a single focus plain of a recorded Z-stack. Vacuoles with an oval and elliptic shape exhibited a decreased signal of VHA-a3-GFP at contact sites between vacuoles. At these sites, mCherry-RABG3f accumulated. (C) shows the orthogonal view of the vacuolar contact site marked with the upper, dense line. The orthogonal XZ view of the recorded Z-stack showed that the contact site contained a small fusion pore. VHA-a3-GFP accumulated at the nexus of the fusion pore and formed a ring-like structure, which enclosed a leaflet of mCherry-RABG3f. (D) displays the orthogonal XZ view of the vacuolar contact site marked with the lower line. The size of the vacuolar fusion pores varied in diameter. Scale bars are equal to 20 µm in (A) and 10 µm in (B).

### 3.5.4 The balance of PI3P at the vacuolar membrane is crucial for proper vacuole fusion

In yeast, the $V_0$ subcomplex of the V-ATPase plays a role in membrane fusion and fission of vacuoles, as the membrane-integral ring of the V-ATPase facilitates lipid mixing during homotypic vacuolar membrane fusion (Baars et al., 2007; Strasser et al., 2011). A previous publication showed that the round vacuoles in the *itt3* mutant of Arabidopsis, which lacks the Qb-SNARE VTI11, fuse with each other to form larger vacuoles after the application of Wortmannin (WM). This indicates that PI3P at the vacuolar membrane prevents homotypic fusion of vacuoles in the *itt3* mutant (Zheng et al., 2014b).

Thus, it was examined whether the fragmented vacuoles in the knockdown of *VPS16* fuse after the application of WM. To investigate a putative function of the V-ATPase in homotypic vacuole fusion in Arabidopsis, vacuole morphology was examined upon Dex-induced knockdown of *VPS16* in Col-0 as well as in the *vha-a2 vha-3* mutant, which lacks V-ATPase complexes at the vacuole.

Vacuoles in Col-0 roots treated with 33 $\mu$M WM did not show the typical vacuolar constrictions (Figure 32 A). The application of WM caused inclusions inside the vacuole, which were not stained with BCECF-AM (arrow). After adding WM and the V-ATPase inhibitor ConcA, the vacuoles displayed one large, rounded compartment lacking vacuolar constrictions. The vacuole phenotype was similar to the one after adding only WM, however, the vacuoles seemed to be slightly more oval in shape (Figure 32 A).

Separated vacuoles in the Dex-induced knockdown against *VPS16* fused after WM treatment and formed large vacuoles (Figure 32 B). The WM-induced fusion of separated vacuoles was not prevented by ConcA indicating that the vacuolar pH does not influence homotypic vacuole fusion.

In the *vha-a2 vha-a3* double mutant lacking V-ATPase complexes at the tonoplast, the Dex-induced knockdown of *VPS16* caused multiple, spherical vacuoles similar to the vacuole morphology in the *VPS16* knockdown in Col-0 (Figure 32 C). As the vacuolar fragmentation phenotype is caused by fission events of the vacuole, the spherical vacuoles in the *vha-a2 vha-a3* double mutant indicate that the V-ATPase

is not required for vacuolar fission events. After adding WM, the multiple round vacuoles fused to form larger compartments. Thus, vacuole fusion does not require the V-ATPase in root cells of Arabidopsis.

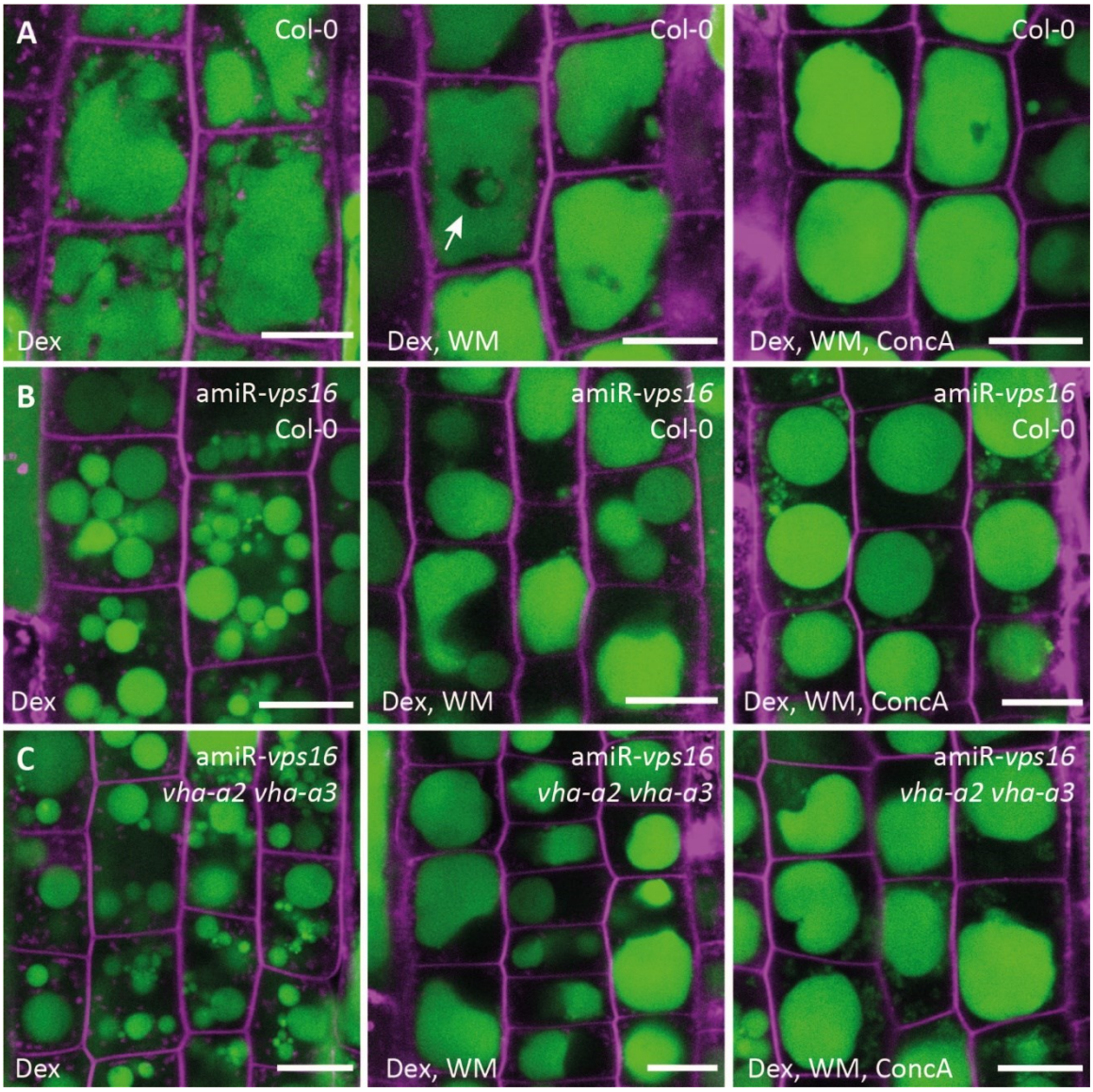


**Figure 32: Wortmannin (WM) induces the fusion of fragmented vacuoles caused by a lack of HOPS and the WM-induced homotypic vacuole fusion does not require the V-ATPase.** Seedlings of Col-0 and the knockdown against *VPS16* in Col-0 and in the *vha-a2 vha-a3* double mutant were treated with 30 µM Dex for 72 hr. To induce fusion of fragmented vacuoles, 33 µM WM was added for 4 hr. V-ATPase complexes were inhibited with 500 nM ConcA for 5 hr. Seedlings were stained with BCECF-AM and FM4-64 to visualize the vacuolar lumen and the plasma membrane. (A) Vacuoles in Col-0 lost the vacuolar constrictions after adding WM. Membranous inclusions formed inside the vacuole (arrow). (B) Fragmented vacuoles in the *VPS16* knockdown fused after adding WM. The fusion was not inhibited by adding ConcA. (C) In the *vha-a2 vha-a3* mutant fragmented vacuoles fused after WM treatment. ConcA did not prevent the WM-induced vacuolar fusion in the *vha-a2 vha-a3* mutant. Scale bars are equal to 10 µm.

Col-0 vacuoles lost the vacuolar constrictions after WM treatment and instead inclusions were formed inside the vacuole. The inclusions in the vacuolar lumen were not observed in Col-0 roots treated with Dex as control for the induced knockdown of *VPS16*. As vacuolar inclusions were not degraded, it can be concluded that a lack of PI3P impacts vacuolar pH and vacuole morphology.

In summary, PI3P accumulated at the tonoplast of fragmented vacuoles in the *VPS16* knockdown (Supplementary Figure 14) and by depleting PI3P with WM the fragmented vacuoles fused. This indicates that PI3P prevents vacuole fusion in the HOPS knockdown similar to the *itt3* mutant.

To further investigate the nature of the vacuolar inclusions and to learn more about the role of PI3P in fusion processes at the vacuole, seedlings expressing VHA-a3-RFP were stained with BCECF-AM to image the tonoplast and the vacuolar lumen at the same time. After WM treatment, vacuoles did not possess vacuolar constrictions or subvolumes in comparison to the DMSO control (Figure 33 A and B) and appeared as balloon-like volumes.

Membranous inclusions formed inside the vacuoles, which were labeled with VHA-a3-RFP, indicating that a part of the vacuolar membrane is pinched off inside the vacuole (Figure 33 B and C). Tonoplast-derived inclusions were partly stained with BCECF-AM (Figure 33 B and C) indicating that these inclusions enclosed vacuolar lumen.

To image the 3D structure of the WM-induced vacuolar inclusions, VHP1-GFP was used. The WM-induced vacuolar inclusions displayed various shapes like tubules and spheres. The inclusions exhibited a bright fluorescence, which points to the assumption that several layers of vacuolar membrane were convolved (Figure 33 D to F). Small vesicles budded from the tonoplast inwards into the vacuolar lumen (Figure 33 E and F) indicating that an inward-directed fission process causes the tonoplast-derived vacuolar inclusions.

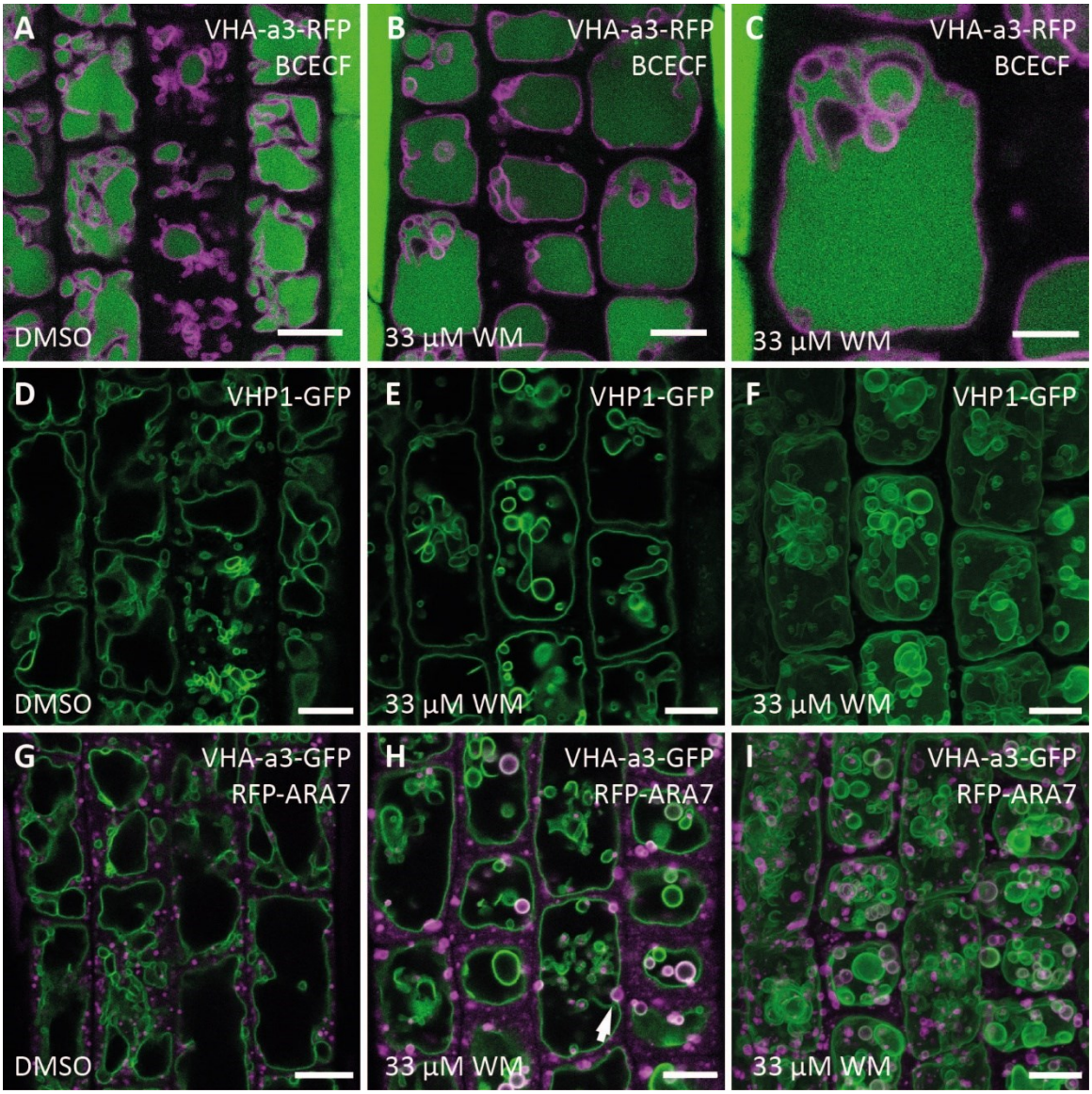


**Figure 33: Lack of PI3P leads to undirected fusion events at the vacuole.** (A to C) Roots expressing VHA-a3-RFP were treated with DMSO (A) or 33 µM Dex for 6 hr (B and C) and stained with BCECF-AM. (B) Vacuoles had an oval appearance and did not show constrictions after the application of WM. (C) Inclusions formed inside the vacuolar lumen, which consisted of vacuolar membrane labeled with VHA-a3-RFP. The lumen of inclusions were stained with BECECF or also not stained with BECF. (D to F) Seedlings expressing VHP1-GFP were treated with DMSO or 33 µM WM for 1 hr to observe the vacuolar membrane. (E) Vacuoles were not constricted and displayed a brick-like morphology in the elongation zone of the root. Inclusions consisted of variously shaped round and tubular structures. (F) In the projected Z-stack, inclusions appeared to contain multiple layers of tonoplast. Small vesicles of the tonoplast budded inwards into the vacuolar lumen. (G to I) Seedlings coexpressing VHA-a3-GFP and RFP-ARA7 in the amiR-*vps16* background were treated with DMSO or 33 µM WM for 1.5 hr. (H) Swollen MVBs/LEs labeled with RFP-ARA7 inside the vacuole were engulfed with a layer of tonoplast marked with VHA-a3-mRFP. (I) Projected Z-stack showed the dense accumulation of tonoplast-derived inclusions. Scale bars are equal to 10 µm, except scale bar in (C) is equal to 5 µm.

WM inhibits the PI3P-Kinase and causes the swelling of MVBs (Takáč et al., 2012). By imaging seedlings coexpressing VHA-a3-GFP and mRFP-ARA7, which marks early MVBs/LEs, it was tested for the presence of endosomes in the vacuolar inclusions. Both fluorescent markers were initially crossed to the Dex-inducible knockdown against VPS16, which remained uninduced for the experiment.

After WM application, swollen, ring-like structures labeled with mRFP-ARA7 were localized in the cytosol. In addition, enlarged mRFP-ARA7 vesicles were present inside the vacuole and were surrounded with an additional membrane layer of tonoplast marked with VHA-a3-GFP (Figure 33 G to I). Enlarged MVBs/LEs do not fuse with the tonoplast but seem to be engulfed with the vacuolar membrane. The tonoplast was deformed inwards to engulf swollen mRFP-ARA7 vesicles (Figure 33 H; white arrow).

Taken together, it can be assumed that the depletion of PI3P with WM leads to the suspension of directed fusion events at the vacuole. Instead, vacuolar constrictions are disintegrated and vacuoles form balloon-like structures with numerous membranous inclusions.

# 4 Discussions

## 4.1 HOPS and CORVET membrane tethering complexes are involved in vacuolar trafficking in Arabidopsis

In Arabidopsis, there are multiple trafficking pathways to the vacuole, which function at the same time. This establishes different transport routes for biosynthetic cargo to the vacuole. The function and importance of the transport routes are of interest to understand vacuole physiology, formation and development.

By now, four different trafficking pathways to the vacuole are known in Arabidopsis: Provacuoles (ER – vacuole), AP-3 vesicles (Golgi – vacuole), MVBs (TGN/EE – vacuole) and RAB5-positive LEs (TGN/EE – vacuole) (Ebine et al., 2014; Viotti et al., 2013; Wolfenstetter et al., 2012). Each transport pathway carries membrane and proteins to the vacuole. A detailed quantification of each transport pathway and its relation to the other transport routes may elucidate the importance of the individual pathway. More detailed investigation of the interplay between the different transport pathways and their contribution to vacuole development seems to be of particular interest for different cell types or developmental stages, where the contribution of the different transport pathways could vary. This study examined the role of the evolutionary conserved membrane tethering complexes HOPS and CORVET in mediating the different transport pathways at the vacuole in Arabidopsis.

Knockdown against the HOPS-specific subunit *VPS41* failed to produce vacuolar inclusions with autophagic content after ConcA treatment. This suggests that the HOPS complex mediates the fusion of autophagosomes with the vacuole, similar to the function of HOPS in yeast and mammalian cells (Balderhaar and Ungermann, 2013). Autophagosomes seem to play a neglectable role in vacuole development under normal growth conditions. The *atg* mutants do not show defects in vacuole development and autophagosomes do not seem to transport newly synthesized proteins to the vacuole (Michaeli et al., 2016).

To investigate the function of HOPS and CORVET in protein trafficking towards the vacuole in Arabidopsis, cargo proteins specific for distinct vacuolar trafficking pathways were used.

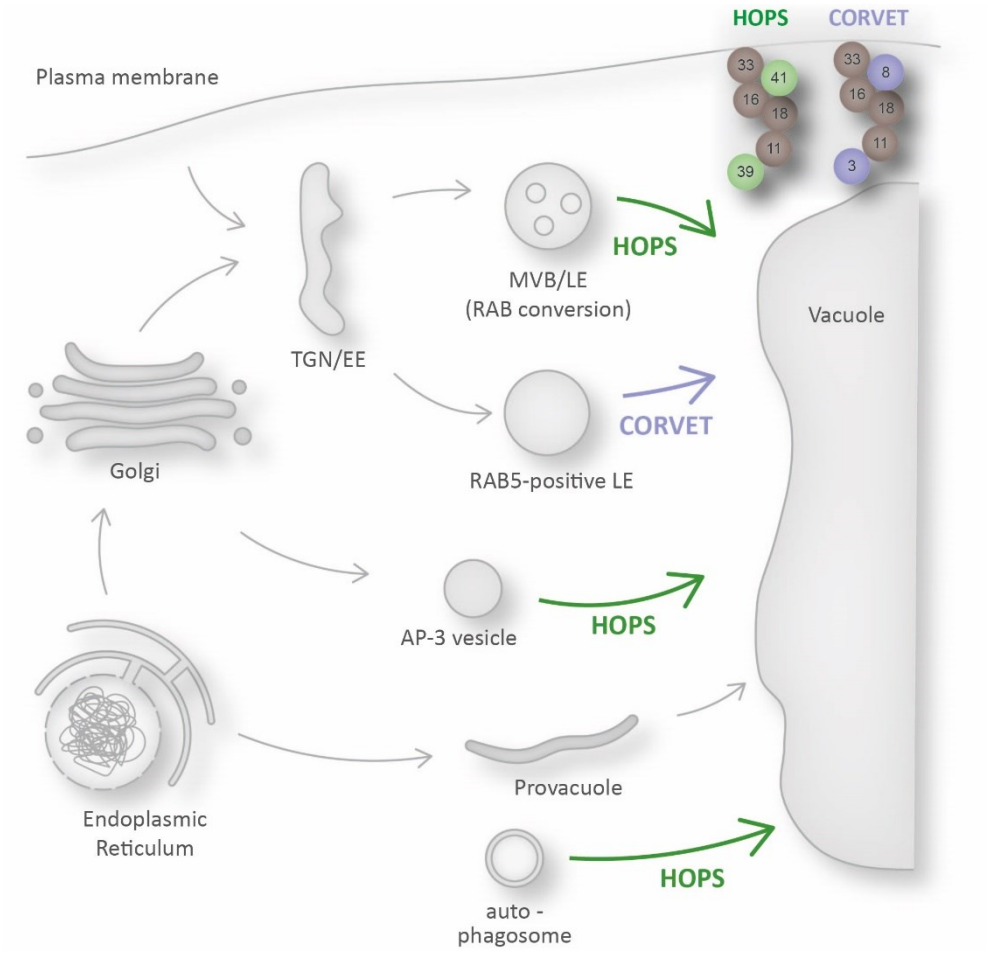


**Figure 34: The evolutionary conserved membrane tethering complexes HOPS and CORVET mediate membrane fusion events at the vacuole in Arabidopsis.** The HOPS complex is involved in the fusion events between autophagosomes, MVBs and AP-3 vesicles with the vacuole. The CORVET complex mediates a plant-specific trafficking pathway to the vacuole via RAB5-positive LEs (Takemoto et al., 2018). The action of HOPS is marked with green arrows and CORVET with a violet arrow.

In the CORVET-specific knockdown, INT1 mislocalized to the plasma membrane and the knockdown of the HOPS-specific subunit led to the accumulation of INT1 in punctae indicating that the trafficking of INT1 relies on CORVET as well as HOPS. This observation is supported by findings from other studies. Expression of ARA7-GDP, the inactive state of the RAB5 GTPase interacting with CORVET, caused mislocalization of INT1 to the TGN/EE and the plasma membrane (Feng

et al., 2017a). In the *mon1-1* mutant defective in MVB maturation, INT1 mislocalized to punctae (Feng et al., 2017b). In addition, vacuolar trafficking of INT1 also depends on RAB7 (Wolfenstetter et al., 2012). INT1 mislocalizes in *vps41-1* pollen showing that the HOPS complex mediates MVB-to-vacuole fusion (Feng et al., 2017a). Taken together, INT1 reaches the vacuole via MVBs that rely on the RAB conversion and by examining the vacuolar trafficking of INT1 it was possible to show that the HOPS complex mediates fusion events between MVBs and the vacuole, similar to the function of HOPS in yeast and mammalian cells. The CORVET complex may function in fusion processes of LEs or early MVBs prior to RAB conversion. This is also supported by the findings that the CORVET-specific subunit VPS3 localizes to MVBs (Delgadillo et al., 2020), but only interacts with RAB5 GTPases (Takemoto et al., 2018). This mechanism would be similar to the sequential action of CORVET and HOPS in the endo-lysosomal pathway in yeast and mammalian cells (Balderhaar and Ungermann, 2013). The molecular mechanism in plant cells remain to be determined.

VAMP711, an R-SNARE and cargo of AP-3 vesicles, mislocalized in the HOPS knockdown. This is in accordance with an independent study, which found that the AP-3 mediated trafficking pathway to the vacuole involves the HOPS membrane tethering complex like in yeast and animal cells (Feng et al., 2017a). The missecretion of VAMP711 to the plasma membrane can also be observed for CBL2 (CALCINEURIN B-LIKE PROTEIN 2), which mislocalized to the plasma membrane and TGN/EE in the ap3 mutant (Feng et al., 2017a).

The plant-specific trafficking route from the TGN/EE to the vacuole via RAB5-positive LEs (Takemoto et al., 2018) was investigated with the help of VTI11 and it turned out that the CORVET complex mediates fusion events between RAB5-positive LEs, which do not require the RAB conversion, and the vacuole. In yeast, CORVET mediates fusion between early and late endosomes, and HOPS between late endosomes and the vacuole. In plants, CORVET developed an new function to also act at the vacuole like HOPS (Ebine et al., 2014; Takemoto et al., 2018). So far it is not known whether RAB5-positive LEs facilitating the RAB conversion independent protein trafficking between the TGN/EE and the vacuole form

intraluminal vesicles (ILVs), similar to MVBs. The subcellular structure and morphology of RAB5-positive LEs remains to be determined.

The approach of investing the subcellular localization of different cargo proteins specific for different trafficking pathways after the Dex-induced knockdown against subunits of the HOPS and CORVET membrane tethering complexes was useful to determine the functions of HOPS and CORVET in vacuolar fusion in Arabidopsis. In metazoans, the HOPS and CORVET complexes diversified to fulfill additional functions.

In Drosophila, a mini-CORVET complex consists of the four subunits Vps8, Vps16A, Vps18 and Vps33A and mediates endosomal fusion events upstream of HOPS. The mini-CORVET seems to interact with Rbsn-5, another early endosomal tether in Drosophila cells (Lőrincz et al., 2016).

The mammalian CORVET complex is recruited via the interaction between Vps8 and Rab5 to tether early endosomes (EEs). In addition, Vps3 and Vps8 co-localize with the CHEVI complex on Rab11-positive recycling endosomes and mediate vesicular transport of Rab4-positive recycling vesicles from the EE to the recycling endosome. There are also indications that Vps3 and Vps8 might act as a heterodimer to recycle β1 integrins to regulate cell adhesion and migration (Jonker et al., 2018).

A subgroup of ciliates lost the HOPS-specific subunits, but the CORVET-specific subunit Vps8 expanded up to 6 paralogs in Tetrahymena. The isoform Vps8a associates with the late endosomal/lysosomal marker Rab7. Thereby, the CORVET complex executes HOPS-like functions indicating that a specificity switch occurred during the evolution of ciliates (Sparvoli et al., 2018).

In Arabidopsis, subunits of the CORVET and HOPS complex are encoded as single genes, which point to an evolutionary conservation. However, the CORVET complex evolved a new function in Arabidopsis and mediates fusion events at the vacuole with RAB5-positive LEs and the R-SNARE VAMP727 (Takemoto et al., 2018). So far, no evidence was found that CORVET or HOPS act in different complex compositions, i.e., mini-CORVET, in Arabidopsis (Brillada et al., 2018; Rojo et al., 2003; Takemoto et al., 2018).

## 4.2 Sar1b-GTP as genetic tool to block ER export to the Golgi

As Brefeldin A (BFA) does not inhibit COPII-mediated ER export in Arabidopsis, unlike in mammalian organisms (Richter et al., 2007), the GTP locked form of Sar1b (Sar1b-GTP) under the control of the Dex-inducible expression system was used to block ER-to-Golgi transport. Since Sar1b-GTP is permanently in the active state and binds to molecular interactors of Sar1b, it outcompetes the endogenous Sar1b over time and titrates away the molecular interactors of Sar1b. Thereby, an inhibitory situation for protein traffic from the ER to the Golgi is established.

As this mechanism was shown in yeast, mammalian cells, tobacco and suspension cells of Arabidopsis (Osterrieder et al., 2010; Takeuchi et al., 2000), the disruption of the COPII-route in Arabidopsis root cells was tested with proteins typically localized to the ER, Golgi and the plasma membrane. The Golgi marker ST (last 58 aa of the rat sialyl transferase; Boevink et al., 1998) and the plasma membrane localized BRI1 (Brassinosteroid Insensitive 1; Geldner et al., 2007) accumulated in the ER and were found in large punctae, at which Sar1b-GTP colocalized (Figure 4). In EM images ER tubules were swollen and Golgi cisternae collapsed after Dex induction (Figure 4). Therefore, the induced expression of the GTP-locked form of Sar1b blocks COPII-mediated ER export to the Golgi and secretory cargo is retained in the ER (Lupanga et al., 2020). As the punctate pattern of Sar1b did not overlap with the ER-localized VMA21 (Supplementary Figure 1) and Golgi remnants in EM images were highly vesiculated, it seems that the Sar1b punctae observed in vivo may be a mixture of COPII vesicles and Golgi remnants (Lupanga et al., 2020).

The punctae of VHA-a1 mostly overlapped with the Sar1b-GTP punctae after the addition of Dex (Figure 5). Likely not only the Golgi but also the TGN/EE is corrupted in the presence of Sar1b-GTP. By observing the effect of Sar1b-GTP on the TGN/EE-localized VHA-a1-GFP, not only was the response of the TGN/EE observed as a compartment in the secretory pathway, but also the difference in trafficking between VHA-a1 and VHA-a3 was underscored (Lupanga et al., 2020). In addition, the second proton pump at the vacuole, VHP1, was not retained in the

ER after Dex induction of Sar1b-GTP. Therefore, COPII-mediated trafficking is not required for the transport of VHA-a3 and VHP1.

The observation that VHA-a3 did not accumulate in the ER could have been also caused by a degradation process in the ER, an insufficient amount of newly synthesized protein, a relatively high turnover rate or a different timing of Dex induction in different Arabidopsis lines. Thus, further experiments were performed to investigate alternative scenarios.

The chimeric protein VHA-a3-a1-TD (Lupanga et al., 2020), which consists of VHA-a3 with the targeting domain of VHA-a1, accumulated in the ER after Dex-induced expression of Sar1b-GTP-CFP but did not localize to the typical Sar1b-GTP punctae (Figure 5; Lupanga et al., 2020). It seems likely that the information for the Sar1b specificity is encoded in a different part of VHA-a1. In addition, the chimeric protein accumulated in the ER without being specifically recognized by Sar1b. This further supports the finding that the COPII route is collapsed by expressing Sar1b-GTP regardless of Sar1 isoform specificities in cargo recognition.

The ER retention of VHA-a3-a1-TD and the observation that the proteasomal inhibitor MG132 had no effect on VHA-a3 after expression of Sar1b-GTP indicate that the lacking ER retention of VHA-a3 is unlikely to be caused by degradation or a low amount of newly synthesized VHA-a3. However, it cannot be out ruled that VHA-a3 may be degraded by the ER-associated degradation (ERAD) pathway (Liu and Li, 2014).

The three-color imaging approach allowed to monitor the disruption of the COPII-mediated pathway simultaneously with the localization of VHA-a3 (Figure 6, Supplementary Figure 3). Thereby, the possibility that a difference in the timing of Dex induction caused the lack of VHA-a3 accumulation in the ER could be ruled out.

To determine the Golgi-dependency of tonoplast-localized proteins, the ER retention of a given protein was examined after Dex-induced expression of Sar1b-GTP. Proteins, which showed no accumulation of fluorescence in the ER, are likely to be transported to the vacuole without passing through the Golgi. These are potential candidates for taking the provacuolar route and require further

examination. The tonoplast-localized protein ERDL6 did not accumulate in the ER after expressing Sar1b-GTP indicating that the trafficking of ERDL6 may be Golgi-independent. Finding more tonoplast-localized proteins, which are transported in a Golgi-independent manner via provacuoles, would indicate that provacuoles do not exclusively transport vacuolar proton pumps to the vacuole. As there is no information about the vacuolar trafficking of ERDL6 in the literature, the membrane trafficking of ERDL6 must be further investigated with the help of trafficking mutants, e.g., *ap-3* mutant, *mon-1* mutant, etc.

It would also be interesting to investigate the trafficking of the Calcineurin B-like (CBL) proteins CBL2, CBL3, CBL6, CBL10. These proteins are tonoplast-localized and transient expression assays using the dominant-negative mutant of the Sar1 tobacco protein demonstrated that CBL10 does not require the COPII pathway for correct localization (Batistič et al., 2009). Therefore, these proteins could also be studied as putative candidates for provacuolar cargo.

Vacuolar trafficking of AHA10 is Golgi-dependent in root cells of Arabidopsis as AHA10 accumulated in the ER and in Sar1b punctae (Figure 7). After 6 hr of Dex induction AHA10 was still detected at the tonoplast. Likewise, residual signal of BRI1 was detected at the plasma membrane (Figure 4). Probably, existing protein populations at the target compartments are not degraded within 6 hr of Dex induction.

VTI11 was shown to be transported through the TGN/EE and interacts with other vacuolar SNAREs (Ebine et al., 2008; Sanderfoot et al., 2001; Uemura et al., 2004). A lower degree of ER retention was observed for tonoplast-localized VTI11 compared to AHA10. The accumulation of VTI11 in the ER was best observed at the cell edges (Figure 8). It is likely that VTI11 is transported via the COPII-mediated ER export but is not specifically recognized by the Sar1b isoform. However, the low ER retention could also be caused by increased degradation in the ER, a low rate of protein biosynthesis, or variations in Dex induction.

For VAMP711 and SUC4, both transported with the AP-3 pathway to the vacuole, no retention in the ER was observed. However, when SUC4 localized to the Golgi in the pat2-2 mutant impaired in the formation of AP-3 vesicles, SUC4 accumulated

in the ER and Sar1b punctae (Figure 8). This indicates that the vacuolar trafficking of SUC4 is COPII-dependent. The Sar1 isoforms were proposed to have different cargo specificities in Arabidopsis (Chung et al., 2016) and vacuolar proteins transported by the AP-3 pathway were indicated to be specific for Sar1c (Feng et al., 2017a). With the conditional expression of Sar1b-GTP used in this study, the isoform specificity can be neglected as the Golgi is corrupted and protein trafficking through the Golgi is not possible. It also may be that VAMP711 and SUC4 are degraded in the ER or that not enough new protein is synthesized so that an accumulation in the ER cannot be observed. Further experiments are needed to clarify why tonoplast-localized proteins that are transported via the Golgi and/or TGN/EE show different reactions to Sar1b-GTP. Nonetheless, the subcellular distribution of VHA-a3 after Dex induction of Sar1b-GTP were studied regarding a degradation process in the ER or a low rate of newly synthesized protein. The results support the finding that VHA-a3 can exit the ER via a COPII-independent route.

In Arabidopsis, Sar1 diversified to five paralogs, which likely recognize different cargo (Chung et al., 2016; Zeng et al., 2015). By using the dominant-negative form of the Sar1b isoform, Golgi stacks dissolved, and secretory cargo accumulated in the ER. This demonstrates that the COPII-mediated ER export was disrupted, and protein traffic was not functional after the expression of Sar1b-GTP. To dispel any remaining doubts, the effects of the GTP-locked form of the isoform Sar1c on the trafficking of secretory cargo could be examined. In addition, the overexpression of Sec12, the guanine nucleotide exchange factor for Sar1, was shown to also block COPII-mediated ER export (daSilva, 2004). As Sec12 is a single-copy gene Arabidopsis, the overexpression could be performed under an inducible expression system to conditionally block protein traffic to the Golgi.

Triple color imaging could also be performed with a red fluorescent fusion of VHA-a3 under the control of the estradiol inducible expression system. After blocking COPII-mediated ER export, the trafficking of freshly synthesized VHA-a3 could be followed to underscore the Golgi-independency and would be a direct proof that VHA-a3 can leave the ER even if the COPII-mediated route is disrupted. This

approach could also be performed for additional tonoplast-localized proteins of interest.

In summary, by using the dominant-negative form of Sar1b to block COPII-mediated transport, further proof was provided that the TGN/EE-localized V-ATPase requires the COPII pathway to exit the ER, whereas the tonoplast-localized V-ATPase can exit the ER independently of the COPII pathway. As Golgi and TGN/EE proteins are retained in the ER by using Sar1b-GTP, it is a useful tool to detect proteins, which pass through the Golgi and the TGN/EE. Putative candidates that take the COPII-independent pathway have been identified. However, the use of Sar1b-GTP also showed limitations. Tonoplast proteins transported by the AP-3 pathway were not retained in the ER after blocking the COPII pathway in Col-0. This illustrates the importance of manipulating and inhibiting trafficking pathways with the help of different approaches to reach a reliable conclusion, e.g., loss-of-function mutants or the expression of dominant-negative GTPase forms.

## 4.3 Tonoplast-localized proton pumps can take two routes to the tonoplast

Certain mutations in the targeting domain of VHA-a1 (VHA-a1-TD), which is crucial for the TGN/EE localization of VHA-a1, lead to a dual localization of VHA-a1 at the TGN/EE and the tonoplast. After blocking COPII-mediated ER export to the Golgi with Sar1b-GTP, the tonoplast localization of VHA-a1-TD mutants increased (Lupanga et al., 2020). This indicates that the VHA-a1-TD mutants are preferably transported via a Golgi-independent trafficking pathway when ER export to the Golgi is not possible. This observation also supports the finding that VHA-a isoforms are not degraded in the ER when the COPII route is disrupted but leave the ER via a Golgi-independent pathway.

In addition, the tonoplast localization of the VHA-a1-TD mutants was also increased in the *vha-a2 vha-a3* mutant. Since no competing VHA-a isoforms remain, the mutated VHA-a1 proteins are more easily sorted into the Golgi-independent route (Lupanga et al., 2020). Similarly, the non-pumping mutant of VHA-a3, VHA-a3R729N, is retained in the ER in Col-0 but localizes to the tonoplast

in the *vha-a2 vha-a3* mutant (Neubert, 2012). Therefore, it can be concluded that the volume for cargo transportation into the Golgi-independent route via provacuoles is variable and adapts to the closure of Golgi-mediated trafficking and to the need of V-ATPase complexes.

Blocking COPII-mediated ER export in an independent approach with the BFA-sensitive GNL1 (GNL1-BFA$^S$) had no effect on the trafficking of VHA-a3 (Viotti et al., 2013). The conditional expression of Sar1b-GTP supports the finding that the trafficking of VHA-a3 and VHP1 does not require COPII-mediated ER export and that the tonoplast-localized proton pumps can take a Golgi-independent route. This Golgi-independent trafficking of the tonoplast-localized proton pumps is mediated by provacuoles. Early stages of provacuoles can be spherical and have a double membrane reminiscent of autophagosomes (Viotti et al., 2013). However, the knockout of autophagy-related genes (ATG) is not required for the trafficking of VHA-a3 (Viotti et al., 2013).

Further investigations about the vacuolar trafficking of the tonoplast-localized proton pumps were concerned with the manipulation of post-Golgi trafficking to underscore the Golgi-independent vacuolar trafficking of VHA-a3. Inhibiting the AP-3 pathway from the Golgi to the vacuole with using the *pat2-2* mutant as well as inhibiting the MVB formation with the *ccz1/mon1* mutant had no effect on the transport of VHA-a3 (Feng et al., 2017b; Viotti et al., 2013). And also the application of BFA or monensin, which disturb trafficking at the TGN/EE, did not alter the trafficking of VHA-a3 (Viotti et al., 2013; Figure 13, Figure 14). In addition, the knockdown against the HOPS complex, which mediates membrane fusion between the vacuole and autophagosomes, AP-3 vesicles and MVBs, did not influence the transport of the tonoplast-localized V-ATPase (Figure 18, Figure 19, Supplementary Figure 7). In the mentioned scenarios of blocking the Golgi and post-Golgi pathways at different points the tonoplast-localized V-ATPase does not show a change in vacuolar trafficking (Figure 35).

The *vha-a1* knockout mutant shows no phenotype in the sporophytic phase but is gametophyte lethal and pollen cannot develop. This indicates that VHA-a3 is at least able to replace VHA-a1 during the vegetative growth phase (Lupanga et al., 2020). The other way around, the mutated VHA-a1-TD proteins, which localize to

the TGN/EE and tonoplast, show a more acidic pH in vacuoles than the *vha-a2 vha-a3* mutant but cannot complement vacuolar pH to Col-0 levels (Lupanga et al., 2020). It is likely that different regulatory mechanisms, pumping activity, proton coupling or interaction partners of the V-ATPases prevent that a complete functional substitution is possible.

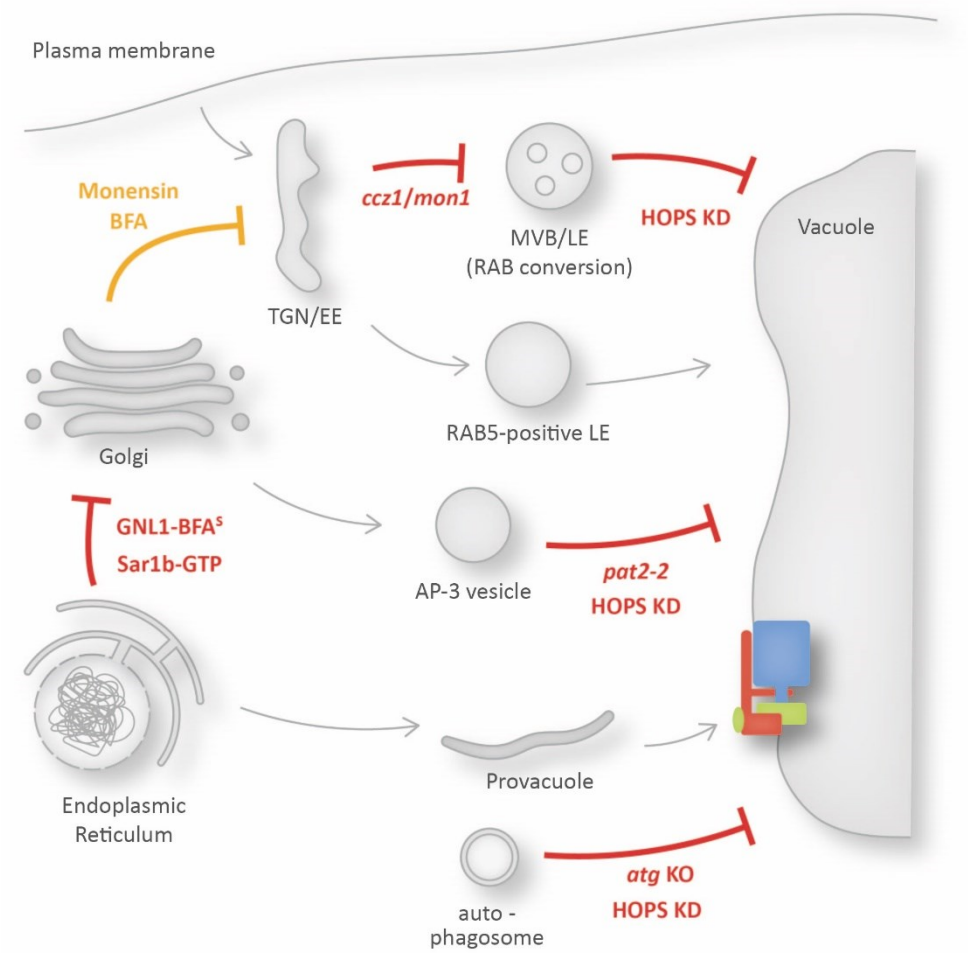


**Figure 35: Scheme summarizing the scenarios, in which Golgi or post-Golgi trafficking pathways to the vacuole are blocked, favoring the Golgi-independent transport of the tonoplast-localized V-ATPase via provacuoles to the tonoplast.** The scheme summarizes the findings on the trafficking of the tonoplast-localized V-ATPase from the present study and published literature, in which inhibition of Golgi and post-Golgi routes did not influence the trafficking of the tonoplast-localized V-ATPase (Feng et al., 2017b; Viotti et al., 2013). Trafficking pathways were inhibited with pharmaceuticals (yellow arrows) and genetic mutations (red arrows). Viotti et al., 2013 showed that the trafficking of VHA-a3 is not altered in *atg* knockout mutants and the *pat2-2* mutant, which is impaired in protein traffic from the Golgi to the vacuole. In addition, the application of BFA and the block of COPII-mediated ER export with the BFA-sensitive GNL1 (GNL1-BFA$^S$) had no effect on the transport of VHA-a3 (Viotti et al., 2013). In the *ccz1/mon1* mutant, which cannot form

MVBs, the trafficking of VHA-a3 was not altered (Feng et al., 2017b). Further evidence shows that neither the expression of Sar1b-GTP (Lupanga et al., 2020), the application of monensin, nor the knockdown against the HOPS complex influences the proper trafficking of VHA-a3. In these scenarios the tonoplast-localized V-ATPase is transported in a Golgi-independent manner via provacuoles to the tonoplast.

Conditional expression of VHA-a3 under the Dex or estradiol inducible expression system caused mislocalization of VHA-a3 at the TGN/EE (Figure 11, Figure 12). The original constructs for constitutional expression of VHA-a3 used the endogenous promotor and the resulting protein is exclusively localized to the tonoplast (Brüx et al., 2008; Dettmer et al., 2006). With conditional expression it is likely that the high amount of synthesized VHA-a3 could not only be transported through provacuoles and led to the additional sorting of VHA-a3 into the trafficking route via the TGN/EE. Inducible expression systems may be subject to processes that diminish the activated transcriptional outcome. This may explain why TGN/EE localization was observed in only a subset of the roots studied.

After inhibiting V-ATPase activity with ConcA the tonoplast-localized proton pumps accumulated at the TGN/EE (Figure 13 and Figure 15). In this study, 500 nM ConcA was applied for 5 hr, whereas 1 $\mu$M ConcA was used for 3 hr or 12 hr in Viotti et al., 2013 to examine the trafficking of VHA-a3 or VHP1. Kinetic measurements of vacuolar pH after application of ConcA to inhibit V-ATPase activity showed that vacuolar alkalinization occurs more slowly with 500 nm ConcA than with 1 $\mu$M ConcA and that 1 $\mu$M ConcA is the concentration at which maximum inhibition is reached (Holzheu et al., 2021). This finding may explain the observation that ConcA had no effect on the localization of VHA-a3 as described in Viotti et al., 2013. The concentration of 500 nM ConcA is probably not sufficient to inhibit all V-ATPase complexes. However, 500 nM ConcA induces the trafficking of the non-pumping mutant VHA-a3R729N, which is retained in the ER under standard conditions (Neubert, 2012; Figure 13). Partial inhibition of V-ATPase complexes seems to temporarily overrule an ER-based quality control as the need for V-ATPase complexes at the TGN/EE is high. ConcA treatment of estradiol inducible VHA-a3 shows that freshly synthesized VHA-a3 is transported to the TGN/EE. Thereby, ConcA may lead to an enhanced sorting of VHA-a3 into COPII vesicles and the Golgi-dependent route.

The knockdown of CORVET lead to the mislocalization of VHA-a3 and VHP1 to the TGN/EE. After expressing the dominant-negative form of the RAB5-GTPase ARA7 (ARA7-GDP) VHA-a3 can be found at the TGN/EE indicating that RAB5-positive LEs transport the tonoplast-localized proton pumps to the vacuole when VHA-a3-containing V-ATPase complexes are sorted into the Golgi-dependent pathway.

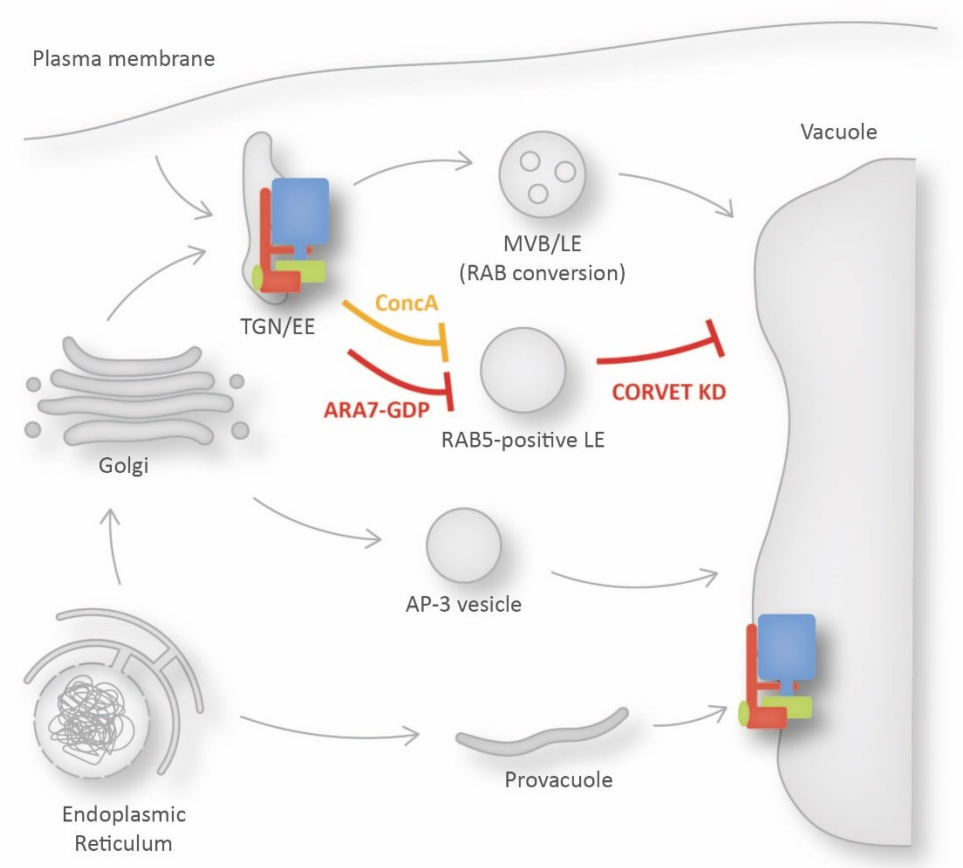


**Figure 36: The population of the tonoplast-localized V-ATPase that takes the Golgi-dependent pathway through the TGN/EE relies on the CORVET mediated pathway to the vacuole.** The population of VHA-a3/VHP1, which is transported via the TGN/EE, requires the fusion of RAB5-positive LEs derived from the TGN/EE with the vacuole. This transport route requires the involvement of ARA7 (RAB5 GTPase) and the CORVET membrane tethering complex. ConcA leads to the accumulation of the tonoplast-localized V-ATPase at the TGN/EE and seems to enhance the sorting of VHA-a3 containing V-ATPase complexes into the Golgi-dependent route.

The observation that both tonoplast-localized proton pumps were found at the TGN/EE after ConcA treatment and the knockdown against the CORVET complex supports the assumption that the dual ER exit is not exclusive for the V-ATPase. It

seems that VHA-a3 and VHP1 contain COPII motifs for the recognition by Sec24 and the sorting into COPII vesicles. Interestingly, VHP1 was further missecreted to the plasma membrane after ConcA treatment and in the induced knockdown against CORVET, whereas VHA-a3 remained at the TGN/EE.

Typically, the tonoplast-localized proton pumps are exclusively detected at the tonoplast in root cells under normal conditions. An exception to this, is the observation that VHP1 localizes to the plasma membrane in very young meristematic root cells close to the Quiescent Center. This observation may be an artifact derived from a possible overexpression. As the proton pumps are exclusively detected at the tonoplast under normal conditions, the protein trafficking of tonoplast-localized proton pumps through the TGN/EE as wells as provacuoles seems to be rather fast.

It is of special interest to further investigate whether tonoplast-localized proton pumps take both ER exits simultaneously and to which amount, as the experimental manipulation does not necessarily reflect the usual preference of VHA-a3 for one or the other ER exit. Of interest would be the conditionally expression of VHA-a3 in plants constitutionally expressing VHA-a1. Thereby, it could be examined how many TGN/EEs are used for the transport of VHA-a3.

In Marchantia polymorpha, VHA-a is encoded by a single gene and shows a dual localization at the TGN/EE and the tonoplast. When expressing VHA-a from Marchantia (MpVHA-a) in Arabidopsis, MpVHA-a localize to the tonoplast but can be found in the typical aggregates after BFA treatment (Lupanga et al., 2020). Contrarily, VHA-a3 cannot be found in BFA compartments (Viotti et al., 2013, Figure 14). The ancient form of the VHA-a isoform is transported through the TGN/EE to the vacuole. As VHA-a3 evolved to leave the ER independent of COPII vesicles, it can be concluded that VHA-a3 is preferentially sorted into provacuoles (Lupanga et al., 2020). This assumption is also supported by the high density of proton pumps on the membrane of provacuoles (Viotti et al., 2013).

This study provides further evidence that a population of the tonoplast-localized V-ATPase enters COPII vesicles and is transported in a Golgi-dependent manner (Lupanga et al., 2020). This population of VHA-a3-containing V-ATPase

complexes is transported via a plant-specific trafficking route involving RAB5-positive LEs and the CORVET complex (Figure 37). Under normal conditions, VHA-a3 containing V-ATPase complexes seem to be preferentially sorted into provacuoles (Lupanga et al., 2020). The sorting of VHA-a3 into provacuoles or COPII vesicles may be subjected to environmental changes. As V-ATPase activity at the TGN/EE is required for salt tolerance (Krebs et al., 2010), the effects of sodium chloride on the trafficking of VHA-a3 could be investigated to gain further insights into the variable sorting at the ER.

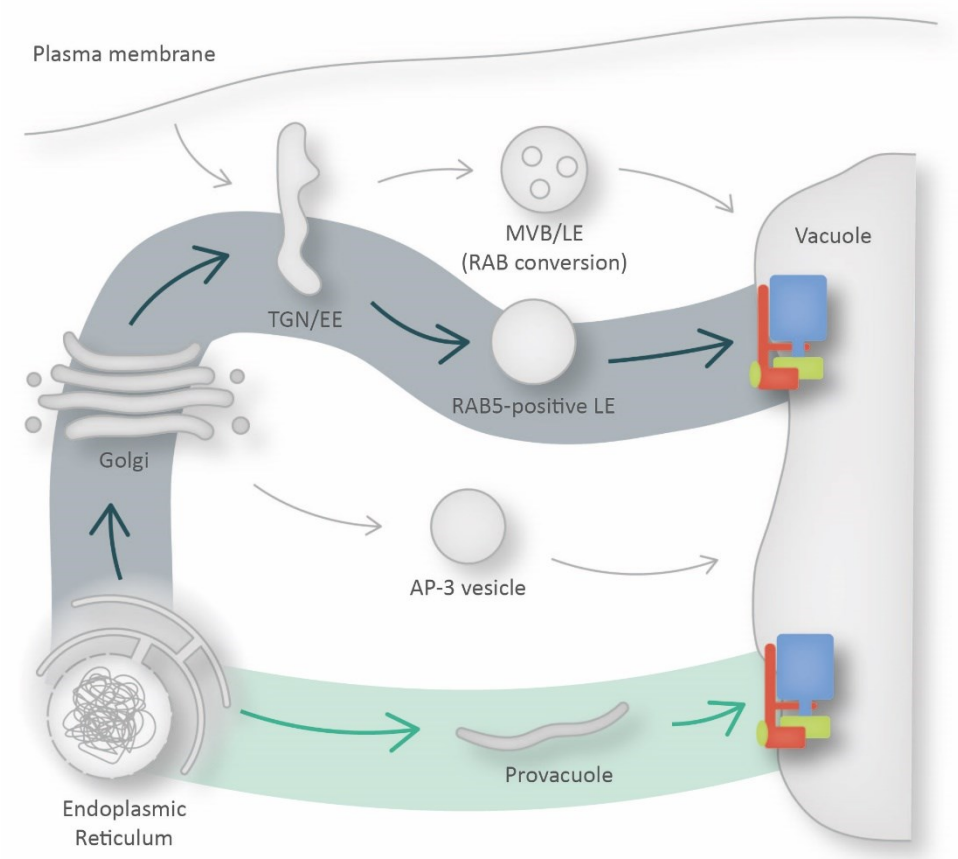


**Figure 37: The tonoplast-localized V-ATPase can take two trafficking pathways.** Based on previous findings (Feng et al., 2017b; Lupanga et al., 2020; Viotti et al., 2013) and observations presented in this study, it can be concluded that the V-ATPase can take two trafficking pathways from the ER to the vacuole in Arabidopsis. On the one hand, the tonoplast-localized V-ATPase is sorted into provacuoles at the ER and does not rely on the Golgi or post-Golgi compartments for trafficking. On the other hand, the tonoplast-localized V-ATPase enters COPII vesicles and is transported via the TGN/EE and RAB5-positive LE

## 4.4 Investigating provacuoles in vivo

Provacuoles were initially identified in sections of high-pressure frozen EM samples. Provacuoles have a double membrane, are spherical or cup-shaped and show a high density of proton pumps (Viotti et al., 2013). Judging from EM images the size of provacuoles range from 500 nm up to 1,8 $\mu$m (Viotti et al., 2013). The visualization of provacuoles in vivo is of great importance to determine the 3D morphology and to measure volume and surface area of provacuoles.

As fluorophores attached to VHA-a3 are exclusively detected at the tonoplast in vivo under normal conditions, trafficking of VHA-a3 happens faster than the maturation of the attached fluorophores (Viotti et al., 2013). Therefore, approaches with inducible expression systems were used to examine provacuoles in vivo.

In the genetic piggyback system, the Dex-induced expression of VHA-a3 caused a shift in localization of VHA-AP2 from the ER to the tonoplast showing that the trafficking of VHA-AP2-GFP to the vacuole depends on the tonoplast-localized V-ATPase. Thereby, the genetic piggyback system allows to follow the transport of VHA-AP2-GFP from the ER to the vacuole (Krüger, 2017, Figure 9). Subcellular structures labeled with VHA-AP2-GFP that are likely to be provacuoles were observed, but with the microscope setup used, it is not possible to distinguish between autofluorescence emitted from endogenous plant components or GFP. Thus, time-gated fluorescence lifetime imaging could help to distinguish between autofluorescence and VHA-AP2-GFP fluorescence marking provacuoles. The discrimination between FM4-64 and mCherry would also be possible with fluorescence lifetime gating to exclude the fraction of VHA-AP2-GFP at the TGN/EE and tonoplast by colocalization. Further experiments with lifetime gating microscopy may also answer the question whether provacuoles exist in root cells of the differentiation zone or in leave cells. The observed structures that may be provacuoles are punctate or tubular and differ from the structures described in Krüger, 2017. It may be that selection processes during propagation changed the strength of the conditional expression system. Nonetheless, the observed punctate and tubular structures seem to fit approximately to the size of provacuoles as seen in EM images.

An ER-localized and/or TGN/EE-localized fluorescent protein could be introduced into the piggyback system. With the help of an ER resident protein, it would be possible to distinguish putative sites of provacuole formation at the ER and the degree of overlap between the ER and provacuoles. The TGN/EE marker would be helpful to discriminate the fraction of VHA-AP2-GFP being part of VHA-a1 containing V-ATPase complexes from VHA-AP2-GFP marking provacuoles. It may also be helpful to attach an mVenus to VHA-AP2 as the fluorescence of mVenus is brighter than GFP (Day and Davidson, 2009) thereby reducing the signal from autofluorescent structures in the Arabidopsis root.

No matter if fluorescent VHA-a3 was expressed with the Dex-induced or the estradiol-induced expression system, a strong tonoplast labeling was observed after 6 hr of induction. However, eGFP seems to mature faster than the traditional GFP in planta and this difference might be accountable for the lacking ER signal in root cells expressing the estradiol-induced VHA-a3-LinkerGFP. This shows that rapidly maturing and bright fluorophores are inevitable to image provacuoles involved in the trafficking of VHA-a3 containing V-ATPase complexes from the ER to the tonoplast. The rather long fluorophore maturation of mCherry is not suitable for the in vivo imaging of provacuoles.

With the help of conditional expression systems, it was possible to gain further insights into the trafficking of the tonoplast localized V-ATPase. With the Dex-inducible expression of VHA-a3-mCherry-eGFP, a signal in the ER was observed, which turned to a pronounced labeling of the tonoplast. Also, punctae and tubular structures independent of the tonoplast were observed. Some of the punctae colocalized with FM4-64 at the TGN/EE (Figure 11). Fusion of provacuoles with the vacuole may lead to brighter areas at the tonoplast, which are in close contact to the nuclear envelope. Lifetime gating with an advanced experimental setup can help to differentiate between autofluorescence from plant structures and emission from fusion proteins with GFP.

Following the trafficking of VHA-a3 in vivo to determine the structure of provacuoles turned out to be difficult as VHA-a3 can enter a Golgi-dependent trafficking pathway. The conditional expression of VHA-a3 may be so strong that the ratio of VHA-a3 to VHA-a1 is increased and more VHA-a3 is sorted into COPII vesicles.

Therefore, mutations of the putative COPII motif in VHA-a3 need to be studied, which are then exclusively sorted into provacuoles.

Notably, VHP1-mCherry localized to the ER and the tonoplast (Supplementary Figure 5). One possible explanation for the localization of VHP1-mCherry in the ER may be the accumulation of freshly synthesized protein, which cannot be transported out of the ER fast enough. Remarkably, no punctae or tubular structures were observed. It may be that too few fluorescent proteins are transported to observe a fluorescent structure with CLSM or that the transport happens too fast to detect transport vesicles or intermediate compartments. This observation stresses the importance of conditional expression systems to study provacuoles in vivo.

A possible alternative to condition expression systems may be to anchor fluorescent VHA-a3 or VHP1 fusion proteins in the ER with a modification of the retention using selective hooks (RUSH) system and to release premade fluorescent protein after the application of Biotin (Boncompain et al., 2012). The protein trafficking could be traced with, e.g., a Spinning Disk microscope for rapid imaging of the trafficking process. Attached fluorophores need to be chosen in accordance with brighter emissions and higher photostability to allow for optimal imaging conditions.

So far it was not possible to isolate knockout mutants impaired in provacuole formation as these mutants probably exhibit lethal phenotypes. Proton pumps are not required for the formation of provacuoles as the *vha-a2 vha-a3 fugu 5*-1 triple mutant possesses lytic vacuoles (Kriegel et al., 2015). Arabidopsis plants expressing VHP1-mCherry could be used for EMS mutagenesis. VHP1-mCherry has the advantage of localizing to the ER and the tonoplast and subsequent screens after EMS mutagenesis for mutants showing punctate or tubular structures independent of the ER and the tonoplast could hint to putatively interesting mutants in provacuole formation. Maybe weak EMS alleles hinder the protein sorting of proton pumps into provacuoles, the formation of provacuoles or the fusion of provacuoles with the vacuole. Such a mutant impaired in provacuole formation should show ER retention after the disruption of the COPII-mediated trafficking pathway, e.g., upon expression of Sar1b-GTP.

The CORVET complex is required for the trafficking of the population of VHA-a3 that passes through the TGN/EE, but the morphology of provacuoles is not altered in the induced knockdown against the CORVET-specific subunit. The *vps3-2* T-DNA knockout mutant embryo was described to form abnormal vacuoles, but from the images presented in the publication membranous structures reminiscent of provacuoles can be observed (Delgadillo et al., 2020). Embryonic cells of the *vps3* T-DNA mutant described in Takemoto et al., 2018 was shown to possess a vacuole, as GFP-VAMP713, which is transported to the vacuolar membrane via the AP-3 pathway, properly localizes to the vacuolar membrane (Takemoto et al., 2018). These observations indicate that CORVET is not involved in the fusion between provacuoles and the vacuole.

The HOPS-specific knockdown did not affect the trafficking of VHA-a3. First evidence shows that fusion events of autophagosomes with the vacuole are mediated by the HOPS complex in Arabidopsis (Supplementary Figure 7) underscoring previous findings that the tonoplast-localized proton pumps are not transported via autophagosomes even though provacuoles have a similar ultrastructure as autophagosomes in EM images (Viotti et al., 2013).

Therefore, the evolutionary conserved HOPS and CORVET membrane tethering complexes seem to not play a role in fusion of provacuoles with the vacuole. The question how provacuoles fuse with the vacuolar network remains open. A novel plant-specific membrane tethering complex could fulfil this role. A motif or other determinant for sorting of the tonoplast-localized proton pumps into provacuoles also remains to be determined.

## 4.5 Membrane tethering complexes are crucial for vacuole development

### 4.5.1 Fragmented vacuoles in HOPS-specific knockdown are the result of a vacuolar network subjected to constant fission processes

Knockout mutants of subunits of the HOPS and CORVET membrane tethering complexes were described to be embryo lethal (Rojo et al., 2001), whereas knockout mutants in yeast are viable. So far, no viable mutant with fragmented vacuoles throughout the complete root was described. Thus, it seems that a connected vacuole network is necessary for the cell's viability and development in the root meristem. Knockdown against single subunits of HOPS and CORVET achieved with an amiRNA can be induced at any developmental stage and are thus useful to study trafficking to the vacuole and vacuole development. Gene silencing mediated by amiRNAs seem to mainly take place through translational inhibition, as the mRNA levels of target genes are changed only slightly (Li et al., 2013). Therefore, real time quantitative PCR (q-RT PCR) may not be the optimal method to analyze the degree of gene silencing. To determine the knockdown efficiency in the induced knockdown against *VPS16* the fluorescent signal from GFP-VPS16 was measured before and after the Dex-induced expression of the amiRNA. There was a 50 % reduction in fluorescence observed (Krüger, 2017). As also endogenous VPS16 protein is targeted in the Col-0 background, it is likely that knockdown efficiency is higher.

The knockdown of *VPS16*, the common subunit of the HOPS and CORVET membrane tethering complex, showed spherical vacuoles and is not distinguishable from the phenotype of the knockdown against the HOPS-specific subunits *VPS39* and *VPS41* (Figure 27). Thereby, it can be concluded that the HOPS complex facilitates homotypic vacuole fusion in yeast and animal cells as well as in plant cells. The role of HOPS in vacuole-to-vacuole or homotypic vacuole fusion is of particular interest in the study of vacuole morphology and connectivity. Previous publications reported opposing findings about vacuole morphology in meristematic root cells: vacuoles either consist of a connected network of tubules (Minina et al., 2021; Viotti et al., 2013) or several separated small vacuoles (SVs)

(Cui et al., 2018). Both models of vacuole biogenesis can explain the formation of multiple, fragmented vacuoles in the HOPS-specific knockdown.

If one follows the model published in Cui et al., 2018, MVBs fuse to form small vacuoles. In the meristematic root zone, each cell contains multiple, round small vacuoles that are fragmented. During developmental differentiation, small vacuoles gradually fuse to form brick-like vacuoles. In the HOPS knockdown, the small, round vacuoles should not be able to fuse. The other model published in Viotti et al., 2013 predicts that the tubular network in meristematic root cells falls apart over time as fission processes still occur. However, the separated vacuolar parts cannot be connected anymore as there are no functional HOPS complexes present. The main difference between the two opposing models of vacuole biogenesis is the function of the HOPS complex in vacuole development. In the model from Cui et al., 2018 HOPS is indispensable for the fusion of MVB-derived small vacuoles to form larger vacuoles. Whereas, the vacuoles in the model of Viotti et al., 2013 are tubular, but connected compartments, which underlie cytoplasmic streaming and fission processes.

Since the knockdown of *VPS16* close to the quiescent center does not seem to be as effective, these cells were shown to have a tubular vacuole network comparable to the vacuole morphology shown in (Minina et al., 2021; Viotti et al., 2013). By following the same cell file in the shootward direction, spherical vacuoles occur indicating that the tubular vacuole network falls apart due to fission processes caused by cytoplasmic streaming and that the separated vacuole subvolumes cannot fuse due to the lacking HOPS complex (Figure 29). Taken together, vacuoles in the root meristem are composed of a tubular network, whose integrity is maintained by the HOPS complex. The HOPS complex mediates homotypic vacuole fusion events to maintain the vacuolar structure as a single compartment. Therefore, the HOPS complex balances fission and fusion events at the developing vacuole. In the late differentiation zone of the root, the differentiated vacuole is no longer subject to cytoplasmic streaming and vacuole fragmentation does not occur.

Vacuole morphology in the CORVET-specific knockdown is highly tubulated in the meristematic root zone and too inflated in the elongation zone (Figure 26). Col-0 roots treated with 250 nm IAA show a similar vacuole morphology (Löfke et al.,

2015; Scheuring et al., 2016) indicating that vacuole morphology is rather a consequence of the stopped root growth.

The role of the cytoskeleton in vacuole fragmentation seems to be neglectable and the microtubule defect in the CORVET-specific knockdown seems to be the result of stopped root growth (Figure 23, Figure 24). Even though microtubules trajected in an unordered manner through meristematic root cells in the knockdown against *VPS16* and *VPS8*, the root cells did not swell unlike to the typical phenotype of genetic mutants affected in genes for the organization or stability of microtubule filaments (Figure 24) (Sugimoto et al., 2003). Due to the altered vacuole morphology, it may be that the turgor pressure is lower and that no swelling is caused by the lack of tension.

### 4.5.2 Vertex rings may play a role in determining the vacuole morphology

In yeast, the HOPS complex was proposed to regulate the formation of intraluminal fragments during vacuole fusion to degrade parts of the vacuolar membrane, such as lipids and transmembrane proteins, for quality control and membrane integrity (Karim et al., 2018). In addition, another study found that the size of vacuoles can be regulated by arrested nanoscopic fusion pores, which are held open by the HOPS complex and SNARE proteins (D'Agostino et al., 2018; Söllner and Malsam, 2018).

As the gene silencing induced by the expressed amiRNA leads to a reduction of VPS16 over time, various gradients of the observed phenotypes and effects become apparent in root cells of Arabidopsis. In the knockdown against *VPS16*, membrane fusion events seem to be arrested in various stages and contact sites between neighboring vacuoles were examined in more detail (Figure 31). In Arabidopsis, vacuolar membrane fusion occurs via vertex ring formation with a leaflet of the RAB7 GTPase RABG3f surrounded by a ring of the tonoplast-localized V-ATPase. Vertex ring and intralumenal fragment formation during homotypic vacuole fusion could function in degradation of tonoplast membrane or tonoplast proteins. As the tubular vacuole network does not fragment into separated tubules, but separated vacuoles, it seems as if vacuoles are not shaped anymore but follow the natural behavior of lipid bilayers. It may be that HOPS acts

as an anchor point for a so far unknown mechanism to determine vacuole morphology. Otherwise, vertex rings and resulting nanopores could function in tubule formation of the vacuolar network. HOPS complexes, which do not dissolve after membrane fusion, could maintain small, constricted joints connecting vacuolar subvolumes. Constricted joints may act as anchor points for proteins, such as NETWORKED 4 A/B (NET4A/B) (Kaiser et al., 2019), which connect the vacuolar membrane with the cytoskeleton.

### 4.5.3 Balance of PI3P level is crucial for proper completion of membrane fusion at the vacuole in Arabidopsis

PI3P (phosphatidylinositol 3-phosphate) is produced through phosphorylation of phosphatidylinositol (PI) by the PI3-kinase Vps34 (Vacuolar Protein Sorting 34) in yeast. Vps34 is part of different complexes in yeast and mammalian cells. Complex I consists of Vps34, Vps15, Vps30/Atg6 and Atg14 and plays a role in autophagy. Complex II shares the subunits Vps34, Vps15 and Vps30/Atg6, but contains Vps38 (or UVRAG in mammals). Complex II functions mostly in endocytic sorting (Rostislavleva et al., 2015).

The signal of 2xFYVE-GFP at the tonoplast was strongest in the differentiation zone of the root in the control treatment (Supplementary Figure 14). This indicates that the level of PI3P at the tonoplast increases during vacuole development. In the knockdown against *VPS16*, the marker for PI3P accumulated at the membrane of the spherical vacuoles (Supplementary Figure 14). By depleting PI3P from the membrane of the spherical vacuoles, the vacuoles fused to larger volumes (Figure 32). The protein amount of VPS16 was shown to be reduced to circa 50 % after Dex-induced knockdown. Therefore, it can be assumed that functional HOPS complexes remain to partially facilitate homotypic vacuole fusion. These observations point to the assumption that a high level of PI3P hinders vacuolar membrane fusion in the absence of HOPS. Whereas, the HOPS-specific subunit VPS41 is recruited by PI3P to the tonoplast and loses its membrane association by adding WM (Brillada et al., 2018). This suggests a delicate balance of PI3P at the vacuolar membrane to regulate membrane fusion. By adding WM to induce the fusion of fragmented vacuoles, the role of the V-ATPase in homotypic vacuole

fusion in Arabidopsis was examined (Figure 32). Neither vacuolar pH nor the V-ATPase is required for vacuole-to-vacuole fusion in Arabidopsis.

As transvacuolar strands and vacuolar tubules are lost and instead membranous inclusions are formed inside the Col-0 vacuole after the application of WM (Figure 33), the vacuolar membrane fusions seem to be unordered and undirected. Low levels of PI3P seems to suppress the proper processing of membrane fusion events at the vacuole. Thus, undirected membrane invaginations inside the vacuolar lumen are formed, which are not observed under normal conditions. Membranous vacuolar inclusions in the vacuole lumen of root cells caused by WM treatment were previously observed in other studies (Feraru et al., 2010; Nováková et al., 2014). In Arabidopsis, the *vps34* knockout mutant is gametophytic lethal (Lee et al., 2008). The vacuole phenotype caused by WM treatment can also be observed in roots lacking VPS38, which is a subunit of the PI3K (phosphatidylinositol-3 kinase) complex II. The *vps38* mutant contains abnormal vacuoles with enlarged vacuoles and undigested content surrounded by several membranes (Lee et al., 2018). An alkalinization of vacuolar pH after WM treatment could lead to the accumulation of undigested membrane material in the vacuolar lumen. However, it may also be that too much material is inside the vacuole to be digested at once.

WM-induced vacuolar inclusions were only partially stained with BCECF (Figure 33). ARA7-positive endosomes did not properly fuse with the vacuole but were engulfed with an extra layer on tonoplast. Partially, vacuolar inclusions showed higher fluorescence for VHA-a3-GFP than the tonoplast indicating that vacuolar inclusions consist of several tonoplast layers (Figure 33). Low levels of PI3P seem to hinder the proper heterotypic fusion with the vacuole and MVBs are engulfed with an additional layer of tonoplast, which may serve for degradation of MVBs through inward budding of the tonoplast and resembles the process of microautophagy (Oku and Sakai, 2018).

The spherical vacuoles in the knockdown against *VPS16* lack the typical trans-vacuolar strands of cytosolic content that run through the vacuolar lumen. And after WM treatment no vacuolar inclusions inside the spherical vacuoles were observed (Figure 32). It may be that the absence of VPS16 has an impact on the fission

machinery needed to pinch off the inclusions inwards to the vacuolar lumen (Praefcke and McMahon, 2004).

# 5 Conclusions

To learn more about the independency of the tonoplast-localized V-ATPase from COPII-mediated ER export (Viotti et al., 2013), the dominant-negative form of Sar1b (Sar1b-GTP) under the control of the Dex-inducible expression system was studied. COPII-mediated trafficking was disrupted after the expression of Sar1b-GTP and it was confirmed that the transport of VHA-a1 is mediated by COPII vesicles, whereas VHA-a3 can be transported independently (Lupanga et al., 2020). Sar1b-GTP can be used as a first approach to determine more tonoplast-localized proteins whose vacuolar trafficking is independent of COPII-mediated trafficking. Further investigation with trafficking mutants and dominant-negative GTPases are then recommended to follow.

The in vivo imaging of provacuoles suggest that provacuoles appear as punctae or tubular stretches when observed with CLSM. Potential fusion sites of provacuoles with the vacuole are likely close to the cell nucleus. However, more sophisticated imaging techniques have to be applied to identify provacuoles in vivo.

In Arabidopsis, the HOPS complex fulfills similar functions as in yeast and mammalian cells. CORVET obtained a new evolutionary role in plants as it acts in heterotypic fusions directly at the vacuole by orchestrating the fusion of RAB5-positive LEs derived from the TGN/EE with the vacuole in Arabidopsis (Takemoto et al., 2018).

When the tonoplast-localized V-ATPase enters the Golgi-dependent pathway (Lupanga et al., 2020), the proton pump is transported via the TGN/EE and plant-specific RAB5-positive LEs, whose fusion with the vacuole is mediated by the CORVET complex. The sorting of the tonoplast-localized V-ATPase into the Golgi-dependent route is likely to be enhanced by a need of V-ATPase complexes at the TGN/EE. However, VHA-a3 is preferably sorted into provacuoles. So far, proof that either HOPS or CORVET plays a role in provacuole-to-vacuole fusion is missing.

HOPS is not only involved in vacuolar trafficking, but also in homotypic (vacuole-to-vacuole) fusion in Arabidopsis. HOPS is required for proper vacuole development in order to maintain the vacuolar network as a single, connected compartment in meristematic root cells. Homotypic vacuole fusion occurs via

vertex ring formation forming luminal leaflets, which could be used for membrane degradation or organelle size determination. Homotypic vacuole fusion is independent of the V-ATPase in Arabidopsis. The balance of PI3P is crucial for directed vacuolar fusion processes at the vacuole.

# 6 Supplementary information

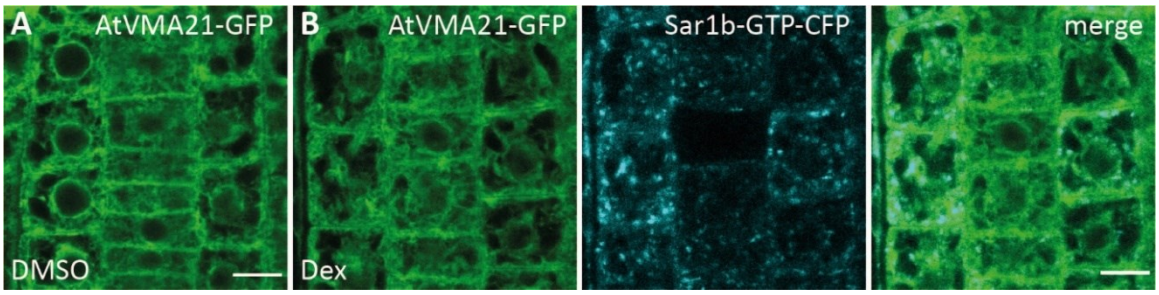


**Supplementary Figure 1: The ER-resident V-ATPase assembly factor VMA21-GFP colocalize with Sar1b-GTP-CFP in the ER after Dex induced expression.** 6-days-old Arabidopsis seedlings were treated with DMSO (A) or 60 µM Dex for 6h (B). After Dex induced expression, Sar1b-GTP-CFP localized to the ER and punctae that were independent of AtVMA21-GFP. Scale bars are equal to 10 µm.

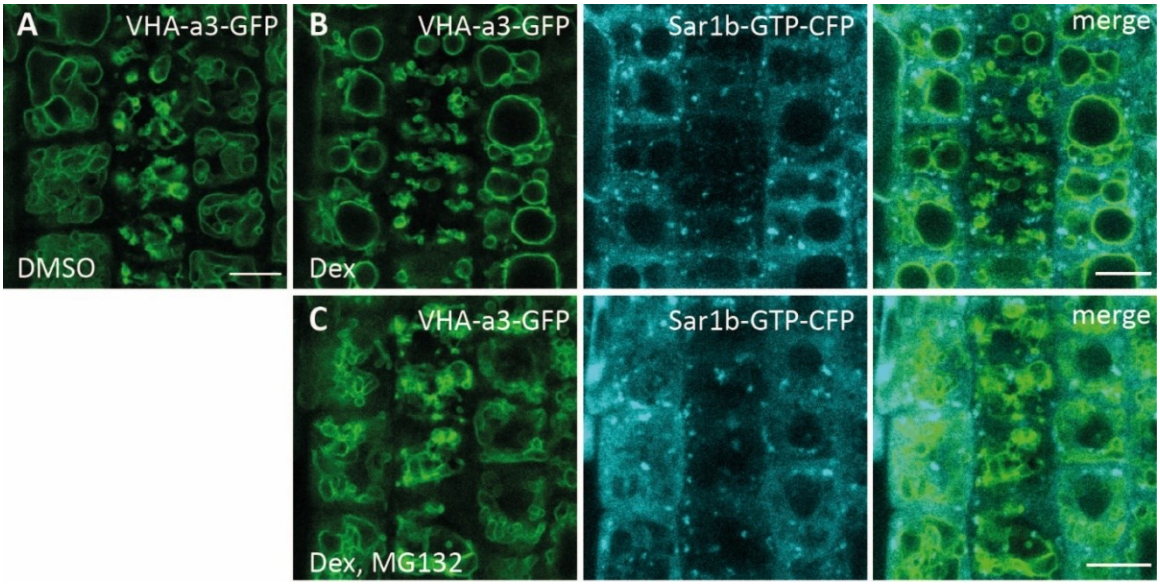


**Supplementary Figure 2: Inhibition of proteasomal degradation with MG132 did not cause an accumulation of VHA-a3-GFP in the ER after Dex induced expression of Sar1b-GTP-CFP.** 6-days-old Arabidopsis seedlings were treated with DMSO or 60 µM Dex for 6 h. To block proteasomal degradation in seedlings with Dex-induced Sar1b-GTP-CFP, 10 µM MG132 was added for 4 hr. Scale bars are equal to 10 µm.

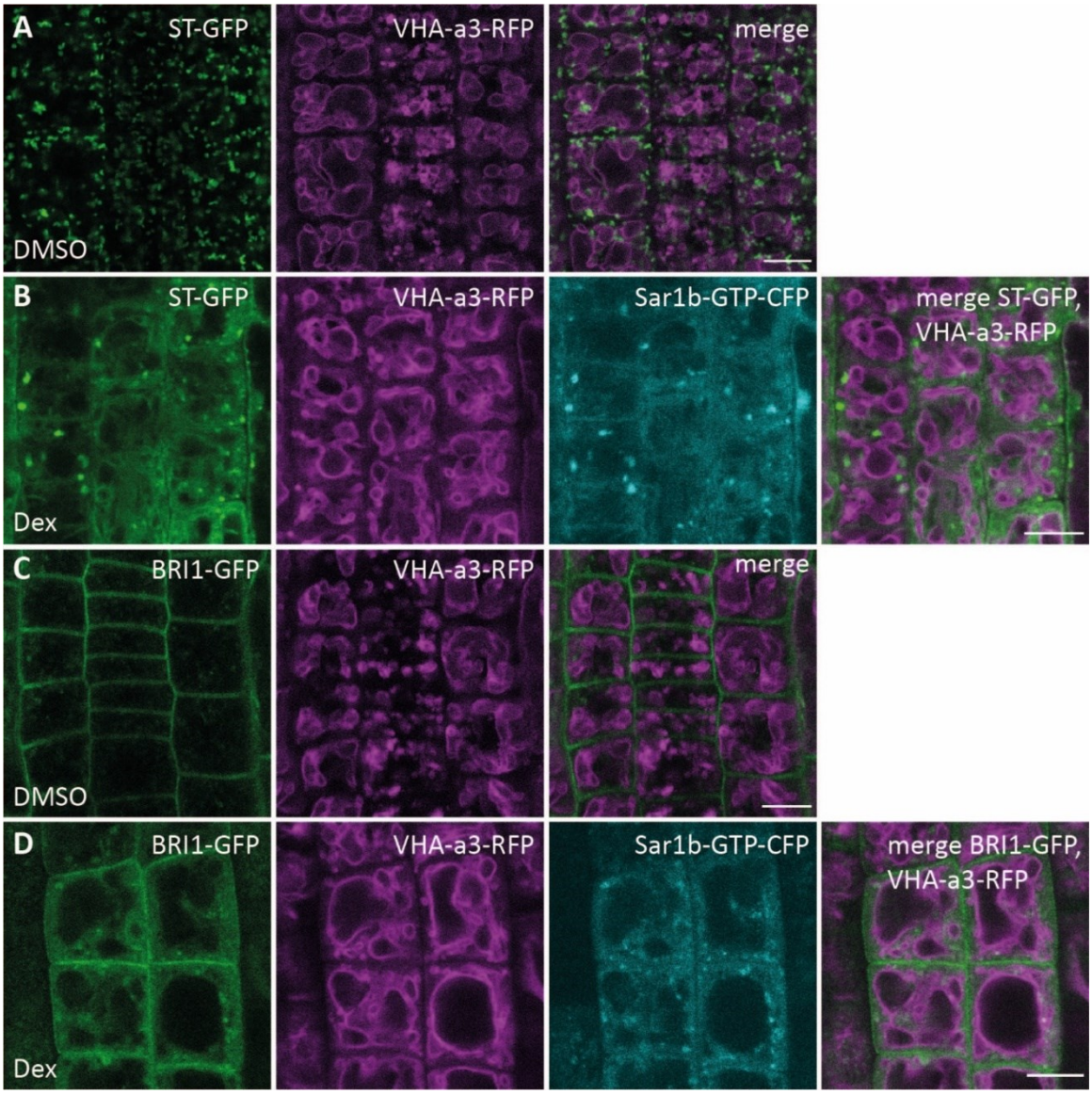


**Supplementary Figure 3: Coexpression of ST-GFP or BRI1-GFP with VHA-a3-RFP and Sar1b-GTP-CFP shows that timing differences in Dex induced gene expression are not the reason why VHA-a3-RFP does not accumulate in the ER.** (A) In the DMSO control ST-GFP localized to the Golgi and VHA-a3-RFP to the tonoplast. (B) After Dex induced expression of Sar1b-GTP-CFP ST-GFP colocalized with Sar1b-GTP-CFP in the ER and punctate structures. VHA-a3-RFP localized to the tonoplast and neither accumulated in the ER nor colocalized with ST-GFP (see merged image). (C) BRI1-GFP was mainly detected at the plasma membrane and a small fraction at intracellular punctae in the DMSO control. VHA-a3-RFP localized to the tonoplast. (D) After Dex treatment BRI1-GFP accumulated in the ER and colocalized with Sar1b-GTP-CFP, whereas VHA-a3-RFP was not retained in the ER and did not colocalize with BRI1-GFP (see merged image). Scale bars are equal to 10 µm.

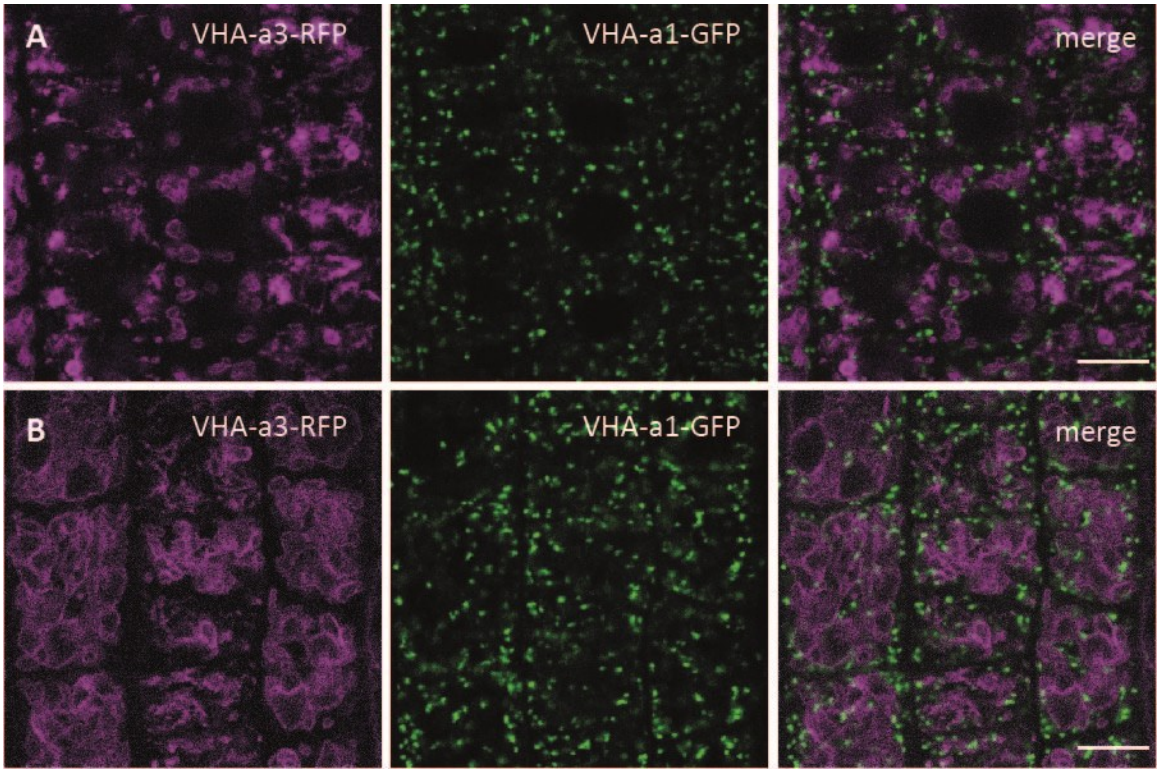


**Supplementary Figure 4: VHA-a3-RFP does not localize to the TGN/EE under standard conditions.** 6-days-old seedlings expressing VHA-a3-RFP (magenta) and VHA-a1-GFP (green) were imaged in the meristematic root zone (A) and the transition zone of the root (B). Scale bars are equal to 10 µm.

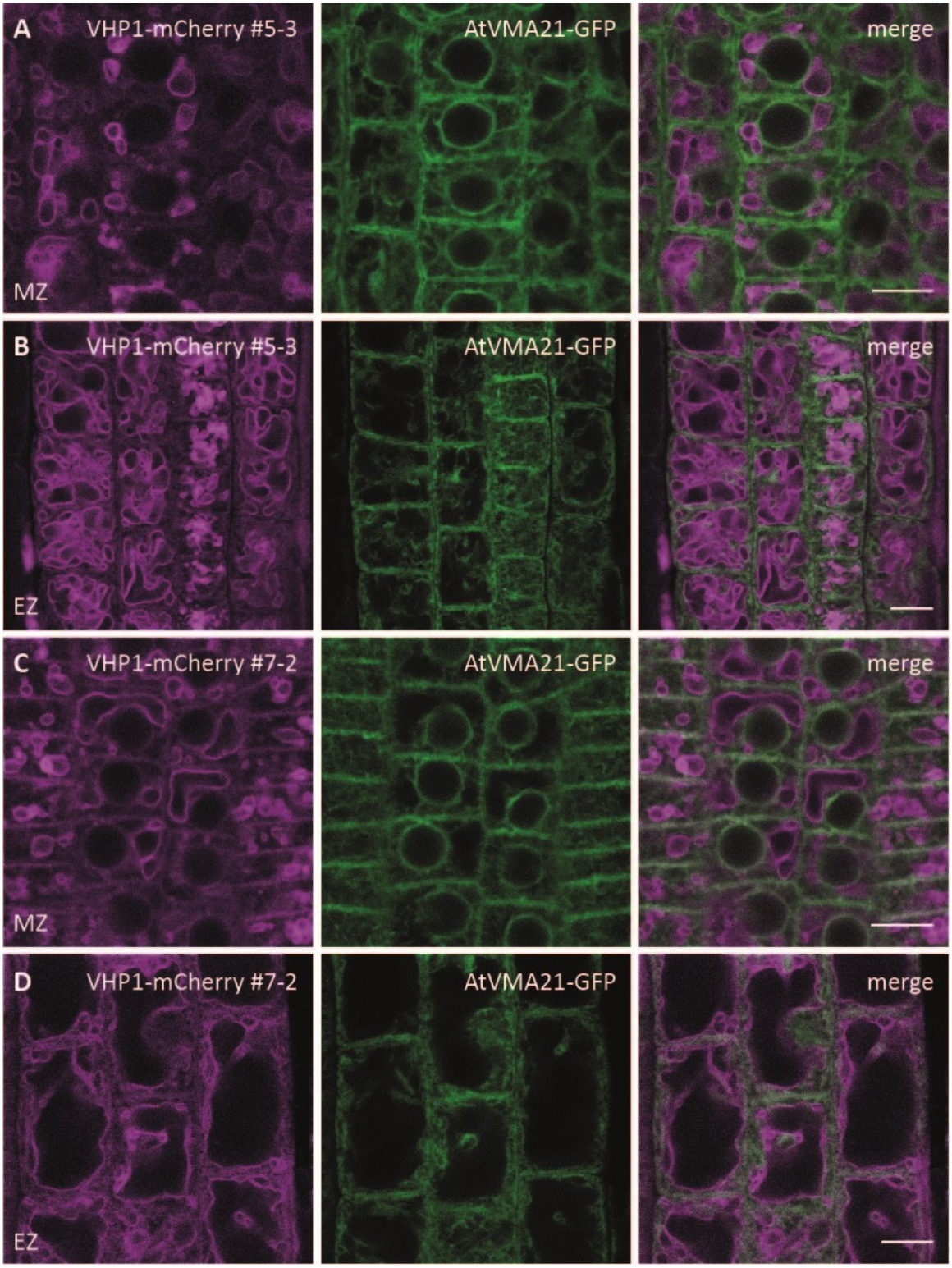


**Supplementary Figure 5: VHP1-mCherry expressed under the UBQ10 promotor localizes to the ER and the tonoplast.** Two independent lines of Col-0 expressing UBQ10:VHP1-mCherry were crossed with the ER-resident V-ATPase assembly factor AtVMA21-GFP. (A and B) VHP1-mCherry #5-3 showed weak overlap with AtVMA21-GFP in the ER and strong tonoplast labeling in meristematic (A) and elongating (B) root cells. (C and D) VHP1-mCherry #7-2 localized to the ER marked by AtVMA21-GFP and the tonoplast in meristematic (C) and elongating (D) root cells. Scale bars are equal to 10 µm.

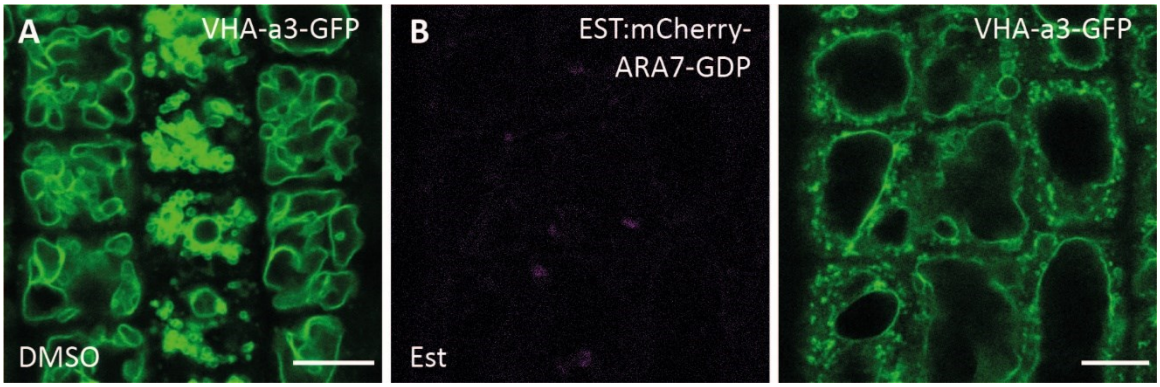


**Supplementary Figure 6: Using the dominant-negative form of ARA7 (ARA7-GDP or ARA7S24N) to block protein transport from the TGN/EE to the vacuole leads to an accumulation of VHA-a3-GFP at the TGN/EE.** (A) VHA-a3-GFP localized to the tonoplast in the DMSO control. (B) After treatment with 60 µM estradiol for 6 hr no fluorescence was detected for mCherrry-ARA7-GDP, but VHA-a3-GFP was found at the tonoplast and in punctae resembling the TGN/EE. Scale bars are equal to 10 µm.

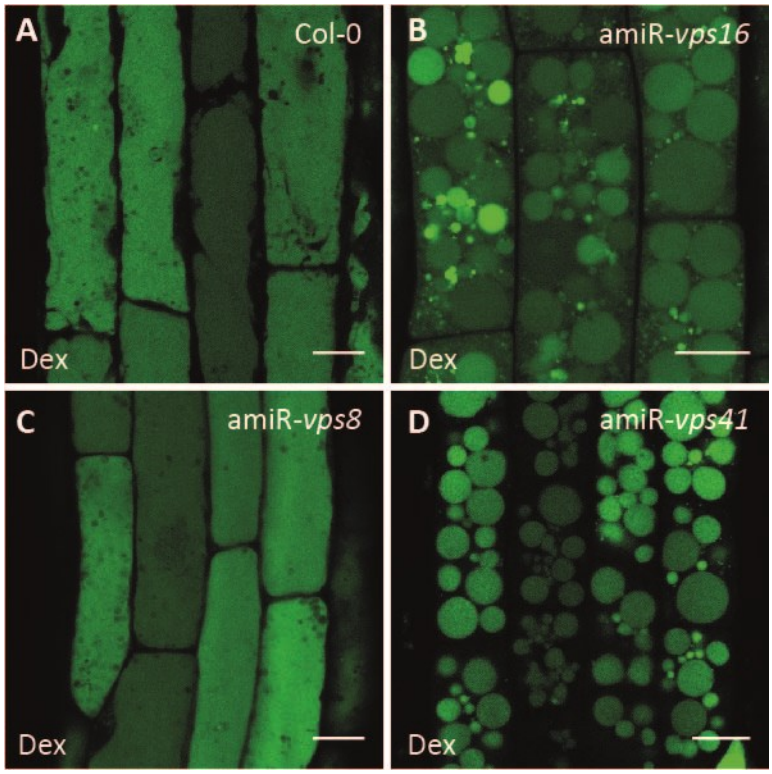


**Supplementary Figure 7: The HOPS complex mediates heterotypic fusion events with autophagosomes and the vacuole in Arabidopsis.** Seedlings were induced for 72 hr with 30 µM Dex to induce the respective gene knockdown. Autophagy was induced with 500 nM ConcA for 5 hr and BCECF was added to visualize the vacuolar lumen. (A) + (C) Autophagic inclusions inside the vacuole, which were not stained with BCECF, were found in Col-0 and the induced knockdown against *VPS8*. (B) + (D) Vacuolar inclusions with autophagic content could not be detected in the *VPS16* and *VPS41* knockdown. Scale bars are equal to 10 µm.

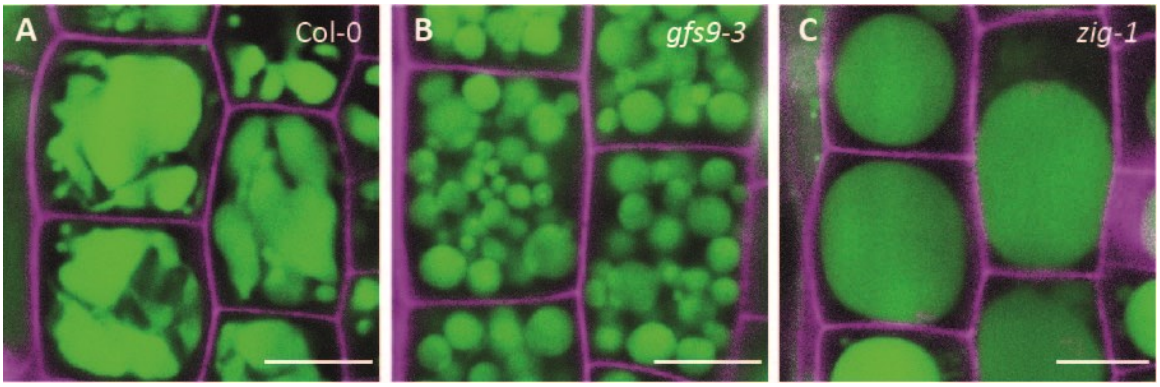


**Supplementary Figure 8: Roots with altered vacuole morphology in elongation zone are viable.** 6-days-old seedlings were stained with BCECF-AM to root cells in the elongation zone were imaged to compare vacuole morphology. (A) Col-0 vacuoles showed constricted subvolumes. (B) Vacuoles in the *gfs9-3* mutant exhibited multiple small and round vacuoles. (C) In cells of the *zig-1* mutant one big, rounded vacuole was observed per cell. Scale bars are equal to 10 µm.

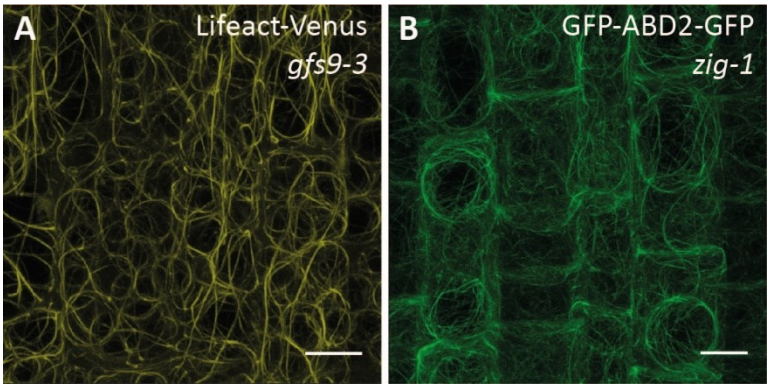


**Supplementary Figure 9: Actin cytoskeleton is intact in mutants with round vacuoles in root cells.** Images show projected Z-stacks of fluorescent actin markers in epidermal root cells. (A) Lifeact-Venus formed spirals around the round vacuoles of the *gfs9-3* mutant. (B) GFP-ABD2-GFP showed intact actin filaments that aligned around the round vacuoles in the *zig-1* mutant. Scale bars are equal to 10 µm.

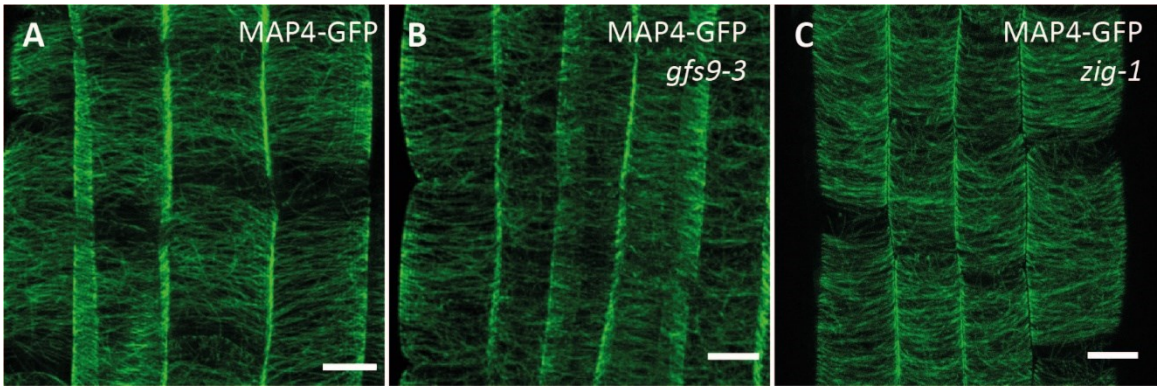


**Supplementary Figure 10: The alignment of Microtubule filaments is not altered in viable mutants with round vacuole morphology.** Images show projected Z-stacks of the epidermal cell layer in the elongation zone of the root. (A) In Col-0 root cells, the microtubule filaments visualized with MAP4-GFP formed a pattern transversal to the growth direction of the root. (B and C) Microtubule filaments in root cells of *gfs9-3* (B) and *zig1* (C) showed a similar orientation as compared to Col-0 roots. Scale bars are equal to 10 µm.

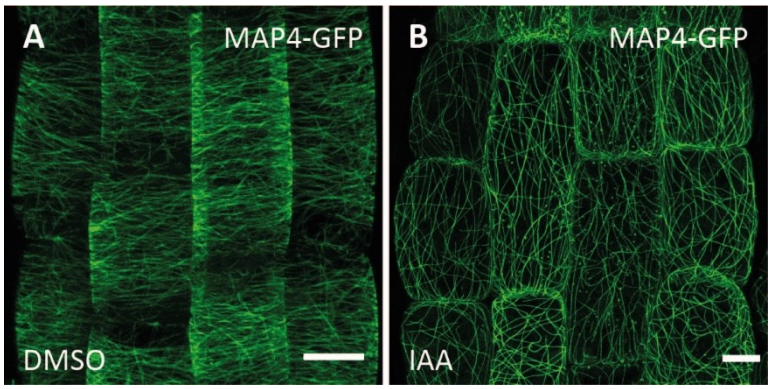


**Supplementary Figure 11: High auxin concentration leads to a disturbed microtubule arrangement in root cells.** Col-0 seedlings expressing MAP4-GFP were treated for 20 hr with DMSO or 10 µM IAA (indole-3-acetic acid). (A) Microtubule filaments were aligned in parallel in the orthogonal direction to the growth axis of the root. (B) After treatment with a high auxin concentration of 10 µM IAA, the microtubule filaments projected in an unordered longitudinal manner through the root cells. Scale bars are equal to 10 µm.

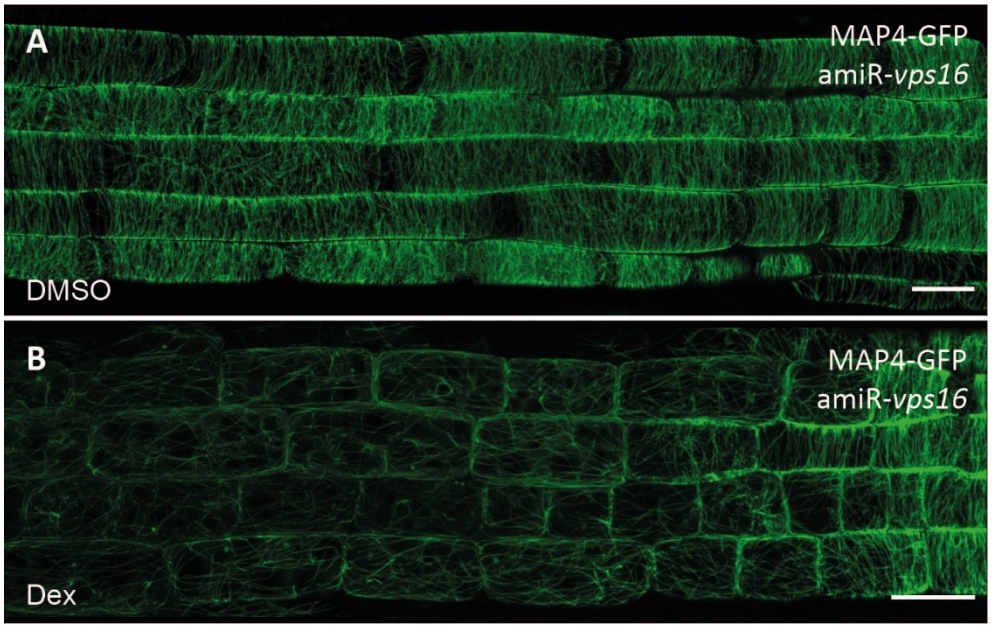


**Supplementary Figure 12: In the knockdown against *VPS16* the microtubule filaments misalign after the transition zone of the root.** Seedlings with Dex-inducible knockdown against *VPS16* and expressing MAP4-GFP were treated with DMSO or 30 µM Dex for 72 hr. Z-stacks of the epidermal cell layer were taken and projected to display 2D images. (A) Microtubule filaments of DMSO-treated control roots exhibited a parallel alignment perpendicular to the root axis. (B) In the Dex-induced knockdown against *VPS16* the arrangement of the microtubule filaments was disturbed in the elongation zone. However, in the meristematic root zone a parallel orientation of microtubules was observed. Scale bars are equal to 20 µm.

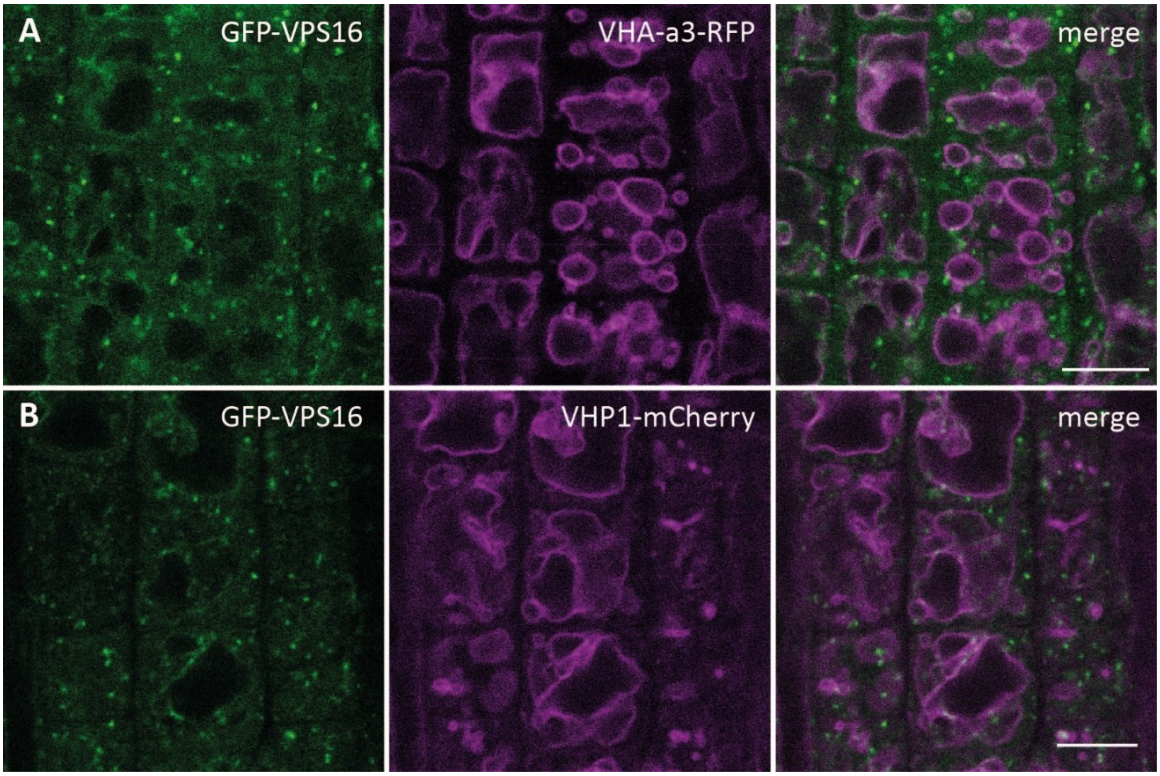


**Supplementary Figure 13: GFP-VPS16 localized to punctae and stretches at the tonoplast.** GFP-VPS16 was observed in punctae and short stretches along the tonoplast that colocalized with VHA-a3-RFP (A) or VHP1-mCherry (B). Scale bars are equal to 10 µm.

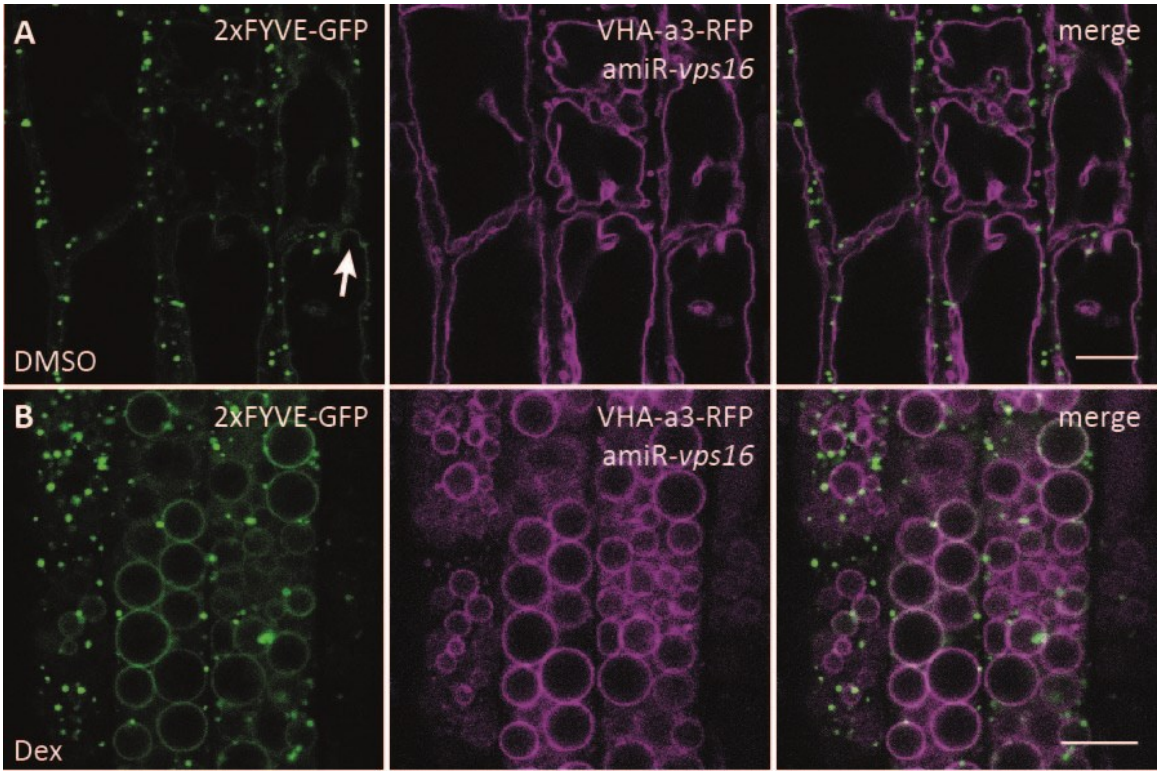


**Supplementary Figure 14: The signaling lipid PI3P accumulated at the tonoplast in the induced *VPS16* knockdown.** Seedlings were treated with 30 µM Dex for 72 hr. (A) In the DMSO control, 2xFYVE-GFP localized to punctae resembling MVBs and exhibited a faint signal at the tonoplast (white arrow) labeled with VHA-a3-RFP. (B) After Dex-induction of the knockdown against *VPS16*, the signal of 2xFYVE-GFP at the tonoplast increased. Scale bars are equal to 10 µm.

# 7 Materials and methods

## 7.1 Media, solutions and buffers

### 7.1.1 Media used for bacteria

LB agar plates or liquid LB medium supplemented with antibiotics were used to grow *Escherischia coli* (E. coli) or *Agrobacterium tumefaciens* (A. tumefaciens, agrobacteria). LB medium was prepared as follows and autoclaved:

LB medium (1 l): 10 g bacto-tryptone

5 g bacto-yeast extract

10 g NaCl

add up to 1 l with dd $H_2O$

LB plates: 15 g bacto-agar

After autoclaving, the respective antibiotics (AB) were added at a temperature between 48 °C and 50 °C.

AB resistance *Escherischia coli* (DH5α):

Ampicillin 150 µg/ml

Spectinomycin 100 µg/ml

AB resistance *Agrobacterium tumefaciens* (ASE:pSOUP$_+$):

Chloramphenicol 25 µg/ml in 50 % Ethanol

Kanamycin 50 µg/ml

Tetracylin 10 µg/ml in 50 % Ethanol

Spectinomycin 100 µg/ml

### 7.1.2 Media used for Arabidopsis

After sterilization of *Arabidopsis thaliana* seeds, the seeds were sown on solid ½ MS (Murashige and Skoog) medium supplemented with 0.5 % sucrose and 0.55 % phtyoagar. For root growth experiments, the ½ MS medium was prepared with

1 % phtyoagar. Seedlings treated with chemical agents were incubated in liquid ½ MS medium supplemented with 0.5 % sucrose. In order to sow seeds directly to soil, seeds were taken up in autoclaved Top-Agar (0.25 g phytoagar/500 ml $ddH_2O$).

The ½ MS medium was prepared as follows. Before filling the volume up to 1 l, the pH of the medium had to be adjusted to pH 5.8 using KOH solution. Medium had to be autoclaved prior to use and antibiotics were added afterwards to the chilled medium having a temperature at around 50 °C.

½ MS medium (1 l): 2.16 g MS

5 g sucrose

add up to 1 l and adjust to pH 5.8

plates: 5.5 g phytoagar (0.55 %) or 10 g phytoagar (1 %)

For Arabidopsis selection the respective selective antiobiotic was used with a concentration of 100 $\mu$g/ml.

### 7.1.3 Floral Dip Solution

To prepare the solution for Floral Dip, 6 g of sucrose was dissolved in 120 ml ddH2O to obtain a 5 % sucrose solution. Then 45 $\mu$l (0.03 %) Silwet L-77 was added.

### 7.1.4 Miniprep buffers

The method used to isolate plasmid DNA consisted of three different buffers P1, P2 and P3.

P1: 6.06 g Tris base and 3.72 g $Na_2EDTA \times 2H_20$ were dissolved in 800 ml $ddH_2O$. pH was adjusted with HCL to pH 8. Afterwards, $ddH_2O$ was added to 1 l and P1 buffer was autoclaved. Then, 10 mg RNase A per 100 ml were added prior to first use. Buffer was stored at 4 °C.

P2: 8 g NaOH and 10 g SDS (or 100 ml 10 % SDS) were dissolved in 1 l $ddH_20$ and sterile filtrated. Buffer was stored at room temperature (RT).

P3: 3 M potassium acetate solution was prepared (294.45 g potassium acetate per 1 l) and pH was adjusted to 5.5 using glacial acetic acid. P3 buffer was autoclaved and stored at 4 °C.

## 7.2 Plant material and plant growth

### 7.2.1 Plant material

The used plant material for transformations, crosses, chemical treatments, subcellular localization studies and other experiments is summarized in Table 3.

Table 3: Tables summarizes the plant material used in this study.

| Name | Published Reference |
|---|---|
| DEX:Sar1b-GTP-CFP (Dex:Sar1BH74L-CFP) | Lupanga et al., 2020 |
| UBQ10:VMA21-GFP | Neubert et al., 2008 |
| DEX:Sar1b-GTP-CFP in UBQ10:VMA21-GFP (T2) | presented study |
| UBQ10:ST-GFP | Lupanga et al., 2020 |
| DEX:Sar1b-GTP-CFP in UBQ10:ST-GFP (T2) | Lupanga et al., 2020 |
| BRI1p:BRI1-GFP | Geldner et al., 2007 |
| DEX:Sar1b-GTP-CFP in BRI1p:BRI1-GFP (T2) | Lupanga et al., 2020 |
| VHA-a1p:VHA-a1-GFP | Dettmer et al., 2006 |
| DEX:Sar1b-GTP-CFP in VHA-a1p:VHA-a1-GFP (T2) | Lupanga et al., 2020 |
| VHA-a3p:VHA-a3-GFP | Dettmer et al., 2006 |
| DEX:Sar1b-GTP-CFP in VHA-a3p:VHA-a3-GFP (T2) | Lupanga et al., 2020 |
| UBQ10:VHA-a3-a1-TD-GFP | Lupanga et al., 2020 |
| DEX:Sar1b-GTP-CFP in UBQ10:VHA-a3-a1-TD-GFP (T2) | Lupanga et al., 2020 |
| VHA-a3p:VHA-a3-RFP | Brüx et al., 2008 |

| | |
|---|---|
| DEX:Sar1b-GTP-CFP in VHA-a3p:VHA-a3-RFP x VHA-a1p:VHA-a1-GFP (F2) | Lupanga et al., 2020 |
| DEX:Sar1b-GTP-CFP in VHA-a3p:VHA-a3-RFP x UBQ10:ST-GFP (F2) | presented study |
| DEX:Sar1b-GTP-CFP in VHA-a3p:VHA-a3-RFP x BRI1p:BRI1-GFP (F2) | presented study |
| pVHP1:VHP1-GFP (A206K) | Segami et al., 2014 |
| DEX:Sar1b-GTP-CFP in pVHP1:VHP1-GFP (A206K) (T2) | presented study |
| UBQ10:ERDL6-GFP | Poschet et al., 2011 |
| DEX:Sar1b-GTP-CFP in UBQ10:ERDL6-GFP (T2) | presented study |
| UBQ10:pHGFP-VTI11 | Takemoto et al., 2018 |
| DEX:Sar1b-GTP-CFP in UBQ10:pHGFP-VTI11 (T2) | presented study |
| UBQ10:mCherry-VAMP711 (WAVE-9R) | Geldner et al., 2009 |
| DEX:Sar1b-GTP-CFP in UBQ10:mCherry-VAMP711 (WAVE-9R) (T2) | presented study |
| 35S:SUC4-GFP | Wolfenstetter et al., 2012 |
| DEX:Sar1b-GTP-CFP in 35S:SUC4-GFP (T2) | presented study |
| DEX:Sar1b-GTP-CFP in 35S:SUC4-GFP *pat2-2* (T2) | presented study |
| UBQ10:VHA-AP2-GFP DEX:VHA-a3-mCherry in *vha-a2 vha-a3* | Krüger, 2017 |
| UBQ10:VHA-a3-mCherry-eGFP (T3) | presented study |
| UBQ10:VMA21-GFP | Neubert et al., 2008 |

| | |
|---|---|
| UBQ10:VHP1-mCherry x UBQ10:VMA21-GFP (F2) | presented study |
| pUXVE2:VHA-a3-LinkerGFP x UBQ10:VHP1-mCherry (F1) | presented study |
| pUXVE2:VHA-a3-LinkerGFP (T2) | presented study |
| VHA-a3p:VHA-a3-RFP x VHA-a1p:VHA-a1-GFP (F2) | presented study |
| UBQ10:VHA-a3R729N-GFP | Lupanga et al., 2020 |
| pUXVE2:mCherry-ARA7-GDP in pVHA-a3:VHA-a3-GFP (T2) | presented study |
| VHA-a3p:VHA-a3-GFP x DEX:amiR-*vps39* (F2) | presented study |
| VHA-a3p:VHA-a3-GFP x DEX:amiR-*vps8* (F2) | presented study |
| pVHP1:VHP1-GFP x DEX:amiR-*vps39* (F1) | presented study |
| pVHP1:VHP1-GFP x DEX:amiR-*vps8* (F1) | presented study |
| DEX:amiR-*vps16* in Col-0 (T3) | Krüger, 2017 |
| DEX:amiR-*vps16* in *vha-a2 vha-a3* (T3) | presented study |
| DEX:amiR-*vps39* (T2,T3) | Takemoto et al., 2018 |
| DEX:amiR-*vps41* (T2,T3) | Brillada et al., 2018 |
| DEX:amiR-*vps3* (T2,T3) | Takemoto et al., 2018 |
| DEX:amiR-*vps8* (T2,T3) | Takemoto et al., 2018 |
| UBQ10:GFP-ABD2-GFP | Dyachok et al., 2014 |
| UBQ10:GFP-ABD2-GFP x DEX:amiR-*vps16* (F1) | presented study |
| UBQ10:GFP-ABD2-GFP x DEX:amiR-*vps41* (F1) | presented study |
| UBQ10:GFP-ABD2-GFP x DEX:amiR-*vps8* (F1) | presented study |

| | |
|---|---|
| 35S:Lifeact-Venus | Era et al., 2009 |
| 35S:MAP4-GFP | Marc et al., 1998 |
| 35S:MAP4-GFP x DEX:amiR-*vps16* (F3) | presented study |
| 35S:MAP4-GFP x DEX:amiR-*vps41* (F1) | presented study |
| 35S:MAP4-GFP x DEX:amiR-*vps8* (F2) | presented study |
| UBQ10:INT1-mTurqoise (T2) | presented study |
| UBQ10:INT1-mTurqoise x DEX:amiR-*vps39* (F1) | presented study |
| UBQ10:INT1-mTurqoise x DEX:amiR-*vps8* (F1) | presented study |
| UBQ10:YFP-VAMP711 (WAVE-9Y) | Geldner et al., 2009 |
| UBQ10:YFP-VAMP711 (WAVE-9Y) x DEX:amiR-*vps16* (F1) | presented study |
| UBQ10:YFP-VAMP711 (WAVE-9Y) x DEX:amiR-*vps39* (F1) | presented study |
| UBQ10:YFP-VAMP711 (WAVE-9Y) x DEX:amiR-*vps8* (F1) | presented study |
| UBQ10:pHGFP-VTI11 x DEX:amiR-*vps16* (F1) | presented study |
| UBQ10:pHGFP-VTI11 x DEX:amiR-*vps39* (F1) | presented study |
| UBQ10:pHGFP-VTI11 x DEX:amiR-*vps3* (F1) | presented study |
| UBQ10:2xFYVE-GFP | Vermeer et al., 2006 |
| UBQ10:2xFYVE-GFP x pVHA-a3:VHA-a3-RFP x DEX:amiR-*vps16* (F2) | presented study |
| UBQ10:GFP-VPS16 | Krüger, 2017 |
| UBQ10:GFP-VPS16 x | presented study |

| | |
|---|---|
| pVHA-a3:VHA-a3-RFP (F2) | |
| UBQ10:GFP-VPS16 x UBQ10:VHP1-mCherry (F2) | presented study |
| UBQ10:mCherry-RABG3f (WAVE-5R) | Geldner et al., 2009 |
| VHA-a3p:VHA-a3-GFP x UBQ10:mCherry-RABG3f (WAVE-5R) x DEX:amiR-*vps16* (F3) | presented study |
| UBQ10:RFP-ARA7 | Scheuring et al., 2011 |
| VHA-a3p:VHA-a3-GFP x UBQ10:RFP-ARA7 x DEX:amiR-*vps16* (F2) | presented study |
| *vha-a2 vha-a3* mutant | Krebs et al., 2010 |
| *pat2-2* mutant | Feraru et al., 2010 |
| *zig1-1* | Kato, 2002 |
| MAP4-GFP x *zig1-1* (F2) | presented study |
| UBQ10:GFP-ABD2-GFP x *zig1-1* (F3) | presented study |
| *gfs9-3* | Ichino et al., 2014 |
| MAP4-GFP x *gfs9-3* (F2) | presented study |
| 35S:Lifeact-Venus x *gfs9-3* (F3) | presented study |

### 7.2.2 Growth of Arabidopsis

*Arabidopsis thaliana* seeds were sterilized before sowing them on ½ MS agar plates. For seed sterilization, two solutions with an increasing Ethanol (EtOH) concentration were subsequently used. The first sterilization solution consisted of 70 % EtOH and 0.05 % TritonX-100. In a 1.5 ml tube, seeds and 700 ml were inverted for 10 min. Afterwards, the seeds were treated with 700 ml of a 95 % EtOH solution for 7 min and dried on sterile filter paper. Seeds were placed on solid ½ MS medium and vernalized in the dark at 4 °C for 48 h.

For Dex induction of knockdowns, seedlings were grown for 5 days on plates and then transferred to liquid medium with 30 µM Dex or the corresponding amount of DMSO.

Dex-induced expression of Sar1b-GTP was induced for 6 hr with 60 $\mu$M Dex or DMSO in liquid ½ MS medium. The estradiol induction system was activated with 60 $\mu$M beta-estradiol or with DMSO as control.

To investigate the morphology of the root tips or the organization of the cytoskeleton ½ MS plates with 1 % phytoagar were used. Plates were covered with autoclaved, square sheets of 100 $\mu$m polyamid sieve mesh (manufactured by Klein & Wieler oHG). Seeds were sown directly into the polyamid mesh, and the mesh was transferred after 5 days to 1 % phytoagar ½ MS plates containing either DMSO or Dex.

To propagate plants, seedlings were transferred after 5 days of growing on ½ MS plates to soil and frequently watered. To sow seeds directly to soil, 20 to 30 seeds were placed in 2 ml tubes, 1.5 ml Top-Agar was added, and seeds were vernalized for 2 nights in the dark at 4 °C. Seeds were directly placed on soil by pipetting 500 – 1,000 µl of Top-Agar with seeds onto the soil. After the seedlings had developed their first true leaves, seedlings had to be thinned out to the wanted number per pot.

Seedlings and plants were grown at 21°C under long day conditions with a photoperiod of 16 hr, 8 hr darkness and a light intensity of approximately 90 - 110 µE/$m_2$/sec. Arabidopsis plants in the vha-a2 vha-a3 mutant background were grown under constant light conditions.

For crossing of two genotypes, the anthers of flowers from one genotype were removed and the remaining stigma (female) were covered in ripe pollen from the other genotype (male). Crossed flowers were separated with paper bags and ripe siliques were harvested.

## 7.3 Plasmid Cloning

### 7.3.1 Cloning strategy

Green Gate Cloning was performed according to Lampropoulos et al., 2013. Correct plasmids were identified with test digests and sequencing. The created destination vectors were transformed to *A. tumefaciens* ASE1 (pSOUP+). Arabidopsis plants were transformed with the checked agrobacteria.

**DEX:Sar1b-GTP-CFP/mVenus**

The DEX:Sar1b-GTP-mVenus construct was cloned by Upendo Lupanga and Philipp Bellon. The DEX:Sar1b-GTP-mVenus construct was similarly cloned to the DEX:Sar1b-GTP-CFP (Dex:Sar1BH74L-CFP) construct published in Lupanga et al., 2020 except for that the used N module was created with mVenus (GSL-mVenus, p2456) instead of CFP (cyan fluorescent protein) and a sulfadiazine resistance (SulfR, pGGF012, Lampropoulos et al., 2013).

In addition to this construct, a DEX:Sar1b-GTP-CFP construct was cloned by Upendo Lupanga and Philipp Bellon, which contained a Hygromycin resistance (HygR, pGGF005) instead of a sulfadiazine resistance. The HygR containing construct was used for the transformation of VHP1-GFP and VHA-a3-a1-TD-GFP expressing Arabidopsis plants.

**UBQ10:INT1-mTurquoise**

This construct was cloned by Marlene Handl as described in (Handl, 2019). The INT1 CDS sequence was amplified with the primers KS-q4287 KS-q4288 (Table *4*) and by Upendo Lupanga. The destination vector was created in a Green Gate reaction (Lampropoulos et al., 2013) with pUBQ10 (A006), B-decoy (B003), PCR fragment of INT1 CDS, pGGD-mCherry (p0846), pGGE-tHSP18.2M (p1296), pGGF012 SulfR (p2783) and pGG-Z003.

**UBQ10:AHA10-mVenus**

This construct was cloned by Meliha Görkem Patir Nebioglu using a conventional cloning method with the barII-UT-mVenus vector (Waadt et al., 2015). AHA10 gDNA was amplified from Col-0 with the primer pair AHA10 Forward and AHA10

Reverse (Table 4) inserting XhoI and SpeI restriction sites. The PCR product was cloned into the pJet1.2 vector for sequencing. Digestion with XhoI and SpeI cut out the AHA10 fragment and the barII-UT-mVenus vector backbone, which were purified using the Qiagen kit and ligated overnight. To verify correct clones test digestion and sequencing was performed. Correct binary vectors were transformed into A. tumefaciens strain GV3101.

**UBQ10:VHA-a3-mCherry-eGFP**

With the CDS of VHA-a3 the vector pGGC-VHA-a3 (pKSC003) was cloned by Ann-Kathrin Schürholz and Stefan Scholl and published in Lupanga et al., 2020. Lotte Bald cloned the D-module containing the two fluorophores mCherry and eGFP (pGGD-mCherry-eGFP, pKSD002). For this mCherry was amplified with primers that removed the STOP codon and a unique overhang between mCherry and eGFP was created (KS-q2193, KS-q2195, KS-q2199, KS-q2194, Table *4*). Lotte Bald performed a Green Gate reaction to create a destination vector with pUBQ10 (pGGA006), N-decoy (pGGB003), pGGC-VHA-a3 (pKSC003), pGGD-mCherry-eGFP, rbcs terminator (pGGE001) and BastaR (pGGF001) in pGGZ001.

**UBQ10:VHP1-mCherry**

The genomic sequence of VHP1 was amplified from Col-0 gDNA. Two parts of the VHP1 genomic sequence were cloned in a B module and D module to insert the fluorophore as a C module within the gDNA sequence of VHP1: pGGB-VHP1-I (pKSB001) and pGGD-VHP1-II (pKSD006). For the PCR amplification of VHP1-I the primers KS-q2422 and KS-q2423 (Table *4*) were used. At end of part 1 of VHP1 (VHP1-I) a Glycin-Serin-Linker was introduced with the primers. To create pGGD-VHP1-II two internal Eco31I sites had to be removed with the primers KS-q2424, KS-q2425, KS-q2426, KS-q2427, KS-q2428 and KS-q2429 (Table *4*). Lotte Bald performed a Green Gate reaction (Lampropoulos et al., 2013) to create a destination vector with pUBQ10 (pGGA006), pGGB-VHP1-I, pGGC-mCherry, pGGD-VHP1-II, rbcs terminator (pGGE001), hygromycin resistance (HygR, pGGF005) in pGGZ001.

**pUXVE2:VHA-a3-LinkerGFP**

pGGC-VHA-a3 (pKSC003) was cloned by Ann-Kathrin Schürholz and Stefan Scholl and published in Lupanga et al., 2020. Together with Florian Hinterberger a Green Gate reaction was performed to create a destination vector with pUXVE2 (p3395), B-decoy (B003), pGGC-VHA-a3 (pKSC003), LinkerGFP (pGGD001, p1005), tHSP18.3M (p1296) and BastaR (p1316) in pGGZ004.

**pUXVE2:mCherry-ARA7-GDP**

This construct was cloned together with Sina Pfleger with the Green Gate method (Lampropoulos et al., 2013). Two PCRs to amplify the ARA7 CDS from the RFP-ARA7 plasmid (Scheuring et al., 2011) were performed to insert the S24N mutation ("TCA" to "AAC") via modified primer overhangs (KS-q3745, KS-q3750, KS-q3749, KS-q3746, Table *4*). The two PCR fragments were ligated into the pGGC vector with a Green Gate reaction (pGGC-ARA7S24N). For creating the destination module a Green Gate reaction with pUXVE2 (p3395, the estradiol inducible expression system published in Denninger et al., 2019), pGGB-mCherry (no Linker, p0832), pGGC-ARA7S24N, C-decoy (pGGD017), tHSP18.2M (p1296) and Basta resistance (pGGF-BarR, p1316) into pGGZ003 was performed.

Table 4: Table listing the used primers for cloning.

| Primer | ID | Sequence |
|---|---|---|
| AHA10 Forward | KS-q3182 | TTT ACT AGT ATG GCC GAG GAT TTG GAC AAG |
| AHA10 Reverse | KS-q3183 | TTT CTC GAG GAC AGT ATG AGC TGC ACG GAT |
| GG-mCherry-fwd | KS-q2193 | TGTGGTCTCTTCAGTTATGGTGAGCAAGGGCGAGG A |
| GG-mCherry-noSTOP-Rev | KS-q2195 | TGTGGTCTCAGTTAACGGCTAACTTGTACAGCTCGT CCA |
| GG-eGFP-fwd | KS-q2199 | TGTGGTCTCATAACGCTAGCATGGTGAGCAAGGGC GAGGA |
| GG-eGFP-rev | KS-q2194 | TGTGGTCTCAGCAGTTACTTGTACAGCTCGTCCA |
| VHP1 B fw | KS-q2422 | ACAGGTCTCAAACAATGGTGGCGCCTGCTTTG |
| VHP1-GS linker C rv | KS-q2423 | ACAGGTCTCTAGCCACCTCCTCCTGATCCA |
| VHP1-II D fw (Fragment 1) | KS-q2424 | ACAGGTCTCATCAGCATCGTCTTCCGGT |
| GG VHP1 Int 1 rv (Fragment 1) | KS-q2425 | TGTGGTCTCTTTCAACTCCAAAGAAGAAACC |

| | | |
|---|---|---|
| GG VHP1 Int 1 fw (Fragment 2) | KS-q2426 | TGTGGTCTCTTGAAACCCTCTCTGGTGTC |
| GG VHP1 Int 2 rv (Fragment 2) | KS-q2427 | TGTGGTCTCGGTCACCAATTGTGTCTCCA |
| GG VHP1 Int 2 fw (Fragment 3) | KS-q2428 | TGTGGTCTCGTGACCCATTGAAGGATACT |
| VHP1-II E rv (Fragment 3) | KS-q2429 | ACAGGTCTCTGCAGTTAGAAGTACTTGAAAAGG |
| INT1 Fw | KS-q4287 | AAC AGG TCT CAG GCT CAA CAA TGA CAT TGA CGA TCC CAA AC |
| INT1 Rev | KS-q4288 | AAC AGG TCT CTC TGA AGA TTG AGA TCC CTG CTC GAG |
| ARA7 fw (Fragment 1) | KS-q3745 | AACAGGTCTCAGGCTCAACAATGGCTGCAGCTGGA AACAAGAGC |
| GG ARA7 S24N Reverse (Fragment 1) | KS-q3750 | AACAGGTCTCTTGTTTTTTCCAGCACCAACATCTCC |
| GG ARA7 S24N Forward (Fragment 2) | KS-q3749 | AACAGGTCTCAAACAGTCTTGTGTTACGGTTTGTCA AAG |
| ARA7 rev (Fragment 2) | KS-q3746 | AACAGGTCTCTCTGAAGCACAACAAGATGAGCTCAC TGCC |

### 7.3.2 Culturing of bacteria

After the transformation of ligated plasmids or retransformation of plasmids, *E. coli* was grown on solid medium supplemented with selective antibiotics over night at 37 °C. To isolate plasmid DNA, liquid bacterial cultures with selective antibiotics were grown over night in the 37 °C shaker.

After the transformation of plasmids, *A. tumefaciens* ASE was grown on solid medium for 2 days at 28 °C. Single colonies were transferred to fresh LB plates with selective antibiotics and grown over night at 28 °C. Then, colonies were inoculated in liquid LB medium with selective antibiotics to grow cultures for minipreps or the transformation of *A. thaliana*.

*A. tumefaciens* GV3101 were grown with Gent, Rif and the respective antibiotic from the transformed plasmid on LB medium at 28 °C.

### 7.3.3 Transformation of E. coli

Transformation competent E. coli were stored in 50 µl aliquots at - 80 °C. Prior to transformation, bacteria were thawed on ice. Either 5 µl of a ligation mix or 1 µl of a miniprep were added to the competent E. coli and mixed by gently tapping the tube. Afterwards, the E. coli cells rested for 30 min on ice, were heat shocked for 45 sec at 42 °C. After 5 min on ice, 1 ml liquid LB medium without selective antibiotics was added. The cells were incubated for 2 hr at 37 °C on a shaker before plating on LB plates containing a selective antibiotic. E. coli bacteria were grown over night at 37 °C.

### 7.3.4 Transformation of A. tumefaciens

Chemically competent agrobacteria were thawed at room temperature. Then 2 µl of the plasmid were added and the cells were placed on ice for 10 min before freezing in liquid nitrogen for 5 min. Agrobacteria were incubated at 37 °C for 5 min and 800 µl liquid LB medium were added and cells were placed on a shaker at 28 °C for up to 4 hr. The GV3101 strain was plated on LB plates containing Rifampicin (chromosomal selection), Gentamycin (Ti-plasmid selection) and the respective antibiotic encoded on the transformed plasmid.

Agrobacteria transformed with Green Gate plasmids (ASE1 strain) were plated on LB medium with Chloramphenicol (chromosomal selection), Kanamycin (Ti-plasmid selection), Tetracycline (pSOUP selection) and Spectinomycin (Green Gate Destination vector).

### 7.3.5 Transformation of Arabidopsis

Transformation of Arabidopsis was performed after a modified protocol from Clough and Bent, 1998. Two days prior to Arabidopsis transformation, agrobacteria were applied to two fresh LB plates with selective antibiotics and grown at 28 °C. Then 15 ml LB medium were added to each of the two LB plates with the grown agrobacteria. Agrobacteria were loosened from the medium with a spatula and dissolved with a 1 ml pipette. LB solution with dissolved agrobacteria were added to the 120 ml solution for floral dip (5 % sucrose, 0.03 % Silwet L-77). Arabidopsis

plants were dipped for approximately 40 to 60 sec. Arabidopsis plants were covered with lids and placed in the dark overnight.

### 7.3.6 Miniprep to isolate plasmid DNA

2 ml of an E. coli culture were transferred to a 2 ml tube, centrifuged at 6800 g and the supernatant was discarded. The cells were resuspended in 200 µl cold buffer P1 before adding 200 µl buffer P2 and the inversion of the tube. Then 200 µl cold buffer P3 were added, and the tube was inverted followed by centrifugation at full speed for 10 min. The supernatant was transferred to a fresh 1.5 ml tube, in which 500 µl isopropanol were placed and the mixture was inverted. Again, the tube was centrifuged at full speed for 10 min. Supernatant was removed and the pellet was washed with 500 µl 70 % Ethanol. The tube was centrifuged at full speed for 3 min and the supernatant was removed with a combination of blue and white pipette tip. Pellet was dried at 70 °C and dissolved in 50 µl dd$H_2O$.

Liquid A. tumefaciens cultures were prepped with the innuPrep Plasmid Mini Kit (analytikjena) and the manual was followed. Afterwards 6 µl of the miniprep was transformed to E. coli for retransformation and test digests to verify the correctness of the transformed plasmids in agrobacteria.

## 7.4 Electron Microscopy

Samples were prepared by Upendo Lupanga, me, Stephanie Gold and Stefan Hillmer and processed as described in Scheuring et al., 2011 and Hillmer et al., 2012. To prevent the rupturing of root cells, the knockdown against *VPS8* was induced for 48 hr with 30 µM Dex. Ultrathin sections were observed in JEM1400 transmission electron microscope (JEOL) operating at 80 kV and images were taken with with a TemCam F416 digital camera (TVIPS) by Stefan Hillmer. Brightness and contrast were adjusted with Image J/FIJI.

## 7.5 Confocal Scanning Laser Microscopy

Confocal Scanning Laser Microscopy (CLSM) was performed with a Leica TCS SP5II microscope equipped with a Leica HCX PL APO lambda blue 63.0 x 1.20 UV water immersion objective and a standard PC operating the Leica Application Suite Advanced Fluorescence software (LASAF). The used imaging settings to record

the different fluorophores are summarized in (Table 5). Z-stacks were recorded with a distance of 0.17 $\mu$m for examination of BCECF stained vacuole morphology and 420 nm for investigating homotypic vacuole fusion and cytoskeletal organization.

Table 5: Used settings for confocal scanning laser microscopy (CLSM).

| Fluorophore/Dye | Laser | Excitation wavelength | Emission detection |
|---|---|---|---|
| CFP, mTurquoise | VIS-Argon | 458 nm | 460 - 480 |
| GFP, eGFP, BCECF | VIS-Argon | 488 nm | 495 – 555 nm |
| mVenus | VIS-Argon | 514 nm | 524 – 570 nm |
| RFP, mCherry | VIS-DPSS 561 | 561 nm | 593 – 636 nm |
| FM4-64 | VIS-DPSS 561 | 561 nm | 700 – 776 nm |

The vacuolar lumen was stained with 10 $\mu$M BCECF-AM for 90 min up to 2 hr followed by an optional wash step of up to an additional hr. To label the plasma membrane and the TGN/EE 1 $\mu$M FM4-64 was applied for 15 to 20 min.

Post-acquisition image processing, such as Gaussian blur between 0.6 and 0.9, Z-stack projection, adjustment of brightness and contrast of the whole image, and overlays of different emission channels, was done with Image J/FIJI. To perform projection of Z-stacks, the “3D projection” macro was applied with total rotation = 0, brightest point as projection method and interpolation activated.

Proteasomal inhibition was done with 10 $\mu$M MG132 for 4 hr. Autophagy in root cells was induced with 500 nm ConcA for 5 hr. To examine if VHA-a3-GFP accumulates in Brefeldin A induced BFA bodies, 25 $\mu$M BFA was added for 4 hr. The sensitivity of VHA-a3-GFP and VHP1-GFP to ConcA was tested with 500 nM ConcA for 5 hr. Monensin was applied in a concentration of 10 $\mu$M for 90 min. To examine the trafficking of estradiol-induced VHA-a3-LinkerGFP 60 $\mu$M β-estradiol, 25 $\mu$M BFA for 6 hr and 1 $\mu$M ConcA for 6 hr were used. To compare the microtubule organization 10 $\mu$M IAA (indole-3-acetic acid) for 20 hr used. To investigate the WM-induced vacuolar fusion 33 $\mu$M WM for 4 hr and 500 nm ConcA for 5 hr were used. The vacuolar inclusions caused by WM were investigated with VHA-a3-RFP stained with BCECF and treated with 33 $\mu$M WM for 6 hr. Further

examinations on vacuolar inclusions were performed with VHP1-GFP and a cross of VHA-a3-GFP and mRFP-ARA7 treated with 33 $\mu$M WM for 1 hr.

# 8 References

**Ando, R., Hama, H., Yamamoto-Hino, M., Mizuno, H., and Miyawaki, A.** (2002). An optical marker based on the UV-induced green-to-red photoconversion of a fluorescent protein. Proc. Natl. Acad. Sci. U. S. A. **99**: 12651–12656.

**Armstrong, J.** (2010). Yeast vacuoles: More than a model lysosome. Trends Cell Biol. **20**: 580–585.

**Askani, J.C.** (2015). The function of tethering complexes in vacuole development in Arabidopsis thaliana. Master Thesis. Faculty of Biosciences of the Ruprecht-Karls-Universität Heidelberg.

**Baars, T.L., Petri, S., Peters, C., and Mayer, A.** (2007). Role of the V-ATPase in regulation of the vacuolar fission-fusion equilibrium. Mol. Biol. Cell **18**: 3873–3882.

**Balderhaar, H.J.K. and Ungermann, C.** (2013). CORVET and HOPS tethering complexes - coordinators of endosome and lysosome fusion. J. Cell Sci. **126**: 1307–1316.

**Balleza, E., Kim, J.M., and Cluzel, P.** (2018). Systematic characterization of maturation time of fluorescent proteins in living cells. Nat. Methods **15**: 47–51.

**Banta, L.M., Robinson, J.S., Klionsky, D.J., and Emr, S.D.** (1988). Organelle assembly in yeast: characterization of yeast mutants defective in vacuolar biogenesis and protein sorting. J. Cell Biol. **107**: 1369–1383.

**Batistič, O., Waadt, R., Steinhorst, L., Held, K., and Kudla, J.** (2009). CBL-mediated targeting of CIPKs facilitates the decoding of calcium signals emanating from distinct cellular stores. Plant J. **61**: 211–222.

**Baxter, I.R., Young, J.C., Armstrong, G., Foster, N., Bogenschutz, N., Cordova, T., Peer, W.A., Hazen, S.P., Murphy, A.S., and Harper, J.F.** (2005). A plasma membrane H+-ATPase is required for the formation of proanthocyanidins in the seed coat endothelium of Arabidopsis thaliana.

Proc. Natl. Acad. Sci. U. S. A. **102**: 2649–2654.

**van der Beek, J., Jonker, C., van der Welle, R., Liv, N., and Klumperman, J.** (2019). CORVET, CHEVI and HOPS – Multisubunit tethers of the endo-lysosomal system in health and disease. J. Cell Sci. **132**.

**Beyenbach, K.W. and Wieczorek, H.** (2006). The V-type H+ ATPase: Molecular structure and function, physiological roles and regulation. J. Exp. Biol. **209**: 577–589.

**Boevink, P., Oparka, K., Cruz, S.S., Martin, B., Betteridge, A., and Hawes, C.** (1998). Stacks on tracks: The plant Golgi apparatus traffics on an actin/ER network. Plant J. **15**: 441–447.

**Boncompain, G., Divoux, S., Gareil, N., de Forges, H., Lescure, A., Latreche, L., Mercanti, V., Jollivet, F., Raposo, G., and Perez, F.** (2012). Synchronization of secretory protein traffic in populations of cells. Nat. Methods **9**: 493–498.

**Brillada, C., Zheng, J., Krüger, F., Rovira-Diaz, E., Askani, J.C., Schumacher, K., and Rojas-Pierce, M.** (2018). Phosphoinositides control the localization of HOPS subunit VPS41, which together with VPS33 mediates vacuole fusion in plants. Proc. Natl. Acad. Sci. **115**: 201807763.

**Brüx, A., Liu, T.-Y., Krebs, M., Stierhof, Y.-D., Lohmann, J.U., Miersch, O., Wasternack, C., and Schumacher, K.** (2008). Reduced V-ATPase Activity in the trans-Golgi Network Causes Oxylipin-Dependent Hypocotyl Growth Inhibition in Arabidopsis. Plant Cell Online **20**: 1088–1100.

**Carter, C., Pan, S., Zouhar, J., Avila, E.L., Girke, T., and Raikhel, N. V** (2004). The vegetative vacuole proteome of Arabidopsis thaliana reveals predicted and unexpected proteins. Plant Cell **16**: 3285–303.

**Chung, K.P., Zeng, Y., and Jiang, L.** (2016). COPII Paralogs in Plants: Functional Redundancy or Diversity? Trends Plant Sci. **21**: 758–769.

**Clough, S.J. and Bent, A.F.** (1998). Floral dip: A simplified method for Agrobacterium-mediated transformation of Arabidopsis thaliana. Plant J. **16**: 735–743.

**Cormack, B.P., Valdivia, R.H., and Falkow, S.** (1996). FACS-optimized mutants of the green fluorescent protein (GFP). In Gene (Elsevier B.V.), pp. 33–38.

**Craft, J., Samalova, M., Baroux, C., Townley, H., Martinez, A., Jepson, I., Tsiantis, M., and Moore, I.** (2005). New pOp/LhG4 vectors for stringent glucocorticoid-dependent transgene expression in Arabidopsis. Plant J. **41**: 899–918.

**Cui, Y. et al.** (2018). A whole-cell electron tomography model of vacuole biogenesis in Arabidopsis root cells. Nat. Plants.

**Cui, Y., Shen, J., Gao, C., Zhuang, X., Wang, J., and Jiang, L.** (2016). Biogenesis of Plant Prevacuolar Multivesicular Bodies. Mol. Plant: 1–13.

**Cui, Y., Zhao, Q., Gao, C., Ding, Y., Zeng, Y., Ueda, T., Nakano, A., and Jiang, L.** (2014). Activation of the Rab7 GTPase by the MON1-CCZ1 Complex Is Essential for PVC-to-Vacuole Trafficking and Plant Growth in Arabidopsis. Plant Cell **26**: 2080–2097.

**D'Agostino, M., Risselada, H.J., Endter, L.J., Comte- Miserez, V., and Mayer, A.** (2018). SNARE - mediated membrane fusion arrests at pore expansion to regulate the volume of an organelle. EMBO J. **37**.

**daSilva, L.L.P.** (2004). Endoplasmic Reticulum Export Sites and Golgi Bodies Behave as Single Mobile Secretory Units in Plant Cells. Plant Cell Online **16**: 1753–1771.

**Day, R.N. and Davidson, M.W.** (2009). The fluorescent protein palette: tools for cellular imaging. Chem. Soc. Rev. **38**: 2887.

**Delgadillo, M.O. et al.** (2020). MTV proteins unveil ER- And microtubule-associated compartments in the plant vacuolar trafficking pathway. Proc. Natl. Acad. Sci. U. S. A. **117**: 9884–9895.

**Denninger, P., Reichelt, A., Schmidt, V.A.F., Mehlhorn, D.G., Asseck, L.Y., Stanley, C.E., Keinath, N.F., Evers, J.F., Grefen, C., and Grossmann, G.** (2019). Distinct RopGEFs Successively Drive Polarization and Outgrowth of Root Hairs. Curr. Biol. **29**: 1854-1865.e5.

**Dettmer, J., Hong-Hermesdorf, A., Stierhof, Y.-D., and Schumacher, K.** (2006). Vacuolar H+-ATPase Activity Is Required for Endocytic and Secretory Traf cking in Arabidopsis. Plant Cell **18**: 715–730.

**Dettmer, J., Schubert, D., Calvo-Weimar, O., Stierhof, Y.D., Schmidt, R., and Schumacher, K.** (2005). Essential role of the V-ATPase in male gametophyte development. Plant J. **41**: 117–124.

**Dragwidge, J.M., Scholl, S., Schumacher, K., and Gendall, A.R.** (2019). NHX-type Na+(K+)/H+antiporters are required for TGN/EE trafficking and endosomal ion homeostasis in Arabidopsis thaliana. J. Cell Sci. **132**.

**Dünser, K., Gupta, S., Herger, A., Feraru, M.I., Ringli, C., and Kleine- Vehn, J.** (2019). Extracellular matrix sensing by FERONIA and Leucine- Rich Repeat Extensins controls vacuolar expansion during cellular elongation in Arabidopsis thaliana . EMBO J. **38**.

**Dyachok, J., Sparks, J.A., Liao, F., Wang, Y.S., and Blancaflor, E.B.** (2014). Fluorescent protein-based reporters of the actin cytoskeleton in living plant cells: Fluorophore variant, actin binding domain, and promoter considerations. Cytoskeleton **71**: 311–327.

**Ebine, K. et al.** (2011). A membrane trafficking pathway regulated by the plant-specific RAB GTPase ARA6. Nat. Cell Biol. **13**: 853–9.

**Ebine, K., Inoue, T., Ito, J., Ito, E., Uemura, T., Goh, T., Abe, H., Sato, K., Nakano, A., and Ueda, T.** (2014). Plant vacuolar trafficking occurs through distinctly regulated pathways. Curr. Biol. **24**: 1375–1382.

**Ebine, K., Okatani, Y., Uemura, T., Goh, T., Shoda, K., Niihama, M., Morita, M.T., Spitzer, C., Otegui, M.S., Nakano, A., and Ueda, T.** (2008). A SNARE complex unique to seed plants is required for protein storage vacuole biogenesis and seed development of Arabidopsis thaliana. Plant Cell **20**: 3006–3021.

**Epp, N., Rethmeier, R., Krämer, L., and Ungermann, C.** (2011). Membrane dynamics and fusion at late endosomes and vacuoles - Rab regulation, multisubunit tethering complexes and SNAREs. Eur. J. Cell Biol. **90**: 779–

785.

**Era, A., Tominaga, M., Ebine, K., Awai, C., Saito, C., Ishizaki, K., Yamato, K.T., Kohchi, T., Nakano, A., and Ueda, T.** (2009). Application of lifeact reveals F-actin dynamics in arabidopsis thaliana and the liverwort, marchantia polymorpha. Plant Cell Physiol. **50**: 1041–1048.

**Feng, Q.-N., Song, S.-J., Yu, S.-X., Wang, J.-G., Li, S., and Zhang, Y.** (2017a). AP3 adaptor protein-dependent vacuolar trafficking involves a subpopulation of COPII and HOPS tethering proteins. Plant Physiol.: pp.00584.2017.

**Feng, Q.-N., Zhang, Y., and Li, S.** (2017b). Tonoplast targeting of VHA-a3 relies on a Rab5-mediated but Rab7-independent vacuolar trafficking route. J. Integr. Plant Biol. **59**: 230–233.

**Feraru, E., Paciorek, T., Feraru, M.I., Zwiewka, M., De Groodt, R., De Rycke, R., Kleine-Vehn, J., and Friml, J.** (2010). The AP-3 Adaptin Mediates the Biogenesis and Function of Lytic Vacuoles in Arabidopsis. Plant Cell **22**: 2812–2824.

**Fink, F.** (2012). The V-ATPase in Arabidopsis thaliana : A closer look to targeting , new interaction partners and its role for ER acidification. Master Thesis. Faculty of Biosciences at the Ruprecht-Karls-Universität Heidelberg.

**Forgac, M.** (2007). Vacuolar ATPases: Rotary proton pumps in physiology and pathophysiology. Nat. Rev. Mol. Cell Biol. **8**: 917–929.

**Fredj, A., Pasquier, H., Demachy, I., Jonasson, G., Levy, B., Derrien, V., Bousmah, Y., Manoussaris, G., Wien, F., Ridard, J., Erard, M., and Merola, F.** (2012). The Single T65S Mutation Generates Brighter Cyan Fluorescent Proteins with Increased Photostability and pH Insensitivity. PLoS One **7**: e49149.

**Gaxiola, R.A., Palmgren, M.G., and Schumacher, K.** (2007). Plant proton pumps. FEBS Lett. **581**: 2204–14.

**Geldner, N., Dénervaud-Tendon, V., Hyman, D.L., Mayer, U., Stierhof, Y.-D., and Chory, J.** (2009). Rapid, combinatorial analysis of membrane compartments in intact plants with a multicolor marker set. Plant J. **59**: 169–

78.

**Geldner, N., Hyman, D.L., Wang, X., Schumacher, K., and Chory, J.** (2007). Endosomal signaling of plant steroid receptor kinase BRI1. Genes Dev. **21**: 1598–1602.

**Handl, M.** (2019). Comparison between different genetic tools in regard to blocking COPII-mediated ER export in Nicotiana benthamiana. Bachelor Thesis. Faculty of Biosciences at the Ruprecht-Karls-Universität Heidelberg.

**Hao, L., Liu, J., Zhong, S., Gu, H., and Qu, L.-J.** (2016). AtVPS41-mediated endocytic pathway is essential for pollen tube–stigma interaction in *Arabidopsis*. Proc. Natl. Acad. Sci.: 201602757.

**Hillmer, S., Viotti, C., and Robinson, D.G.** (2012). An improved procedure for low-temperature embedding of high-pressure frozen and freeze-substituted plant tissues resulting in excellent structural preservation and contrast. J. Microsc. **247**: 43–47.

**Höfte, H.** (2015). The yin and yang of cell wall integrity control: brassinosteroid and FERONIA signaling. Plant Cell Physiol. **56**: 224–231.

**Holzheu, P., Krebs, M., Larasati, C., Schumacher, K., and Kummer, U.** (2021). An integrative view on vacuolar pH- homeostasis in Arabidopsis thaliana : Combining mathematical modeling and experimentation. Plant J.: tpj.15251.

**Hoole, S. and Leeuwenhoek, A. van** (1800). The select works of Antony van Leeuwenhoek : containing his microscopical discoveries in many of the works of nature / translated from the Dutch and Latin editions published by the author, by Samuel Hoole. (G. Sidney,: London :).

**Hunter, P.R., Craddock, C.P., Di Benedetto, S., Roberts, L.M., and Frigerio, L.** (2007). Fluorescent reporter proteins for the tonoplast and the vacuolar lumen identify a single vacuolar compartment in Arabidopsis cells. Plant Physiol. **145**: 1371–1382.

**Hurtado-Lorenzo, A., Skinner, M., El Annan, J., Futai, M., Sun-Wada, G.H.,**

**Bourgoin, S., Casanova, J., Wildeman, A., Bechoua, S., Ausiello, D.A., Brown, D., and Marshansky, V.** (2006). V-ATPase interacts with ARNO and Arf6 in early endosomes and regulates the protein degradative pathway. Nat. Cell Biol. **8**: 124–136.

**Ichino, T., Fuji, K., Ueda, H., Takahashi, H., Koumoto, Y., Takagi, J., Tamura, K., Sasaki, R., Aoki, K., Shimada, T., and Hara-Nishimura, I.** (2014). GFS9/TT9 contributes to intracellular membrane trafficking and flavonoid accumulation in Arabidopsis thaliana. Plant J. **80**: 410–23.

**Ito, E., Ebine, K., Choi, S., Ichinose, S., Uemura, T., Nakano, A., and Ueda, T.** (2018). Integration of two RAB5 groups during endosomal transport in plants. Elife **7**: 1–22.

**Jonker, C.T.H., Galmes, R., Veenendaal, T., Ten Brink, C., Van Der Welle, R.E.N., Liv, N., De Rooij, J., Peden, A.A., Van Der Sluijs, P., Margadant, C., and Klumperman, J.** (2018). Vps3 and Vps8 control integrin trafficking from early to recycling endosomes and regulate integrin-dependent functions. Nat. Commun. **9**: 1–12.

**Kaiser, S., Eisa, A., Kleine-Vehn, J., and Scheuring, D.** (2019). NET4 Modulates the Compactness of Vacuoles in Arabidopsis thaliana. Int. J. Mol. Sci. **20**: 4752.

**Kalinowska, K., Nagel, M.-K., Goodman, K., Cuyas, L., Anzenberger, F., Alkofer, A., Paz-Ares, J., Braun, P., Rubio, V., Otegui, M.S., and Isono, E.** (2015). Arabidopsis ALIX is required for the endosomal localization of the deubiquitinating enzyme AMSH3. Proc. Natl. Acad. Sci.: 201510516.

**Karim, M.A., McNally, E.K., Samyn, D.R., Mattie, S., and Brett, C.L.** (2018). Rab-Effector-Kinase Interplay Modulates Intralumenal Fragment Formation during Vacuole Fusion. Dev. Cell **47**: 80-97.e6.

**Kato, T.** (2002). SGR2, a Phospholipase-Like Protein, and ZIG/SGR4, a SNARE, Are Involved in the Shoot Gravitropism of Arabidopsis. PLANT CELL ONLINE **14**: 33–46.

**Kawasaki-Nishi, S., Bowers, K., Nishi, T., Forgac, M., and Stevens, T.H.**

(2001). The Amino-terminal Domain of the Vacuolar Proton-translocating ATPase a Subunit Controls Targeting and in Vivo Dissociation, and the Carboxyl-terminal Domain Affects Coupling of Proton Transport and ATP Hydrolysis. J. Biol. Chem. **276**: 47411–47420.

**Khmelinskii, A. and Knop, M.** (2014). Analysis of Protein Dynamics with Tandem Fluorescent Protein Timers. Methods Mol. Biol. **1174**: 195–210.

**Kim, B.Y., Ueda, M., Nakamura, Y., Kohsaka, S., and Akazawa, C.** (2004). Expression of the mammalian homologue of vacuolar protein sorting 16 (Vps16p) in the mouse and rat brain. Neurosci. Lett. **355**: 217–220.

**Kolb, C., Nagel, M.-K., Kalinowska, K., Hagmann, J., Ichikawa, M., Anzenberger, F., Alkofer, A., Sato, M.H., Braun, P., and Isono, E.** (2015). FYVE1 Is Essential for Vacuole Biogenesis and Intracellular Trafficking in Arabidopsis. Plant Physiol. **167**: 1361–1373.

**Kotzer, A.M., Brandizzi, F., Neumann, U., Paris, N., Moore, I., and Hawes, C.** (2004). AtRabF2b (Ara7) acts on the vacuolar trafficking pathway in tobacco leaf epidermal cells. J. Cell Sci. **117**: 6377–6389.

**Krebs, M., Beyhl, D., Görlich, E., Al-Rasheid, K. a S., Marten, I., Stierhof, Y.-D., Hedrich, R., and Schumacher, K.** (2010). Arabidopsis V-ATPase activity at the tonoplast is required for efficient nutrient storage but not for sodium accumulation. Proc. Natl. Acad. Sci. U. S. A. **107**: 3251–3256.

**Kreis, T.E., Lowe, M., and Pepperkok, R.** (1995). COPs Regulating Membrane Traffic. Annu. Rev. Cell Dev. Biol. **11**: 677–706.

**Kriegel, A. et al.** (2015). Job Sharing in the Endomembrane System: Vacuolar Acidification Requires the Combined Activity of V-ATPase and V-PPase. Plant Cell: tpc.15.00733.

**Krüger, F.** (2017). Vacuole biogenesis in Arabidopsis thaliana. Dissertation. Ruprecht-Karls-Universität Heidelberg.

**Krüger, F. and Schumacher, K.** (2017). Pumping up the volume – vacuole biogenesis in Arabidopsis thaliana. Cell Dev. Biol.

**Lampropoulos, A., Sutikovic, Z., Wenzl, C., Maegele, I., Lohmann, J.U., and Forner, J.** (2013). GreenGate - A Novel, Versatile, and Efficient Cloning System for Plant Transgenesis. PLoS One **8**: e83043.

**Lee, H.N., Zarza, X., Kim, J.H., Yoon, M.J., Kim, S.-H., Lee, J.-H., Paris, N., Munnik, T., Otegui, M.S., and Chung, T.** (2018). Arabidopsis VPS38 is required for vacuolar trafficking but dispensable for autophagy. Plant Physiol.: pp.01297.2017.

**Lee, Y., Kim, E.-S., Choi, Y., Hwang, I., Staiger, C.J., Chung, Y.-Y., and Lee, Y.** (2008). The Arabidopsis Phosphatidylinositol 3-Kinase Is Important for Pollen Development. Plant Physiol. **147**: 1886–1897.

**Li, J.-F., Chung, H.S., Niu, Y., Bush, J., McCormack, M., and Sheen, J.** (2013). Comprehensive Protein-Based Artificial MicroRNA Screens for Effective Gene Silencing in Plants. Plant Cell **25**: 1507–1522.

**Li, S.C. and Kane, P.M.** (2009). The Yeast Lysosome-Like Vacuole: Endpoint and Crossroads. Biochim Biophs Acta. **1793**: 650–663.

**Liu, Y. and Li, J.** (2014). Endoplasmic reticulum-mediated protein quality control in Arabidopsis. Front. Plant Sci. **5**: 162.

**Löfke, C., Dünser, K., Scheuring, D., and Kleine-Vehn, J.** (2015). Auxin regulates SNARE-dependent vacuolar morphology restricting cell size. Elife **4**.

**Lőrincz, P. et al.** (2016). MiniCORVET is a Vps8-containing early endosomal tether in Drosophila. Elife **5**: e14226.

**Luo, Y. et al.** (2015). V-ATPase activity in the TGN/EE is required for exocytosis and recycling in Arabidopsis. Nat. Plants **1**: 15094.

**Lupanga, U., Röhrich, R., Askani, J., Hilmer, S., Kiefer, C., Krebs, M., Kanazawa, T., Ueda, T., and Schumacher, K.** (2020). The Arabidopsis V-ATPase is localized to the TGN/EE via a seed plant specific motif. Elife **9**.

**Manolson, M.F., Wu, B., Proteau, D., Taillon, B.E., Roberts, B.T., Hoyt, M.A., and Jones, E.W.** (1994). STV1 gene encodes functional homologue of 95-

kDa yeast vacuolar H+- ATPase subunit Vph1p. J. Biol. Chem. **269**: 14064–14074.

**Marc, J., Granger, C., Brincat, J., Fisher, D., Kao, T., McCubbin, A., and Cyr, R.** (1998). A GFP-MAP4 reporter gene for visualizing cortical microtubule rearrangements in living epidermal cells. Plant Cell **10**: 1927–1940.

**de Marcos Lousa, C. and Denecke, J.** (2016). Lysosomal and vacuolar sorting: not so different after all! Biochem. Soc. Trans. **44**: 891–897.

**Marti, L., Fornaciari, S., Renna, L., and Stefano, G.** (2010). COPII-mediated traffic in plants. Trends Plant Sci. **15**: 522–528.

**Marty, F.** (1978). Cytochemical studies on GERL, provacuoles, and vacuoles in root meristematic cells of Euphorbia. Proc. Natl. Acad. Sci. U. S. A. **75**: 852–6.

**Marty, F.** (1999). Plant vacuoles. Plant Cell **11**: 587–600.

**Matile, P. and Moor, H.** (1968). Vacuolation: origin and development of the lysosomal apparatus in root-tip cells. Planta **80**: 159–175.

**Maugarny-Calès, A. and Laufs, P.** (2018). Getting leaves into shape: A molecular, cellular, environmental and evolutionary view. Dev. **145**.

**Mesquita, J.F.** (1969). Electron microscope study of the origin and development of the vacuoles in root-tip cells of Lupinus albus L. J Ultrastruct Res **26**: 242–250.

**Michaeli, S., Galili, G., Genschik, P., Fernie, A.R., and Avin-Wittenberg, T.** (2016). Autophagy in Plants - What's New on the Menu? Trends Plant Sci. **21**: 134–144.

**Miller, E.A., Beilharz, T.H., Malkus, P.N., Lee, M.C.S., Hamamoto, S., Orci, L., and Schekman, R.** (2003). Multiple cargo binding sites on the COPII subunit Sec24p ensure capture of diverse membrane proteins into transport vesicles. Cell **114**: 497–509.

**Minina, E.A., Scheuring, D., Askani, J., Krueger, F., and Schumacher, K.** (2021). Light at the end of the tunnel: FRAP assay reveals that plant

vacuoles start as a tubular network. bioRxiv: 444058.

**Morel, N., Dedieu, J.C., and Philippe, J.M.** (2003). Specific sorting of the a1 isoform of the V-H+ATPase a subunit to nerve terminals where it associates with both synaptic vesicles and the presynaptic plasma membrane. J. Cell Sci. **116**: 4751–4762.

**Nakanishi-Matsui, M., Sekiya, M., Nakamoto, R.K., and Futai, M.** (2010). The mechanism of rotating proton pumping ATPases. Biochim. Biophys. Acta - Bioenerg. **1797**: 1343–1352.

**Neubert, C.** (2012). Assembly and quality control of the V- ATPase in Arabidopsis. Dissertation. Ruprecht-Karls-Universität Heidelberg.

**Neubert, C., Graham, L.A., Black-Maier, E.W., Coonrod, E.M., Liu, T.-Y., Stierhof, Y.-D., Seidel, T., Stevens, T.H., and Schumacher, K.** (2008). Arabidopsis has Two Functional Orthologs of the Yeast V-ATPase Assembly Factor Vma21p. Traffic **9**: 1618–1628.

**Niihama, M., Takemoto, N., Hashiguchi, Y., Tasaka, M., and Morita, M.T.** (2009). ZIP genes encode proteins involved in membrane trafficking of the TGNPVC/Vacuoles. Plant Cell Physiol. **50**: 2057–2068.

**Nováková, P. et al.** (2014). SAC phosphoinositide phosphatases at the tonoplast mediate vacuolar function in Arabidopsis. Proc. Natl. Acad. Sci. U. S. A. **111**: 2818–23.

**Oku, M. and Sakai, Y.** (2018). Three Distinct Types of Microautophagy Based on Membrane Dynamics and Molecular Machineries. BioEssays **40**: 1–6.

**Osterrieder, A., Hummel, E., Carvalho, C.M., and Hawes, C.** (2010). Golgi membrane dynamics after induction of a dominant-negative mutant Sar1 GTPase in tobacco. J. Exp. Bot. **61**: 405–422.

**Panteris, E., Adamakis, I.D.S., Daras, G., Hatzopoulos, P., and Rigas, S.** (2013). Differential responsiveness of cortical microtubule orientation to suppression of cell expansion among the developmental zones of Arabidopsis thaliana root apex. PLoS One **8**: e82442.

**Poschet, G., Hannich, B., Raab, S., Jungkunz, I., Klemens, P.A.W., Krueger, S., Wic, S., Neuhaus, H.E., and Büttner, M.** (2011). A novel arabidopsis vacuolar glucose exporter is involved in cellular sugar homeostasis and affects the composition of seed storage compounds. Plant Physiol. **157**: 1664–1676.

**Praefcke, G.J.K. and McMahon, H.T.** (2004). The dynamin superfamily: universal membrane tubulation and fission molecules? Nat. Rev. Mol. Cell Biol. **5**: 133–47.

**Raymond, C.K., Howald-Stevenson, I., Vater, C.A., and Stevens, T.H.** (1992). Morphological classification of the yeast vacuolar protein sorting mutants: Evidence for a prevacuolar compartment in class E vps mutants. Mol. Biol. Cell **3**: 1389–1402.

**Reyes, F.C., Buono, R., and Otegui, M.S.** (2011). Plant endosomal trafficking pathways. Curr. Opin. Plant Biol. **14**: 666–73.

**Richardson, S.C.W., Winistorfer, S.C., Poupon, V., Luzio, J.P., and Piper, R.C.** (2004). Mammalian late vacuole protein sorting orthologues participate in early endosomal fusion and interact with the cytoskeleton. Mol. Biol. Cell **15**: 1197–210.

**Richter, S., Geldner, N., Schrader, J., Wolters, H., Stierhof, Y.D., Rios, G., Koncz, C., Robinson, D.G., and Jürgens, G.** (2007). Functional diversification of closely related ARF-GEFs in protein secretion and recycling. Nature **448**: 488–492.

**Rojo, E., Gillmor, C.S., Kovaleva, V., Somerville, C.R., and Raikhel, N. V.** (2001). VACUOLELESS1 Is an Essential Gene Required for Vacuole Formation and Morphogenesis in Arabidopsis. Dev. Cell **1**: 303–310.

**Rojo, E., Zouhar, J., Kovaleva, V., Hong, S., and Raikhel, N. V** (2003). The AtC-VPS protein complex is localized to the tonoplast and the prevacuolar compartment in arabidopsis. Mol. Biol. Cell **14**: 361–9.

**Rostislavleva, K., Soler, N., Ohashi, Y., Zhang, L., Pardon, E., Burke, J.E., Masson, G.R., Johnson, C., Steyaert, J., Ktistakis, N.T., and Williams,**

**R.L.** (2015). Structure and flexibility of the endosomal Vps34 complex reveals the basis of its function on membranes. Science (80-. ). **350**: aac7365–aac7365.

**Sanderfoot, a a, Kovaleva, V., Bassham, D.C., and Raikhel, N. V** (2001). Interactions between syntaxins identify at least five SNARE complexes within the Golgi/prevacuolar system of the Arabidopsis cell. Mol. Biol. Cell **12**: 3733–3743.

**Sauer, M., Robert, S., and Kleine-Vehn, J.** (2013). Auxin: Simply complicated. J. Exp. Bot. **64**: 2565–2577.

**Scheuring, D., Löfke, C., Krüger, F., Kittelmann, M., Eisa, A., Hughes, L., Smith, R.S., Hawes, C., Schumacher, K., and Kleine-Vehn, J.** (2016). Actin-dependent vacuolar occupancy of the cell determines auxin-induced growth repression. Proc. Natl. Acad. Sci. U. S. A. **113**: 452–457.

**Scheuring, D., Viotti, C., Krüger, F., Künzl, F., Sturm, S., Bubeck, J., Hillmer, S., Frigerio, L., Robinson, D.G., Pimpl, P., and Schumacher, K.** (2011). Multivesicular bodies mature from the trans-Golgi network/early endosome in Arabidopsis. Plant Cell **23**: 3463–81.

**Schumacher, K. and Krebs, M.** (2010). The V-ATPase: small cargo, large effects. Curr. Opin. Plant Biol. **13**: 724–30.

**Schwab, R., Ossowski, S., Riester, M., Warthmann, N., and Weigel, D.** (2006). Highly Specific Gene Silencing by Artificial MicroRNAs in Arabidopsis[W][OA]. Plant Cell **18**: 1121–1133.

**Segami, S., Makino, S., Miyake, A., Asaoka, M., and Maeshima, M.** (2014). Dynamics of vacuoles and H+-pyrophosphatase visualized by monomeric green fluorescent protein in Arabidopsis: artifactual bulbs and native intravacuolar spherical structures. Plant Cell **26**: 3416–34.

**Shima, D.T., Cabrera-poch, N., Pepperkok, R., and Warren, G.** (1998). An Ordered Inheritance Strategy for the Golgi Apparatus: Visualization of Mitotic Disassembly Reveals a Role for the Mitotic Spindle. **141**: 955–966.

**Singh, M.K., Krüger, F., Beckmann, H., Brumm, S., Vermeer, J.E.M., Munnik, T., Mayer, U., Stierhof, Y.-D., Grefen, C., Schumacher, K., and Jürgens, G.** (2014). Protein Delivery to Vacuole Requires SAND Protein-Dependent Rab GTPase Conversion for MVB-Vacuole Fusion. Curr. Biol. **24**: 1383–1389.

**Söllner, T.H. and Malsam, J.** (2018). Uncovering the "secret" lives of vacuolar fusion pores in living cells. EMBO J. **37**: 1–3.

**Sparvoli, D. et al.** (2018). Remodeling the Specificity of an Endosomal CORVET Tether Underlies Formation of Regulated Secretory Vesicles in the Ciliate Tetrahymena thermophila. Curr. Biol. **28**: 697-710.e13.

**Strasser, B., Iwaszkiewicz, J., Michielin, O., and Mayer, A.** (2011). The V-ATPase proteolipid cylinder promotes the lipid-mixing stage of SNARE-dependent fusion of yeast vacuoles. EMBO J. **30**: 4126–4141.

**Sugimoto, K., Himmelspach, R., Williamson, R.E., and Wasteneys, G.O.** (2003). Mutation or drug-dependent microtubule disruption causes radial swelling without altering parallel cellulose microfibril deposition in Arabidopsis root cells. Plant Cell **15**: 1414–1429.

**Sze, H., Schumacher, K., Müller, M.L., Padmanaban, S., and Taiz, L.** (2002). A simple nomenclature for a complex proton pump: VHA genes encode the vacuolar H+-ATPase. Trends Plant Sci. **7**: 157–161.

**Takáč, T., Pechan, T., Šamajová, O., Ovečka, M., Richter, H., Eck, C., Niehaus, K., and Šamaj, J.** (2012). Wortmannin treatment induces changes in arabidopsis root proteome and Post-Golgi compartments. J. Proteome Res. **11**: 3127–3142.

**Takemoto, K., Ebine, K., Askani, J.C., Krüger, F., Gonzalez, Z.A., Ito, E., Goh, T., Schumacher, K., Nakano, A., and Ueda, T.** (2018). Distinct sets of tethering complexes, SNARE complexes, and Rab GTPases mediate membrane fusion at the vacuole in Arabidopsis. Proc. Natl. Acad. Sci.: 201717839.

**Takeuchi, M., Ueda, T., Sato, K., Abe, H., Nagata, T., and Nakano, A.** (2000).

A dominant negative mutant of Sar1 GTPase inhibits protein transport from the endoplasmic reticulum to the Golgi apparatus in tobacco and Arabidopsis cultured cells. Plant J. **23**: 517–525.

**Toyomura, T., Murata, Y., Yamamoto, A., Oka, T., Sun-Wada, G.H., Wada, Y., and Futai, M.** (2003). From lysosomes to the plasma membrane. Localization of vacuolar type H+-ATPase with the a3 isoform during osteoclast differentiation. J. Biol. Chem. **278**: 22023–22030.

**Uemura, T., Nakano, R.T., Takagi, J., Wang, Y., Kramer, K., Finkemeier, I., Nakagami, H., Tsuda, K., Ueda, T., Schulze-Lefert, P., and Nakano, A.** (2019). A golgi-released subpopulation of the trans-golgi network mediates protein secretion in arabidopsis 1[OPEN]. Plant Physiol. **179**: 519–532.

**Uemura, T., Suda, Y., Ueda, T., and Nakano, A.** (2014). Dynamic behavior of the trans-golgi network in root tissues of arabidopsis revealed by super-resolution live imaging. Plant Cell Physiol. **55**: 694–703.

**Uemura, T. and Ueda, T.** (2014). Plant vacuolar trafficking driven by RAB and SNARE proteins. Curr. Opin. Plant Biol. **22**: 116–21.

**Uemura, T., Ueda, T., Ohniwa, R.L., Nakano, A., Takeyasu, K., and Sato, M.H.** (2004). Systematic analysis of SNARE molecules in Arabidopsis: Dissection of the post-Golgi network in plant cells. Cell Struct. Funct. **29**: 49–65.

**Vermeer, J.E.M., Van Leeuwen, W., Tobeña-Santamaria, R., Laxalt, A.M., Jones, D.R., Divecha, N., Gadella, T.W.J., and Munnik, T.** (2006). Visualization of PtdIns3P dynamics in living plant cells. Plant J. **47**: 687–700.

**Viotti, C. et al.** (2010). Endocytic and Secretory Traffic in Arabidopsis Merge in the Trans-Golgi Network/Early Endosome, an Independent and Highly Dynamic Organelle. Plant Cell **22**: 1344–1357.

**Viotti, C. et al.** (2013). The endoplasmic reticulum is the main membrane source for biogenesis of the lytic vacuole in Arabidopsis. Plant Cell **25**: 3434–3449.

**Vukašinović, N. and Žárský, V.** (2016). Tethering Complexes in the Arabidopsis Endomembrane System. Front. cell Dev. Biol. **4**: 46.

**Waadt, R. et al.** (2015). Identification of Open Stomata1-interacting proteins reveals interactions with Sucrose Non-Fermenting1-Related Protein Kinases2 and with type 2A protein phosphatases that function in abscisic acid responses. Plant Physiol. **169**: 760–779.

**Wagner, C.A., Finberg, K.E., Breton, S., Marshansky, V., Brown, D., and Geibel, J.P.** (2004). Renal vacuolar H+-ATPase. Physiol. Rev. **84**: 1263–1314.

**Wang, R., Long, T., Hassan, A., Wang, J., Sun, Y., Xie, X.S., and Li, X.** (2020). Cryo-EM structures of intact V-ATPase from bovine brain. Nat. Commun. **11**: 1–9.

**Wickner, W.** (2010). Membrane fusion: five lipids, four SNAREs, three chaperones, two nucleotides, and a Rab, all dancing in a ring on yeast vacuoles. Annu. Rev. Cell Dev. Biol. **26**: 115–136.

**Wolfenstetter, S., Wirsching, P., Dotzauer, D., Schneider, S., and Sauer, N.** (2012). Routes to the Tonoplast: The Sorting of Tonoplast Transporters in Arabidopsis Mesophyll Protoplasts. Plant Cell **24**: 215–232.

**Zeng, Y., Chung, K.P., Li, B., Lai, C.M., Lam, S.K., Wang, X., Cui, Y., Gao, C., Luo, M., Wong, K.-B., Schekman, R., and Jiang, L.** (2015). Unique COPII component AtSar1a/AtSec23a pair is required for the distinct function of protein ER export in *Arabidopsis thaliana*. Proc. Natl. Acad. Sci. **112**: 14360–14365.

**Zhang, G.F., Driouich, A., and Staehelin, L.A.** (1993). Effect of monensin on plant Golgi: Re-examination of the monensin-induced changes in cisternal architecture and functional activities of the Golgi apparatus of sycamore suspension-cultured cells. J. Cell Sci. **104**: 819–831.

**Zheng, H. and Staehelin, L.A.** (2011). Protein storage vacuoles are transformed into lytic vacuoles in root meristematic cells of germinating seedlings by multiple, cell type-specific mechanisms. Plant Physiol. **155**: 2023–35.

**Zheng, J., Han, S.W., Munnik, T., and Rojas-Pierce, M.** (2014a). Multiple vacuoles in impaired tonoplast trafficking3 mutants are independent

organelles. Plant Signal. Behav. **9**: e972113.

**Zheng, J., Han, S.W., Rodriguez-Welsh, M.F., and Rojas-Pierce, M.** (2014b). Homotypic Vacuole Fusion Requires VTI11 and Is Regulated by Phosphoinositides. Mol. Plant **7**: 1026–1040.

**Zouhar, J. and Rojo, E.** (2009). Plant vacuoles: where did they come from and where are they heading? Curr. Opin. Plant Biol. **12**: 677–684.

# 9 List of abbreviations

| | |
|---|---|
| % | percent |
| °C | degree Celsius |
| 6x OP | 6x Operator-Promoter |
| aa | amino acid |
| AB | antibiotics |
| amiR | artificial micro RNA |
| AP-3 | adaptor protein-3 |
| ATP | adenosine-triphosphate |
| AU | Airy unit |
| BCECF | 2',7'-bis(2-carboxyethyl)-5(6)-carboxyfluorescein |
| BFA | Brefeldin A |
| bp | base pair(s) |
| CCV | clathrin-coated vesicle |
| cDNA | complementary DNA |
| CDS | coding sequence |
| CFP | cyan fluorescent protein |
| CLSM | confocal laser scanning microscopy |
| cm | centimetre(s) |
| Col-0 | Columbia-0 |
| ConcA | Concanamycin A |
| COPI/II | coat protein complex I / II |
| CORVET | Class C Core Vacuole/Endosome Tethering |
| Dex | dexamethasone |

| | |
|---|---|
| DMSO | dimethylsulfoxid |
| DNA | deoxyribonucleic acid |
| E. coli | Escherichia coli |
| e.g. | exempli gratia/ for example |
| eGFP | enhanced monomeric green fluorescent protein |
| EM | electron microscopy |
| ER | Endoplasmic Reticulum |
| Est | β-estradiol |
| F | filial generation |
| FM 4-64 | (N-(3-triethylammoniumpropyl)-4-(6-(4- (diethylamino) phenyl) hexatrienyl) pyridinium dibromide) |
| FRAP | Fluorescence Recovery After Photobleaching |
| gDNA | genomic DNA |
| GDP | Guanosine diphosphate |
| GTP | Guanosine-5'-triphosphate |
| HOPS | Homotypic Protein Sorting |
| hr | hour(s) |
| i.e. | lat.: *id est*; eng.: that is |
| kb | kilobases |
| l | litre(s) |
| LE | late endosome |
| M | molar |
| min | minute(s) |
| ml | millilitre(s) |

| | |
|---|---|
| mM | millimolar |
| MS | Murashige & Skoog |
| MVB/LE | multivesicular body/late endosome |
| ng | nanogram |
| nm | nanometre(s) |
| nM | nanomolar |
| ORF | open reading frame |
| PCR | polymerase chain reaction |
| pH | potential of hydrogen (*pondus hydrogenii)* |
| PI3K | phosphatidylinositol 3-kinase |
| PI3P | phosphatidyl 3-phosphate |
| $PP_i$ | pyrophosphate |
| PSV | protein storage vacuole |
| RFP | monomeric red fluorescent protein |
| RNA | ribonucleic acid |
| rpm | rounds per minute |
| RT | room temperature (22°C) |
| sec | second(s) |
| SNARE | soluble N-ethylmaleimidine sensitive factor attachment receptor |
| SV | small vacuole |
| T | transgenic generation |
| T-DNA | transfer DNA |
| TGN/EE | *trans*-Golgi network/ early endosome |

| | |
|---|---|
| V-ATPase | vacuolar-type proton ATPase |
| V-PPase | VHP $H^+$- pyrophosphatase |
| WM | Wortmannin |
| WT | wild type |
| µE m-2 s-1 | micro Einstein per square meter per second |
| µg | micro gram |
| µl | micro litre |
| µM | micro molar |
| µm | micrometre(s) |

# 10 Acknowledgements

I would like to express my greatest gratitude to Prof. Dr. Karin Schumacher for the valuable opportunity to perform my PhD study in her lab, including numerous times supporting and advising me. These years were very formative for me and above all also personally important. The open exchange with other laboratories inside and outside Europe has greatly enriched me and my work.

The Schumacher Lab was always very special to me. And Dr. Melanie Krebs is a central part of this lab, unlimitedly providing her knowledge and always curious for the new.

Big thanks to Prof. Dr. Alexis Maizel who is my second examiner and has accompanied me as a TAC member through the years giving treasured advice and guiding discussions. I also highly appreciate the participation of my other TAC members Dr. Sebastian Wolf and Dr. Michael Raissig. Thank you for the support and guidance through the years. I also thank Prof. Dr. Rüdiger Hell and Prof. Dr. Gislene Pereira for agreeing to be referees in my oral examination.

Many thanks to Falco Krüger for introducing me into the beauty of plant endomembrane trafficking and vacuole biogenesis. I highly appreciate that he never got tired to discuss any new hypotheses or experimental outcome.

I want to thank Eleonore Holzwart for her support and lasting friendship. Thanks to Marlene Handl for her great work in the lab and the fun times while working together.

I also would like to thank Upendo Lupanga for her advice and support. Thanks to Stefan Scholl for Tips and Tricks in the daily bench work. Thanks to Fabian Fink for the great work atmosphere and constant good mood.

Thanks to Barbara Jesenofsky, Beate Schöfer and Ines Steins for being a rescue net whenever it was needed. Thanks to Rachel Röhrich for being understanding and supportive. Thanks to Zaida Andrés for the social interaction, scientific advice and guidance. Thanks to Stefanie Gold and Stefan Hillmer for their assistance in electron microscopy.

Special thanks to Alyona Minina, Paula Ragel de la Torre, Catharina Larasati, Rainer Waadt, Jonathan Dragwidge, Nana Keinath, Anne Kriegel, Philipp Belon, Simon Delang, Borja Garnelo Gómez, Zhenni Li, Ann-Kathrin Schürholz, Sebastian Augustin, Amaya Vilches Barro, Leonie Martin and Sina Pfleger for the great time in the lab.

I also want to thank my friends and my family. Especially, as my family is fundamental to my well-being. No words can say how much I love you and how much I am thankful for your love and support. To the same extent, I am grateful to Marco.